

What makes long DNA short?

Modulation of DNA structure by Dps protein: cooperating & reorganizing

Vtyurina, Natalia

DOI

[10.4233/uuid:14080918-3a6e-48ad-8c47-906538f689ac](https://doi.org/10.4233/uuid:14080918-3a6e-48ad-8c47-906538f689ac)

Publication date

2016

Document Version

Final published version

Citation (APA)

Vtyurina, N. (2016). *What makes long DNA short? Modulation of DNA structure by Dps protein: cooperating & reorganizing*. [Dissertation (TU Delft), Delft University of Technology].
<https://doi.org/10.4233/uuid:14080918-3a6e-48ad-8c47-906538f689ac>

Important note

To cite this publication, please use the final published version (if applicable).
Please check the document version above.

Copyright

Other than for strictly personal use, it is not permitted to download, forward or distribute the text or part of it, without the consent of the author(s) and/or copyright holder(s), unless the work is under an open content license such as Creative Commons.

Takedown policy

Please contact us and provide details if you believe this document breaches copyrights.
We will remove access to the work immediately and investigate your claim.

Modulation of DNA structure by Dps protein: cooperating & reorganizing



Natalia Vtyurina

What makes long DNA short?

Modulation of DNA structure by Dps protein: cooperating & reorganizing

Natalia Vtyurina

What makes long DNA short?

Modulation of DNA structure by Dps protein: cooperating & reorganizing

Proefschrift

ter verkrijging van de graad van doctor
aan de Technische Universiteit Delft,
op gezag van de Rector Magnificus prof. ir. K.C.A.M. Luyben;
voorzitter van het College voor Promoties,
in het openbaar te verdedigen op
9 september 2016 om 10.00 uur

door

Natalia VTYURINA

Master of Science in de natuurkunde,
Lomonosov Staatsuniversiteit van Moskou, Rusland
geboren te Moskou, Rusland

This dissertation has been approved by the

promotor: Prof.dr.ir. N. H. Dekker

Delft University of Technology

copromotor: Dr. E. A. Abbondanzieri

Delft University of Technology

Composition of the doctoral committee:

Rector Magnificus

chairman

Independent members:

Prof.dr. A. H. Engel

Delft University of Technology

Prof.dr. T. S. Shimizu

VU University Amsterdam

Prof.dr. G. J.L. Wuite

VU University Amsterdam

Dr.ir. J. S.T. van Noort

Leiden University

Dr. D. Grainger

University of Birmingham, UK

Reserve member

Prof.dr. M. Dogterom

Delft University of Technology



Keywords: single-molecule, DNA condensation, Dps protein, cooperativity, reorganization, hysteresis, Ising model

Printed by: Proefschriftmaken.nl

Front & back cover design: Jinhee Kim

Copyright © 2016 by N.N. Vtyurina

Casimir PhD series, Delft-Leiden 2016-10

ISBN 978.90.8593.262.8

An electronic version of this thesis is available at <http://repository.tudelft.nl/>

*This dissertation is dedicated to my parents
who made my life meaningful for me.
To my father who inspired me to become a scientist
and accomplish a PhD.
To my mother who provided me love and care.
June 2016*

Abbreviations

| | |
|-----------------------|--|
| AF | Assisting Force |
| CS | Conformational Spread model |
| Cy5 | Cyanine (fluorescent dye) |
| DNA | DeoxyriboNucleic Acid |
| Dps | DNA-binding Protein from Starved cells |
| DTW | Dwell Time Window |
| <i>E. coli</i> | <i>Escherichia coli</i> |
| KNF | Koshland-Némethy-Filmer model |
| MWC | Monod-Wyman-Changeux model |
| NAP | Nucleoid-Associated Proteins |
| OF | Opposing Force |
| PEG | PolyEthylene Glycol |
| RNA | RiboNucleic Acid |
| mRNA | Messenger RNA |
| RNAP | RNA Polymerase |
| WLC | Worm-Like Chain model |
| YOYO-1 | Yellow Oxazole (fluorescent dye) |

Table of Contents

| | |
|---|-----------|
| Abbreviations | i |
| Table of Contents..... | iii |
| 1. Introduction..... | 1 |
| 1.1 Life is confined in the DNA of each single cell | 3 |
| 1.2 Proteins execute myriad functions in the cell..... | 4 |
| 1.3 DNA packaging: fitting kilometers into a tennis ball | 4 |
| 1.4 What is Dps and why it is important? | 6 |
| 1.5 How Dps compacts DNA?..... | 9 |
| 1.6 Thesis overview | 9 |
| References | 11 |
| 2. <i>In vitro</i> single-molecule techniques: from technology to biology..... | 15 |
| 2.1 Introduction | 17 |
| 2.2 Preparing DNA and Dps for interaction..... | 18 |
| 2.2.1 DNA isolation and labeling..... | 18 |
| 2.2.2 Dps purification and labeling..... | 19 |
| 2.3 Activity of Dps on DNA molecule tested in bulk experiments | 20 |
| 2.4 Sample preparation and experimental configuration | 24 |
| 2.4.1 Preparation of glass slides and coverslips | 24 |
| for fluorescent measurements | |
| 2.4.2 Fluorescence assay: imaging Dps binding to DNA | 25 |
| 2.4.3 Magnetic tweezers assay: | 26 |
| controlling DNA compaction by Dps with force | |
| 2.5 Conclusions | 28 |
| References | 29 |
| 3. Cooperativity and hysteresis combined in Ising model | 31 |
| 3.1 Introduction | 33 |
| 3.2 Dps induces DNA compaction via cooperative binding..... | 34 |
| 3.2.1 Bulk experimental data of Dps binding to DNA | 34 |
| 3.2.2 Tracking Dps binding to DNA under fluorescent microscope | 35 |
| 3.3 Reversible DNA compaction by Dps reveals hysteresis..... | 38 |
| 3.3.1 Past concentrations of Dps influences DNA compaction | 38 |

| | |
|--|-----------|
| 3.3.2 Tracking Dps binding to DNA under tension | 39 |
| 3.3.3 Hysteresis remains extremely stable over hour-long timescales..... | 42 |
| 3.3.4 Artificial point mutation changes Dps cooperativity..... | 43 |
| 3.4 Standard cooperativity models..... | 44 |
| 3.5 A modified Ising model of cooperativity predicts hysteresis..... | 44 |
| 3.5.1 Ising model from ferromagnetism..... | 44 |
| 3.5.2 Derivation of the binding probability of non-cooperative ligands | 46 |
| 3.5.3 Derivation of the binding probability using the Hill model..... | 47 |
| 3.5.4 Derivation of the binding probability using the Ising model | 48 |
| 3.5.5 The effects of DNA tension in each binding model..... | 50 |
| 3.5.6 Derivation of inflection points for Ising model | 52 |
| 3.6 Conclusions..... | 54 |
| References | 55 |
| 4. Kinetics of Dps binding to DNA..... | 59 |
| 4.1 Introduction | 61 |
| 4.2 Salt modulates cooperativity of Dps | 62 |
| 4.3 Tension modulates the affinity of Dps for DNA..... | 65 |
| 4.4 Kinetic interpretation of the hysteresis..... | 69 |
| 4.4.1 Global free energy diagram for an Ising mechanism | 69 |
| 4.4.2 Tilting the global free energy with force and ionic strength | 73 |
| 4.5 Hysteresis in other models of cooperativity..... | 74 |
| 4.5.1 Ising and KNF mechanisms of hysteresis | 74 |
| 4.5.2 Global free energy diagram for an MWC mechanism | 75 |
| 4.5.3 Global free energy diagram for a CS mechanism..... | 76 |
| 4.6 Conclusions..... | 78 |
| References | 79 |
| 5. Electrostatics drives Dps-DNA interactions | 81 |
| 5.1 Introduction | 83 |
| 5.2 Dps-induced compaction of DNA is influenced by salt, magnesium,..... | 84 |
| pH, and crowding conditions | |
| 5.3 Compare an Ising model to empirical data | 86 |
| 5.4 Biological implication of cooperative hysteresis..... | 90 |
| 5.5 Conclusions..... | 90 |
| References | 91 |

| | |
|--|------------|
| 6. How does DNA supercoiling affect Dps affinity? | 93 |
| 6.1 Introduction | 95 |
| 6.2 Affinity of Dps for DNA supercoils, U-shape and stretched DNA | 97 |
| 6.3 Dps-DNA complex accommodates excess of the DNA | 101 |
| 6.4 Coiling of DNA at constant stretching forces and presence of Dps | 102 |
| 6.4.1 Rotation-extension DNA curves are influenced by Dps | 102 |
| 6.4.2 Dps compensates force and stabilize plectonemes | 102 |
| 6.5 Force-extension curves of coiled DNA | 108 |
| 6.6 Conclusions | 110 |
| References | 112 |
| 7. RNAP transcription through Dps-DNA complexes | 115 |
| 7.1 Introduction | 117 |
| 7.2 Methods for tracking RNAP translocation along the DNA | 118 |
| 7.2.1 DNA constructs and RNAP labeling for magnetic tweezers assay | 119 |
| 7.2.2 Flow cell preparation | 120 |
| 7.2.3 RNAP transcription assay | 121 |
| 7.3 Analyzing RNAP translocation along the DNA | 122 |
| 7.3.1 RNAP transcription traces | 122 |
| 7.3.2 Dwell time analysis | 123 |
| 7.4 RNAP transcription at assisting and opposing forces in the presence of Dps | 123 |
| 7.4.1 RNAP transcription at assisting force in the presence of Dps | 123 |
| 7.4.2 RNAP transcription at opposing force in the presence of Dps | 124 |
| 7.4.3 Comparison of assisting and opposing force configurations | 125 |
| 7.5 Tracking RNAP transcription in fully compacted Dps-DNA complexes | 127 |
| 7.6 Conclusions | 128 |
| References | 129 |
| Summary | 133 |
| Samenvatting | 141 |
| Acknowledgements | 149 |
| A.I Story of my PhD adventure | 151 |
| A.II Story of my live during PhD adventure | 154 |
| Curriculum Vitae | 157 |
| List of Publications | 159 |
| Propositions | 161 |

Chapter 1

Introduction



1.1 Life is confined in the DNA of each single cell

Of all that surrounds us, the most inexplicable seems to be life. We are used to the fact that life is around us and in us. Ultimately, one may take it for granted and stop being curious what is actually hidden behind the word “life” and the meaning of “being alive”. Therefore, before you start reading the thesis and focus on the deep details of a particular biological question – look around and think what are the common properties and features that unite all living organisms in one group, whether they be human or an invisible microbe?

The answer begins with the first observation of life under the microscope performed by Antony Van Leeuwenhoek in Delft 340 years ago. Two centuries of research passed before 'cell theory' was formulated, stating that all living organisms are made from cells: the basic structural unit that can independently function and replicate (1, 2). The simplest forms of life, like bacteria, consist of one single cell. Higher organisms, such as humans, represent communities of cells, or colonies of individual cells, that perform specialized functions. The plan of how the organism will develop after birth is confined inside each single cell – particularly in the DNA molecule (3).

DNA is a long natural polymer that is built from repeating blocks called nucleotides and twisted into a double helix (4, 5), therefore, reminiscent of a ladder (**Fig.1**).



Fig.1. First drawn schematic representation of DNA (5).

A tremendous amount of information is stored in this molecule: the color of hair or feathers; legs or wings; lips or a beak; and many other properties.

Overall, each cell carries the information about the entire organism. Imagine if every brick of a building would contain a tiny plan of the whole construction. Then, if archeologists find at least one stone left from an ancient building, historians would not have any need to reckon how it looked like back in time. Therefore, to be living means to have a molecule that is enclosed within cell boundaries and represents the carrier of genetic material (i.e. DNA).

1.2 Proteins execute myriad functions in the cell

Along with the importance of the DNA molecule as a genetic carrier, we should not forget about the role of proteins, without which neither the genome nor the cell could function. Proteins are the building blocks from which cells are assembled. In addition to providing the cell with its shape and structure, proteins (or enzymes) also execute many of other myriad functions: they promote intracellular metabolism, control the passage of nutrients, carry a message from one cell to another, and act as hormones. They are even capable of activating or disabling particular genes and play a crucial role in DNA replication, repair and protection.

Before we can truly understand how neurons deliver signals to the brain, how muscles contract, how embryos develop, and how diseases spread, we must understand how DNA and genes work, accompanied by number of proteins. One group of proteins releases after expression into the cellular interior to perform their functions (6). Another group of proteins is not only encoded on the DNA, but after expression directly interacts back with the DNA as the protein's functions must be accomplished there (7-9). In this thesis, we will only focus on the last type - DNA-binding proteins. Therefore, closer attention will be paid to one of the proteins that physically binds to DNA molecules.

1.3 DNA packaging: fitting kilometers into a tennis ball

The direct access of DNA-binding proteins to the DNA molecule makes them vitally important. One of their roles is the compaction of long DNA inside the cell. They organize DNA into particular structures so that it is still accessible

to many other proteins and enzymes that replicate, repair, and transcribe genes to produce new proteins (7-12). Taking into account the large amount of information that has to be condensed inside of a small cell volume and the length of DNA that has mechanical properties of an entropic spring, helps to imagine how complex the task is.

In bacteria, the task of packaging the comparatively enormous DNA (1.6 mm) inside of the utterly tiny cell ($1\text{ }\mu\text{m}^3$) is accomplished by a family of nucleoid-associated proteins (NAPs) (9, 13, 14). This geometry is equivalent to packing kilometers of extremely fine thread into a tennis ball (15). NAPs bind to and fold the DNA, generating a series of coils and loops that provide increasingly higher levels of organization (12). The binding of one single protein from this family to DNA may activate or deactivate a particular gene by simply influencing its shape (8, 9), i.e. one protein may directly affect the global genetic regulation. Incorrect functioning of one or more of these types of proteins subsequently can be life treating for the cell and, furthermore, for the entire organism.

The examples given above demonstrate the intimate relation between DNA-binding proteins and DNA inside of the bacteria. The beneficial function of genome packaging performed by NAPs is at the same time potentially harmful, in case of incorrect regulation. This feature makes the topic exceptionally fascinating: while fighting with life-threatening diseases caused by bacterial pathogens on a daily basis worldwide, dysfunction of NAPs in pathogen may be fatal to them and therefore beneficial to us. Additionally, gained knowledge about bacterial DNA compaction mediated by proteins may be translated and applied in other living systems that contain analogous proteins. Without this knowledge, we do not possess a complete picture of the vitally important processes in the cell. Furthermore, we might be losing a very promising pipeline of new antibiotics discoveries that might be utilized for a treatment of many bacterial diseases.

1.4 What is Dps and why it is important?

In order to understand the nature of the DNA packaging process, we need to identify parameters of the system that drive it. However, the variety of the proteins that are involved in this process makes the system extremely complicated to describe. To simplify the problem, we need to focus on particular proteins separately, especially the ones that protect bacteria against external treatment. For instance, under conditions of cell stress and starvation, an NAP called Dps (DNA-binding protein from starved cells) becomes abundant (**Fig.2**), playing a major role in DNA protection (16-22). Dps is highly expressed in stationary phase (4-7) and is also involved in the cellular response to oxidative (4, 8-10), UV (8, 11), thermal (8), pH shocks (8) and antibiotic treatment (23). In addition, Dps has been implicated in biofilm formation and tolerance to bacteriophage attacks (12). Therefore, helping bacteria to survive antibiotics, Dps makes the fight against pathogens difficult. Moreover, besides DNA protection Dps plays an important role in DNA compaction (18, 21, 24).

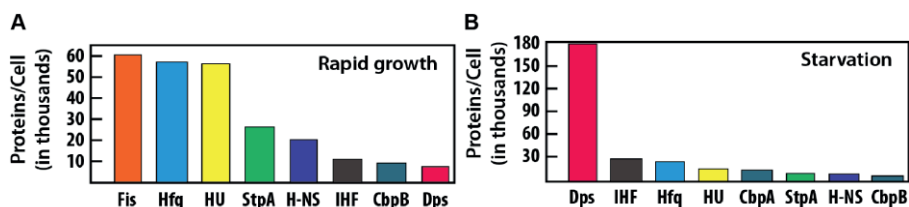


Fig.2. Growth phase-dependent variation in the intracellular levels of DNA-binding proteins in *E. coli*. (A) The expression levels among the DNA-binding proteins in exponential growth phase (25). (B) The expression levels among the DNA-binding proteins at late stationary growth phases (25).

Dps monomers have a molecular mass of 19 kDa and assemble into a dodecameric shell (**Fig.3**). The resulting complex binds to both supercoiled and linear DNA to form a dense biocrystal structure (16, 19, 21, 26). This biocrystal protects DNA from damage and increases cell survival rates under a diverse range of stresses (18, 21, 22, 27). While the crystal structure of the

Dps dodecamer has been solved (28), no atomic scale structure of Dps-DNA assemblies currently exists.

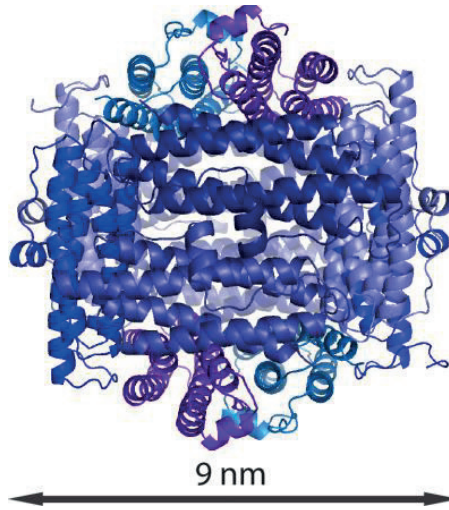


Fig.3. Dps spherical dodecamer. Dps 12-mers form a shell-like structure 8-9 nm in diameter (28).

Different techniques have been applied to the visualization of Dps-DNA complexes. Electron microscopy (EM) images reveal that Dps dodecamers form ordered crystalline structures *in vitro* both in absence and presence of the DNA (**Fig.4A and 4B respectively**) (19). Interestingly, Dps dodecamers without DNA are also tightly packed implying existence of extensive Dps-Dps interactions (18). Atomic force microscopy (AFM) images show that Dps causes clustering of distal DNA loci (**Fig.4C**) (29). EM observations of *E. coli* cells after the onset of starvation have shown a massive reorganization of the nucleoid mediated by Dps. These cells contained two structurally distinct morphologies: toroidal (24 hours starved bacteria) and rectangular (36 hours starved bacteria) (**Fig.4D and 4E respectively**) (26). *Ex vivo* AFM experiments conducted on lysed cells in stationary phase describe a tightly packed structure that is modulated by Dps protein (**Fig.4F**) (24). While other NAPs form markedly different structures on DNA *in vitro* and *in vivo*, Dps can assemble into rectangular bio-crystals in both contexts (16, 19, 21, 26).

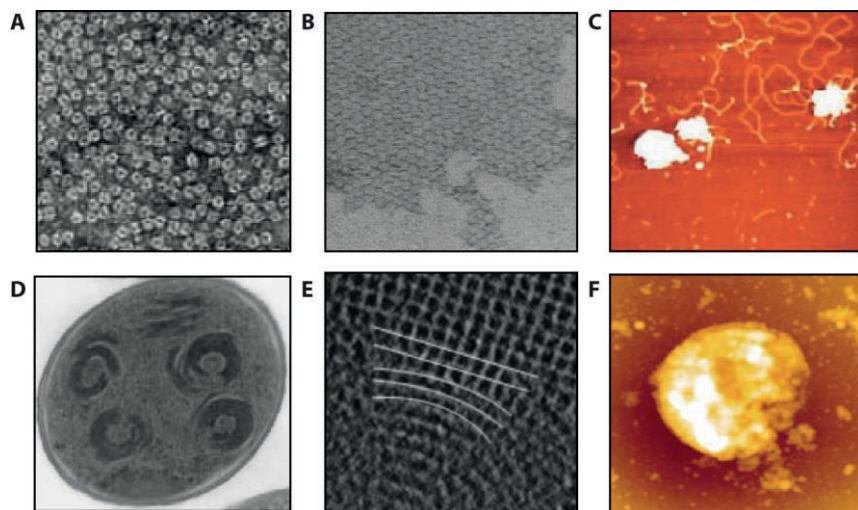


Fig.4. Images of Dps and Dps-DNA complexes. **(A)** Electron microscopy image of Dps incubated alone (19). **(B)** Electron microscopy image of Dps-DNA complexes (16). **(C)** Atomic force microscopy image of Dps-DNA complexes (29). **(D)** Electron microscopy image of *E. coli* cell starved for 24 hours (26). **(E)** Electron microscopy image of *E. coli* cell starved for 36 hours (26). **(F)** *Ex vivo* atomic force microscopy image of *E. coli* cell after the expression of the Dps protein was induced with IPTG in the stationary phase (24).

However, fewer efforts have been made in studying the mechanism behind the transition from dispersed DNA structure to extremely compact and highly ordered morphology. In bulk gel shift assays, it has been shown that Dps forms a few intermediate sized complexes before it transitions to a massive complex with DNA (29). This transition into a compact Dps-DNA state has been repeatedly observed and described by a standard Hill model for cooperative binding (22). However, little evidence of structural intermediates has been reported in AFM and EM studies performed *in vitro*. Therefore, based on only static images of preformed Dps-DNA complexes, we cannot identify any dynamic features of its formation and, consequently, mechanisms by which it protects bacteria.

There are several groups worldwide working with Dps and carrying out mostly purely biological research. However, biophysical approaches have never been applied for the characterization of Dps-DNA complex formation.

Additionally, available single-molecule techniques, which have been established in studying of other DNA-binding proteins (30, 31), have not been used yet to explore Dps binding to DNA, especially for real time observations. Therefore, existing knowledge of Dps mediated DNA compaction does not fully describe the kinetic features and biophysical parameters of Dps-DNA complex formation. The questions how this complex forms and how it is regulated remain unknown.

1.5 How Dps compacts DNA?

This thesis examines the question of how Dps compacts DNA into a complex *in vitro*. Particularly, the study investigates the dynamics of the complex formation in real time and reveals biophysical properties of the Dps-DNA interaction. In this research, we propose a new model of cooperative binding that reveals the intrinsic features of Dps-Dps and Dps-DNA neighboring interactions in response to the environmental changes. These experiments give a detailed biophysical view of Dps binding to DNA and gives us a better insight into the process of cell functioning. Elucidation of the properties of Dps may have important medical impact for treatment of the bacterial diseases. Further characterization and modeling of the processes of DNA compaction by Dps provide substantial information to the whole picture of genome organization together with other proteins.

1.6 Thesis overview

In this study, we developed two single-molecule assays to resolve the process of DNA compaction by Dps: fluorescent microscopy and magnetic-tweezers measurements, which are described in **Chapter 2**. Utilizing these techniques, the interaction between DNA and Dps were recorded in real time *in vitro*.

Chapter 3 is devoted to the nature of the interactions between Dps and DNA. Probing the binding activity of Dps to DNA, we find that Dps is a highly cooperative protein. Moreover, we surprisingly discovered a reproducible hysteresis in the process of compaction and decompaction of the Dps-DNA complex. Further, we point out that this process cannot be fit to standard

cooperativity models. Inspired by the Ising model of ferromagnetism, we describe the observation of cooperative Dps binding that exhibits hysteresis with a modified Ising model of cooperativity.

The obtained data on Dps binding and unbinding processes provide us with kinetic features of Dps-DNA complex formation. In **Chapter 4** we examine these processes by following DNA compaction dynamics and tuning various factors that affect Dps activity. Utilizing fluorescent assays, we compare how different amounts of monovalent salt change the affinity of Dps for DNA. Applying magnetic tweezers, we measure the mechanical forces that characterize the interactions between Dps and DNA and testing how tension applied to the DNA molecule modulates binding and dissociation rates of Dps. In order to understand why our modified Ising model gives rise to hysteresis, we discuss hysteresis in a scope of kinetics by comparing the energy diagrams between several other cooperative models.

In **Chapter 5**, several buffer variations that mimic changes in the cellular environment upon a stress, were applied in order to probe electrostatic interactions between Dps and DNA. With the developed Ising model for Dps-DNA complex we relate the amount of hysteresis to each of the tested conditions.

In the previous chapters, we demonstrate that torsionally relaxed DNA is compacted by Dps through a cooperative Ising mechanism. In **Chapter 6**, we focus on the affinity of Dps for other DNA conformations, paying particular attention to plectonemic DNA. Using fluorescence microscopy, we test preferences of Dps in binding to different DNA shapes and if the preformed Dps-DNA complexes can bind an additional amount of free DNA. With magnetic tweezers we examine how presence of Dps influences DNA coiling under constant tension. Further, we explore how preformed supercoiled DNA state influences Dps activity.

Lastly, after we characterized the process of DNA compaction by Dps from kinetic, physiological and biophysical perspectives at single- molecule level, we modified a magnetic tweezers assay particularly in order to characterize the dynamic process of RNAP transcription through preformed Dps-DNA

complexes in **Chapter 7**. We apply an assisting force (AF) to the RNAP molecules and allow it to transcribe through Dps-DNA complexes located downstream of RNAP. A second configuration allows us to apply an opposing force (OF) to the RNAP while transcribing through stretched bare DNA with Dps-DNA complex located upstream of RNAP. Further, we compare dwell-time distributions for these two configurations. We also examine the degree to which RNAPs can transcribe through completely compacted Dps-DNA complex at very low opposing force.

References

1. Mazzarello P (1999) A unifying concept: the history of cell theory. *Nat Cell Biol* 1(1):E13-15.
2. Wolpert L (1996) The evolution of 'the cell theory'. *Curr Biol* 6(3):225-228.
3. Watson JD & Crick FHC (1953) Genetical Implications of the Structure of Deoxyribonucleic Acid. *Nature* 171(4361):964-967.
4. Watson JD & Crick FHC (1953) The Structure of DNA. *Cold Spring Harb Sym* 18:123-131.
5. Watson JD & Crick FHC (1953) Molecular Structure of Nucleic Acids - a Structure for Deoxyribose Nucleic Acid. *Nature* 171(4356):737-738.
6. Crick F (1970) Central Dogma of Molecular Biology. *Nature* 227(5258):561-&.
7. Narlikar GJ, Fan HY, & Kingston RE (2002) Cooperation between complexes that regulate chromatin structure and transcription. *Cell* 108(4):475-487.
8. Browning DF, Grainger DC, & Busby SJW (2010) Effects of nucleoid-associated proteins on bacterial chromosome structure and gene expression. *Curr Opin Microbiol* 13(6):773-780.
9. Dillon SC & Dorman CJ (2010) Bacterial nucleoid-associated proteins, nucleoid structure and gene expression. *Nat Rev Microbiol* 8(3):185-195.
10. Kornberg RD (1974) Chromatin structure: a repeating unit of histones and DNA. *Science* 184(4139):868-871.
11. Badrinarayanan A, Reyes-Lamoth R, Uphoff S, Leake MC, & Sherratt DJ (2012) In Vivo Architecture and Action of Bacterial Structural Maintenance of Chromosome Proteins. *Science* 338(6106):528-531.
12. Wang XD, Llopis PM, & Rudner DZ (2013) Organization and segregation of bacterial chromosomes. *Nat Rev Genet* 14(3):191-203.
13. Luijsterburg MS, Noom MC, Wuite GJL, & Dame RT (2006) The architectural role of nucleoid-associated proteins in the organization of bacterial chromatin: A molecular perspective. *J Struct Biol* 156(2):262-272.
14. Muskhelishvili ATaG (2010) The Topology and Organization of Eukaryotic Chromatin. *Bacterial Chromatin Chapter* 11.

15. B. Alberts AJ, J. Lewis, M. Raff, K. Roberts and P. Walter (2002) *Molecular Biology of the Cell*. Garland Science, New York, USA, 4th edition.
16. Almiron M, Link AJ, Furlong D, & Kolter R (1992) A novel DNA-binding protein with regulatory and protective roles in starved *Escherichia coli*. *Genes & development* 6(12B):2646-2654.
17. Martinez A & Kolter R (1997) Protection of DNA during oxidative stress by the nonspecific DNA-binding protein Dps. *J Bacteriol* 179(16):5188-5194.
18. Nair S & Finkel SE (2004) Dps protects cells against multiple stresses during stationary phase. *J Bacteriol* 186(13):4192-4198.
19. Wolf SG, et al. (1999) DNA protection by stress-induced biocrystallization. *Nature* 400(6739):83-85.
20. Calhoun LN & Kwon YM (2011) Structure, function and regulation of the DNA-binding protein Dps and its role in acid and oxidative stress resistance in *Escherichia coli*: a review. *J Appl Microbiol* 110(2):375-386.
21. Frenkiel-Krispin D, et al. (2001) Regulated phase transitions of bacterial chromatin: a non-enzymatic pathway for generic DNA protection. *Embo J* 20(5):1184-1191.
22. Karas VO, Westerlaken I, & Meyer AS (2015) The DNA-Binding Protein from Starved Cells (Dps) Utilizes Dual Functions To Defend Cells against Multiple Stresses. *J Bacteriol* 197(19):3206-3215.
23. Calhoun LN & Kwon YM (2011) The ferritin-like protein Dps protects *Salmonella enterica* serotype Enteritidis from the Fenton-mediated killing mechanism of bactericidal antibiotics. *Int J Antimicrob Agents* 37(3):261-265.
24. Kim J, et al. (2004) Fundamental structural units of the *Escherichia coli* nucleoid revealed by atomic force microscopy. *Nucleic Acids Res* 32(6):1982-1992.
25. Azam TA, Iwata A, Nishimura A, Ueda S, & Ishihama A (1999) Growth phase-dependent variation in protein composition of the *Escherichia coli* nucleoid. *J Bacteriol* 181(20):6361-6370.
26. Frenkiel-Krispin D, et al. (2004) Nucleoid restructuring in stationary-state bacteria. *Mol Microbiol* 51(2):395-405.
27. Kavita Algu VSCC, Ravinder S. Dhami, Dallas A. K. Duncan (2007) Dps confers protection of DNA sequence integrity in UV-irradiated *Escherichia coli*. *Journal of Experimental Microbiology and Immunology (JEMI)* 11:60-65.
28. Grant RA, Filman DJ, Finkel SE, Kolter R, & Hogle JM (1998) The crystal structure of Dps, a ferritin homolog that binds and protects DNA. *Nat Struct Biol* 5(4):294-303.
29. Ceci P, et al. (2004) DNA condensation and self-aggregation of *Escherichia coli* Dps are coupled phenomena related to the properties of the N-terminus. *Nucleic Acids Res* 32(19):5935-5944.
30. Xiao B, Johnson RC, & Marko JF (2010) Modulation of HU-DNA interactions by salt concentration and applied force. *Nucleic Acids Res* 38(18):6176-6185.
31. Xiao BT, Zhang HY, Johnson RC, & Marko JF (2011) Force-driven unbinding of proteins HU and Fis from DNA quantified using a thermodynamic Maxwell relation. *Nucleic Acids Res* 39(13):5568-5577.

Chapter 2

In vitro single-molecule techniques: from technology to biology



2.1 Introduction

Starting from the last decade of the nineteenth century, *in vitro* measurements have been used to perform procedures in a controlled environment outside of a living organism. These measurements have provided valuable knowledge about the structure and function of biological systems. However, further understanding of them required deeper knowledges in physics and chemistry of biologically important molecules that build the cell and interact with each other. Only by measuring microscopic forces of interactions between the individual molecules and detecting molecular intermediates, we can provide additional information about thermodynamics and kinetics of biomolecular processes. This information could not be obtained via traditional bulk assays. Therefore, the possibility of manipulating individual molecules inspired the scientist and has eventually become a major research topic in modern biophysics.

The great progress made in molecular biology and biochemistry in twentieth century afforded the resolution for the direct observation of interaction between individual molecules. Nowadays, we are able to build complex scientific instruments of high resolution and manipulate molecules one at a time, making it possible to ask and answer entirely new types of biological questions. Therefore, these novel techniques have been applied more and more frequently to study various DNA-binding proteins (1-4).

What makes long DNA short? How does the Dps protein compact DNA molecule? What are the kinetic features of Dps binding to DNA? In fact, the answers to these questions can be found if the interaction between isolated DNA and Dps molecules is studied at the single-molecule level. This chapter offers a detailed description of the experiments carried out utilizing two single-molecule techniques: fluorescence microscopy and magnetic-tweezers. These experiments for the first time were developed specifically to allow thorough study of the dynamic process of DNA compaction by Dps.

In this chapter we describe the experimental techniques and methods that were used in the research. **Section 2.2** provides DNA isolation and Dps

purification protocols together with the chemical modification protocols on DNA and Dps molecules designed practically for the single-molecule measurements. The activity of the Dps protein after performed modifications was validated with control experiments that presented in the **section 2.3**. Sample preparations, special experimental procedures and details of setup configurations are described in the **sections 2.4**. Concluding remarks are represented in **section 2.5**.

2.2 Preparing DNA and Dps for interaction

Both single-molecule assays used in this research, fluorescent microscopy and magnetic tweezers, required additional chemical modifications on isolated molecules in order to make them suitable for the experiments. Here, we provide the protocols for DNA plasmids isolation and Dps protein purification. Subsequently, we describe the methodology of modifications on DNA and wild type Dps protein specifically designed for the measurements with single-molecule techniques.

2.2.1 DNA isolation and labeling

A 20.6 kb DNA was isolated from *E.coli* cells carrying the pSupercos lambda 1,2 plasmid (kindly provided by S. Hage from TU Delft, the Netherlands) by midiprep (Qiagen). The construct was made by digestion of the plasmid with XhoI (New England Biolabs) and fill-in of the 5'-overhang by the Klenow fragment of DNA polymerase I with dCTP, dGTP, dTTP and Biotin-labelled-dATP (Invitrogen/Life Technologies). Further, the plasmid was digested with NotI-HF (New England Biolabs). To create the handle, a 1200 bp fragment was amplified by PCR from pBluescript Sk+ (Stratagene/ Agilent Technologies, Inc, Santa Clara, CA) in the presence of Digoxigenin-11-dUTP (Roche Diagnostics) using forward primer GACCGAGATAGGGTTGAGTG and reversed primer CAGGGTCGGAACAGGAGAGC. This fragment was digested with NotI-HF (New England Biolabs), ligated to the NotI-HF-digested 20.6 kbp fragment and gel-purified. The construct was made by Theo van Laar (TU Delft, the Netherlands). The biotin and digoxigenin labels provided the DNA binding to the surface of the flow cell at one or to the magnetic particles at another end,

depending on experimental setup requirements (**Fig.1A**). For DNA labeling an intercalating dye was used at ratio about 1 molecule of YOYO-1 (Thermo Fisher Scientific) per 200 bp of DNA (**Fig.1B**).

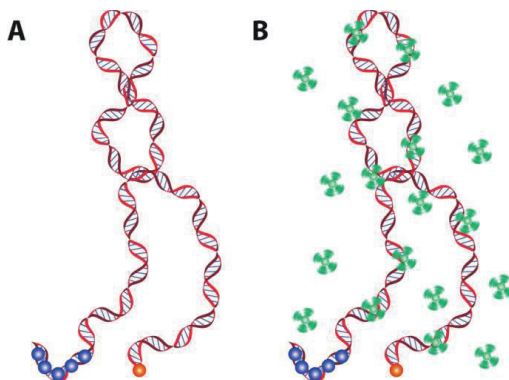


Fig.1. DNA construct and labeling. (A) Cartoon of the DNA construct with digoxigenin handle (blue circles) at one end and single biotin molecule (orange circle) at another end designed for the magnetic tweezers assay. (B) Cartoon of the DNA construct with a digoxigenin handle (blue) at one end and a single biotin molecule (orange circle) at another end designed for the fluorescent assay. The construct is labeled with intercalating fluorescent dye YOYO-1 (green stars).

2.2.2 Dps purification and labeling

Dps monomers have a molecular mass of 19 kDa and assemble into a dodecameric shell (**Fig.2**) (5). We expressed and purified wild-type Dps protein from *E. coli* BL21(DE3) cells carrying the pET17b-dps plasmid (6). This plasmid was designed for high expression of proteins under the T7 promotor. Cells were grown at 37°C with shaking at 250 rpm O.D.₆₀₀ 0.4-0.6. The production of Dps was induced by addition of 0.3 mM IPTG. After the cells were disrupted with a French press, Dps protein was precipitated with ammonium sulfate from cell lysates that were passed through a DEAE Sepharose CL-6B column (GE Healthcare) equilibrated with 50 mM HEPES-KOH, 100 mM NaCl, pH 7.3. Further buffer exchange to 50 mM HEPES-KOH, 0.1 mM EDTA, pH 7.3 using a PD-10 column, lowered the ionic strength. Sample was loaded onto SP-Sepharose column (GE Healthcare), and Dps was eluted with a 0 mM to 1 M NaCl gradient followed by buffer exchange with 50 mM

Hepes-KOH, 100 mM NaCl, pH 7.3. The monomer concentration of purified Dps sample was determined by measuring the absorbance at 280 nm, using a molar extinction coefficient of $15470 \text{ M}^{-1} \text{ cm}^{-1}$ (6).

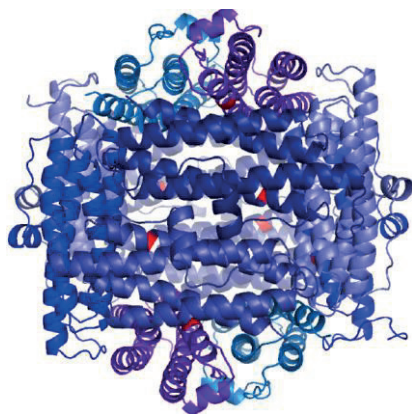


Fig.2. Dps spherical dodecamer T79C. Fluorescent dye is attached to a cysteine residue (*red*) at position 79 (T79C) facing a 4-5 nm internal cavity of Dps. The crystal structure of the Dps dodecamer has been solved by Grant R.A. et al (5).

For Dps labeling, plasmid encoding the *dps* gene pLysS pET17b *dps* 2-1 was modified to insert a cysteine at position 79 (T79C) (**Fig.2**), then expressed and purified as described for wild-type Dps. Cy5 Maleimide (GE Healthcare) was incubated at room temperature for 45 min with Dps monomers at a molar ratio of 1:15 Dps monomer to dye in a buffer of 50 mM Hepes-KOH, 400 mM NaCl, 10% glycerol, 5 M GdmCl, pH 7.3. Labeled Dps was subsequently diluted 5x with unlabeled Dps. Then, the sample was dialyzed against 50 mM Hepes-KOH, 100 mM NaCl, pH7.3, resulting in a labelling efficiency of ~10% (~1 dye per Dps dodecamer).

2.3 Activity of Dps on DNA molecule tested in bulk experiments

The chemical modifications performed on isolated DNA and Dps molecules made them suitable for the single-molecule experiments. All of them were designed with an aim of introducing as little distortion in the interaction

between DNA and Dps as possible. Even though, such modifications might still affect activity, properties and functions of the molecules of interest. Here we present control experiments that were carried out in bulk in order to validate activity of Dps protein on DNA molecule after each step of introducing a modification.

Activity of Dps protein is defined as its ability to bind and compact DNA. Therefore, before we started the major experiments at single-molecule level, we determined the base condition suitable for all future measurements. A gel shift assay is a straightforward way to quantify the binding affinity of Dps protein for DNA in bulk. Different amounts of Dps monomers were incubated with 2.5 nM of 331 bp DNA in 100 mM NaCl, 50 mM Hepes-KOH pH 7.3, allowing binding for 30 min. Directly after incubation, Dps-DNA complexes were loaded and ran on an agarose gel. For the visualization of the DNA bands, the agarose gels were washed in SYBR Gold (Thermo Fisher Scientific) for 30 min and directly scanned with Typhoon Trio (GE Healthcare). The amount of bound DNA was monitored by the fluorescence at the position on the agarose gel corresponding to non-bound DNA (**Fig.3A,C**). Through comparison to a reference DNA sample incubated without Dps, the bound DNA fraction was determined, calibrated from 0 to 100% and fit with a Hill equation (7) (**Fig.3B,D**).

First, using the gel shift assay we probed binding affinity of wild type Dps protein for DNA molecules labeled with YOYO-1 at different ratios of dye per DNA base pairs (**Fig.3A**). We showed that the ratio of 1 dye molecule per more than 100 base pairs of DNA has a minor effect on binding affinity of Dps for DNA (**Fig.3B**).

Second, using the gel shift assay we probed binding affinity of T79C Dps mutant, labeled T79C Dps mutant (dye:monomer 1:12) for non-labeled and labeled with YOYO-1 DNA molecules (dye:bp 1:100) (**Fig.5C**). We showed that each step of inducing a modification to the molecules slightly reduced the binding affinity of Dps for DNA. (**Fig.3D**).

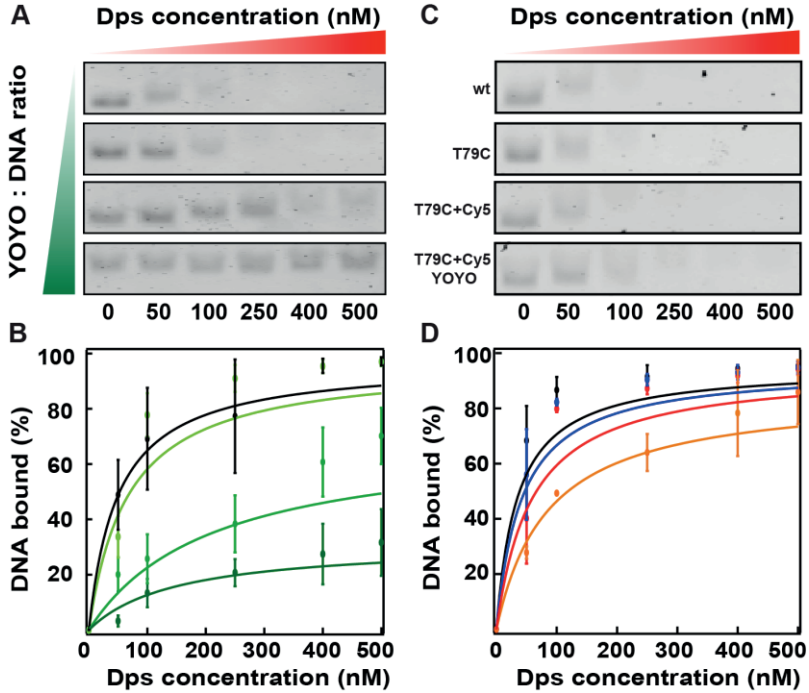


Fig.3. Binding affinity of Dps for DNA tested with DNA gel shift assay and fit to Hill equation. **(A)** Different amounts of Dps were incubated with YOYO-1 labeled DNA molecules and run on an agarose gel. The fluorescent signal on the agarose gel (*lines*) corresponds to non-bound DNA. From the top to bottom the ratio of YOYO-1 molecules to DNA base pairs equals: non-labeled, 1:100, 1:20, and 1:10. **(B)** The fraction of Dps-bound DNA (*circles; mean, SE*) were fit with a Hill equation (*lines*) and the effective dissociation constant for each dye:bp ratio was determined: non-labeled ($K_D = 50$ nM, *black*), 1:100 ($K_D = 67$ nM, *light green*), 1:20 ($K_D = 150$ nM, *green*), and 1:10 ($K_D = 210$ nM, *dark green*). **(C)** Different amounts of wild type Dps and Dps mutant T79C were incubated with DNA and ran on an agarose gel. The fluorescence signal on the agarose gel (*lines*) corresponds to non-bound DNA. From top to bottom: wild type Dps, T79C Dps, T79C Dps labeled with Cy5 incubated with non-labeled DNA, and T79C Dps labeled with Cy5 (dye:monomer 1:12) incubated with YOYO-1 labeled DNA molecules at ratio (dye:bp 1:100). **(D)** The amounts of bound DNA (*circles; mean, SE*) were fit with a Hill equation (*lines*) and the effective dissociation constant was determined: wild type Dps ($K_D = 35$ nM, *black*), T79C Dps ($K_D = 42$ nM, *blue*), T79C Dps labeled with Cy5 ($K_D = 59$ nM, *red*), T79C Dps labeled with Cy5 and incubated with YOYO-1 labeled DNA ($K_D = 85$ nM, *orange*).

Lastly, we checked if labelling of Dps affected the binding affinity of Dps for DNA with magnetic-tweezers assay (see section 2.5.3 for the details) in a buffer of 100 mM NaCl, 50 mM Hepes-KOH pH 7.3 (**Fig.4**). The DNA force-extension curve measured in the presence of 2 μ M wild type Dps almost completely overlapped with the force-extension curve measured at the same concentration of labelled T79C Dps mutant. This result demonstrates that neither generated point mutation in Dps monomers nor Dps labelling, do not influence Dps affinity for DNA.

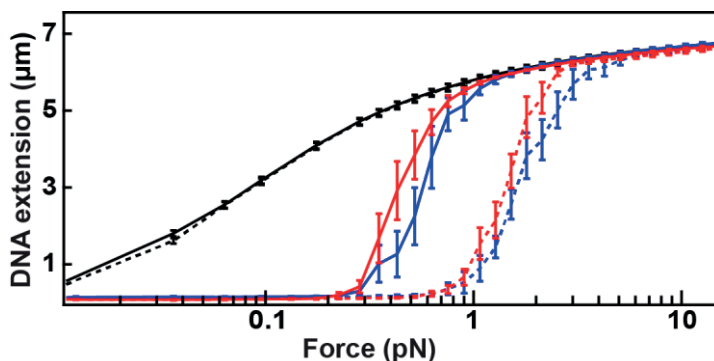


Fig.4. Binding affinity of fluorescently labeled Dps mutant T79C for DNA tested with magnetic tweezers. Decreasing and increasing force records are represented by solid and dashed lines respectively. Force-extension curves recorded in the presence of 2 μ M Dps mutant T79C (red) are compared to force-extension curves recorded with 2 μ M wild type Dps (blue). The DNA force-extension curve without Dps (black) is shown. Each curve is generated from the mean of 5 to 10 molecules and the bars correspond to standard errors in the mean.

Therefore, all performed control experiments validated activity of the labeled Dps protein, as it still remained able to bind labeled DNA and compact it sufficiently for further investigation. To make the binding of Dps even more efficient, we have chosen lower salt condition than used for tests described above and performed most of the experiments in the reaction buffer containing 50 mM NaCl, 50 mM Hepes-KOH pH 7.3 unless noted otherwise.

2.4 Sample preparation and experimental configuration

The glass surfaces of the microfluidic chambers used for *in vitro* measurements were cleaned and functionalized prior to all experiments. Here the cleaning and functionalization protocols are provided. The attachment protocols of individual DNA molecules to the glass surfaces described accordingly to the fluorescence and magnetic tweezers assays. Specific strategy of surface passivation was developed in order to reduce the nonspecific binding of Dps protein. Lastly, sample preparation, experimental procedures and setups configurations are described.

2.4.1 Preparation of glass slides and coverslips for fluorescent measurements.

Cleaning procedure and functionalization of the glass slides and coverslips were performed in the Kavli Nanolab Delft research facility in two steps. First, the microscope glass slides (Thermo Fisher Scientific) and coverslips (VWR) were loaded into the teflon holder. The holder was placed into the glass beaker filled with a pure nitric acid HNO_3 (Sigma Aldrich) and sonicated for 20 min. After sonication the slides and coverslips were thoroughly rinsed with MiliQ water and dried with a nitrogen pistol. Second, plasma cleaning was used to remove left organic or mineral oil residues and activate chemical bonds on the glass surfaces for further functionalization. The glass surfaces of the slides and coverslips were functionalized by incubating them for 20 min in 1.5% APTES, 94% methanol and 4.5% acetic acid (Sigma Aldrich). All the actions above should be taken in the fume hood (except of plasma cleaning).

Further, the slides and coverslips were coated with a mixture of mPEG and biotin-PEG at ration 3:1 (5K, Laysan Bio) diluted in 2 ml of 100 mM sodium bicarbonate buffer (Sigma Aldrich) and incubated overnight in a high humidity. Subsequently, a second layer of 10x diluted MS(PEG)4 (Methyl-PEG-NHS-Ester Reagent, Thermo Fisher Scientific) was introduced overnight in order to improve surface quality from the nonspecific binding of proteins.

After all the preparation steps the slides and coverslips were thoroughly rinsed with MiliQ water and dried with a nitrogen pistol.

2.4.2 Fluorescence assay: imaging Dps binding to DNA

We developed a novel fluorescence assay to directly visualize the process of Dps-DNA complex formation at the single-molecule level without applied tension. Linear DNA molecules were attached to the surface of a flow cell and were labeled with YOYO-1 (**Fig.5, green stars**). To induce DNA compaction, a reaction buffer with Dps labeled with Cy5 (**Fig.5, red stars**) was added.

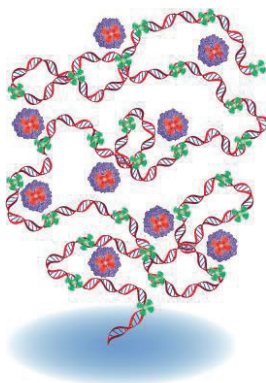


Fig.5. Cartoon of the fluorescent assay showing an immobilized DNA molecule labeled with YOYO-1 (*green stars*) and diffusing Dps dodecamers labeled with Cy5 (*red stars*).

All experiments were carried out in the flow cells assembled by hand from microscope slides (Thermo Fisher Scientific) and coverslips (VWR) with double-sided sticky tape spacers. To reduce the nonspecific binding of Dps protein, the surfaces of the flow cells were passivated with blocking aid solution (Invitrogen) for 1 hour followed by 0.2 mg/ml streptavidin coating (Sigma Aldrich) for 3 min. Unbound streptavidin was washed with 100 μ l of buffer T50 (10 mM Tris-HCl pH 8.0, 50 mM NaCl). 100 μ l of the DNA molecules (150 pg/ μ l) were injected into the flow cell and attached to the surface via the biotin-streptavidin linker, leaving the remaining DNA end unbound. Further, T50 buffer was substituted with reaction buffer containing 50 mM NaCl, 50 mM Hepes-KOH pH 7.3 and intercalating dye YOYO-1 (Thermo Fisher

Scientific) for DNA visualization at molar ratio less than 100:1 respectively. After injection of a given concentration of Cy5 labelled T79C Dps mutant in reaction buffer (50 mM NaCl, 50 mM Hepes-KOH pH 7.3 unless noted otherwise) into the flow cell, the process of DNA compaction was immediately recorded. To prevent bleaching all the buffers used during the imaging contained scavenger system: 10% glucose, glucose oxidase (0.3 µg/ul), catalase (40 ng/ul), and 2mM trolox (Sigma Aldrich).

Single-molecule fluorescence measurements were performed on a total internal reflection fluorescence microscope (IX81, Olympus). Cy5 and YOYO-1 molecules were excited using 640 nm and 488 nm lasers, respectively (CMR-LAS-640-100-D, CMR-LAS-488-150, Olympus). Fluorescence signals of Cy5 and YOYO-1 were collected through an oil immersion objective (U Apochromat 150X TIRF, NA 1.45, Olympus) by exciting the sample with two lasers simultaneously in epi (488 nm) and TIRF (640 nm) modes.

A series of images with 100 ms exposure time were recorded at 1 Hz using dual EMCCD cameras (iXon 3 897, Andor Technology) with a TuCam adapter. The image series was read using custom-made Matlab (MathWorks) software. After a linear drift correction, the Cy5 and YOYO-1 signals were co-localized by summing intensities over all frames and finding the linear transformation between spot locations of Dps and DNA. Individual spots were selected and cropped (ROI of 30x30 pixels). For each ROI the positions of the center of mass of DNA fluorescence and the maximum fluorescence intensities of Dps were extracted. Fluctuations in the DNA center of mass between frames were calculated. For measurements of DNA collapse, records were time-shifted so that the collapse occurred at $t=0$, and a 5-point median filter was applied to the DNA fluctuation data. Records were then averaged over many molecules.

2.4.3 Magnetic tweezers assay: controlling DNA compaction by Dps with force

We made use of a magnetic tweezer instrument (8-10) that allowed us to modulate the force applied to individual DNA molecules in the presence of Dps (**Fig.6**). We developed a protocol for probing Dps-DNA complexes for the

assembly and disassembly, which consisted of applying a slowly decreasing force (from 15 to 0.01 pN over >40 min) followed by a slowly increasing force (from 0.01 to 15 pN over >40 min). The choice of this experimental timescale was based on the characteristic timescales of bead fluctuations at each applied force that define the minimum measurement time for a desired statistical accuracy (8).

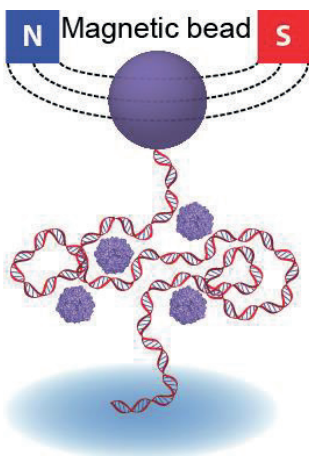


Fig.6. Cartoon of the magnetic tweezers assay showing a DNA molecule attached by one end to a microscope coverslip and by the other end to a magnetic bead. A pair of small permanent magnets controls the magnetic field.

The magnetic tweezers apparatus used in this study has been described previously (8-10). Briefly, light transmitted through the sample was collected by an oil-immersion objective (CFI Plan 50XH, Nikon) and projected onto a 12-Mpixels CMOS camera (12M Falcon2, Teledyne Dalsa). The images were acquired at a frequency of 25 Hz. The magnetic field was generated by a pair of horizontally aligned permanent neodymium-iron-boron magnets (SuperMagnet) separated by a distance of 1 mm, vertically translated by a motorized stage (M-126.PD2, Physik Instrumente) above the flow cell. Images, collected by the camera, were processed in real-time to create records of the bead positions in Cartesian coordinates with a custom written software in C++, CUDA and LabView (National Instruments) (10). The forces experienced

by the DNA tethers have previously been calibrated using a custom routine (8, 9).

The sample preparation used in this study has been described in detail elsewhere (8-12). In short, the DNA molecules were mixed and incubated for 2 min with 20 μ l streptavidin-coated superparamagnetic beads with a diameter of 2.89 μ m (M270 Dynabeads, Invitrogen/Life Technologies) at room temperature in Tris buffer (10 mM Tris-HCl pH 8.0, 150 mM NaCl, 1 mM EDTA, 0.01% Triton X-100). The mixture was then incubated for 30 min in flow cell coated with anti-digoxigenin (0.5mg/ml) (Roche Diagnostics) and overnight passivated with BSA (10 mg/ml) (New England Biolabs). Non-tethered beads were removed by flushing the flow cell with 5 ml Tris buffer. Tris buffer was then replaced with reaction buffer containing 50 mM NaCl, 50 mM Hepes-KOH pH 7.3 and 0.1 mg/ml BSA unless noted otherwise. After a careful screening of beads tethered by multiple DNA molecules using magnet rotation-extension records, we acquired a full DNA force-extension cycle by changing the vertical position of the magnet and applying a force ramp down (from 15 to 0.01 pN) followed by a force ramp up (from 0.01 to 15 pN). The force-extension relationship of DNA was measured and fit to the worm-like chain model (persistence length $L_p = 43.4$ nm, contour length $L_c = 6.97$ μ m) (13). Further, we injected a reaction buffer containing a given concentration of wild-type Dps protein. During the buffer solution exchange, the force applied to the beads was maintained at 15 pN to prevent DNA compaction by the Dps. Reagents used in the buffers were purchased from Sigma Aldrich (hepes, sodium chloride, magnesium chloride) and Promega (PEG 8000).

2.5 Conclusions

The molecules of interest for this study Dps and DNA were specifically modified to be able to be manipulated with two powerful single-molecule techniques: fluorescent microscopy and magnetic-tweezers. The activity of the protein Dps was validated with bulk experiments and the most suitable condition for future experiments was determined. All these adjustments made it possible to test easily wide range of different conditions by simply varying

few parameters (i.e. buffer conditions, Dps concentration or force) one by one and explore the process of Dps binding to DNA and Dps-DNA complex formation at the single-molecule level in real time.

References

1. Xiao B, Johnson RC, & Marko JF (2010) Modulation of HU-DNA interactions by salt concentration and applied force. *Nucleic Acids Res* 38(18):6176-6185.
2. Xiao BT, Zhang HY, Johnson RC, & Marko JF (2011) Force-driven unbinding of proteins HU and Fis from DNA quantified using a thermodynamic Maxwell relation. *Nucleic Acids Res* 39(13):5568-5577.
3. Skoko D, et al. (2006) Mechanism of chromosome compaction and looping by the *Escherichia coli* nucleoid protein Fis. *J Mol Biol* 364(4):777-798.
4. Luo Y, North JA, & Poirier MG (2014) Single molecule fluorescence methodologies for investigating transcription factor binding kinetics to nucleosomes and DNA. *Methods* 70(2-3):108-118.
5. Grant RA, Filman DJ, Finkel SE, Kolter R, & Hogle JM (1998) The crystal structure of Dps, a ferritin homolog that binds and protects DNA. *Nat Struct Biol* 5(4):294-303.
6. Karas VO, Westerlaken I, & Meyer AS (2013) Application of an in vitro DNA protection assay to visualize stress mediation properties of the Dps protein. *J Vis Exp* (75):e50390.
7. Barcroft J & Hill AV (1910) The nature of oxyhaemoglobin, with a note on its molecular weight. *J Physiol-London* 39(6):411-428.
8. Yu Z, et al. (2014) A force calibration standard for magnetic tweezers. *Review of scientific instruments* 85(12):123114.
9. Velthuis AJWT, Kerssemakers JWJ, Lipfert J, & Dekker NH (2010) Quantitative Guidelines for Force Calibration through Spectral Analysis of Magnetic Tweezers Data. *Biophys J* 99(4):1292-1302.
10. Cnossen JP, Dulin D, & Dekker NH (2014) An optimized software framework for real-time, high-throughput tracking of spherical beads. *Review of Scientific Instruments* 85(10):103712
11. Janissen R, et al. (2014) Invincible DNA tethers: covalent DNA anchoring for enhanced temporal and force stability in magnetic tweezers experiments. *Nucleic Acids Res* 42(18):e137.
12. Dulin D, et al. (2015) Elongation-Competent Pauses Govern the Fidelity of a Viral RNA-Dependent RNA Polymerase. *Cell Rep* 10(6):983-992.
13. Bustamante C, Marko JF, Siggia ED, & Smith S (1994) Entropic Elasticity of Lambda-Phage DNA. *Science* 265(5178):1599-1600.

Chapter 3

Cooperativity and hysteresis combined in Ising model



3.1 Introduction

Cooperativity has been a fundamental concept in the understanding of biological systems for over one hundred years. Nature uses cooperative interactions to accelerate or enhance specific processes. For instance, ecosystems like flocks of birds or a hive of bees act cooperatively in order to achieve the common task more efficiently. On a smaller scale of biological systems cooperativity has “as much variety as it has ubiquity” (1). It is important in cell-cell signaling (2) and collective survival strategies of cancer cells (3). If we zoom in even more, to the microscopic level, we find evidence that individual molecules can also act cooperatively.

In the cooperative process of a molecule binding, the first binding event, increases the affinity of the second binding event providing highly efficient and rapid reaction. Therefore, a minimal concentration shift of binding molecules causes a much bigger change in activity of the system, thus it reacts very sensitively.

Cooperative interactions enable and regulate function of the system at many different levels of organization, from single-molecules to multimolecular complexes. The higher the complexity of the cooperation among the interacting molecules, the more difficult it is for understanding, but the greater the role of cooperativity in regulating system's functions. Without cooperativity many biological events would be simply imposed by physical and chemical laws when considered at the molecular level. Therefore, cooperativity allows the system to circumvent the energetic, spatial and temporal constraints and become essential for its functioning (4).

The classic example of cooperativity at molecular level is the binding of oxygen to hemoglobin (5). Later, cooperativity was found as a key emergent property in protein folding (6), transcriptional control (7, 8) and replication of many eukaryotic viruses (9, 10). The self-interacting properties of Dps protein have also been reported previously (11, 12) and binding mechanism of Dps to DNA was characterized as cooperative (13, 14). However, despite of this curious fact and the ability of Dps to protect DNA, no efforts have been done in

order to probe these mechanisms further and expand it neither experimentally nor theoretically.

In this chapter, we describe a cooperative process of DNA compaction by Dps that was probed by fluorescent microscopy and magnetic-tweezers (see Chapter 2). In **section 3.2**, real-time *in vitro* records demonstrate a highly cooperative nature of Dps binding to DNA characterized by an abrupt collapse of the DNA extension, even under applied tension. Surprisingly, following Dps-mediated DNA compaction and subsequent decompaction, we discovered that the Dps-DNA complex exhibits reproducible hysteresis (i.e. memorization) between these two processes. In **section 3.3**, we provide a detailed view of Dps binding transitions and show that the observed hysteresis is extremely stable over timescales ranging from seconds to hours. Unfortunately, the presence of cooperative hysteresis makes it very difficult to fit the system to the standard models of cooperativity (discussed in **section 3.4**). Instead, in **section 3.5**, we theoretically develop a simple way to explain and fit an observed hysteresis by modifying an Ising model from ferromagnetism specifically for our Dps-DNA system. Concluding remarks are represented in **section 3.6**.

3.2 Dps induces DNA compaction via cooperative binding

3.2.1 Bulk experimental data of Dps binding to DNA

The transition into a compact Dps-DNA state has been reported to be cooperative (14) based on bulk gel shift assays, where Dps forms a massive complex with DNA and shows few intermediate sized complexes (15). In our gel shift assay different amounts of Dps monomers were incubated with 40 pM of 20.6 kbp DNA in the reaction buffer (50 mM NaCl, 50 mM Hepes-KOH pH 7.3). Directly after incubation, Dps-DNA complexes were loaded and ran on an agarose gel (**Fig.1A**). Through comparison to a reference DNA sample incubated without Dps, the bound DNA fraction was determined, calibrated from 0 to 100% and fit with a Hill equation (16) (**Fig.1B**). The effective

dissociation constant $K_D = 0.63 \pm 0.17 \mu\text{M}$ and cooperativity coefficient $N_H = 2.20 \pm 0.53$ ($N=2$, mean, SD) were determined.

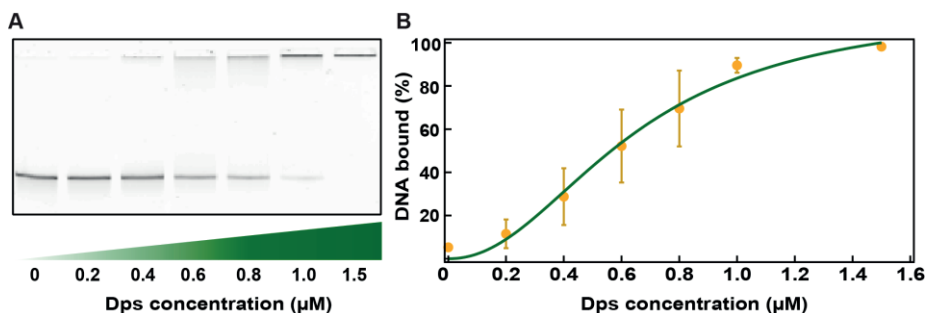


Fig.1. Dps-DNA gel shift assay fit to Hill equation. (A) The amounts of bound DNA monitored by the fluorescence at the position on the agarose gel corresponding to non-bound DNA (lines) and bound DNA (wells). (B) The amounts of bound DNA (yellow circles) fit with a Hill equation (green line).

3.2.2 Tracking Dps binding to DNA under fluorescent microscope

Applying a single-molecule fluorescent microscopy (see chapter 2) we were able to observe in real time Dps binding to DNA and subsequent transition from long, flexible DNA molecule into compact Dps-DNA complex without applied tension (**Fig.2**).

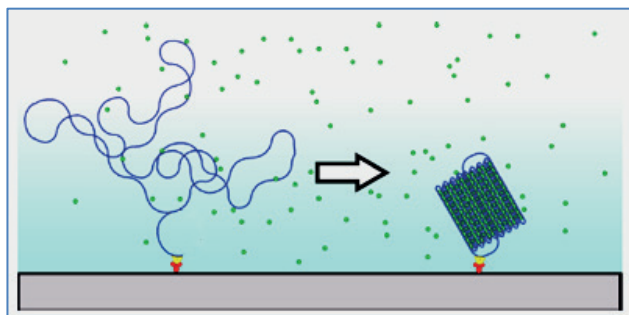


Fig.2. Cartoon of the fluorescent assay showing an immobilized on a glass slide 20.6 kbp DNA molecule (blue) and diffusing Dps dodecamers (green circles). After binding of Dps to DNA a compact Dps-DNA structure forms.

To induce DNA compaction, a reaction buffer with 0.2 μM Dps labeled with Cy5 was added into the flow cell. We followed the binding of Dps proteins onto DNA molecules over tens of minutes using fluorescent microscopy. We deliberately chose low Dps concentrations, as determined by a bulk gel shift assay (**Fig.1**), to slow down the arrival of Dps and resolve the process of DNA compaction in real time. A sequence of frames for one such DNA molecule is shown in **Fig.3**. Initially, the DNA molecule moved freely around the attachment point (0-720 s). The binding of Dps to the DNA (frames 900-1620 s) resulted in a rapid co-localization of these two molecules into a smaller, immobile Dps-DNA complex.

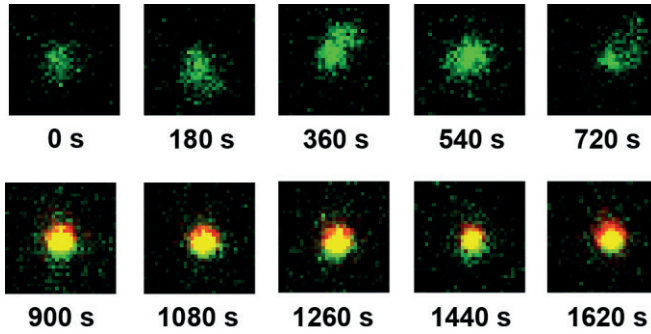


Fig.3. DNA compaction by Dps observed with fluorescence in real time. Fluorescent images show a single DNA molecule (*green*) in the presence of 0.2 μM Dps undergoing thermal fluctuations in position (0-720 s). When Dps (*red*) binds to the DNA, these molecules co-localize into an immobile Dps-DNA complex (900-1620 s).

To further analyze the transition of the DNA into an immobile state, we measured the fluctuations of the DNA between frames and the maximum fluorescence intensity of the Dps in individual complexes (**Fig.4A,B**). We attribute the uniform increase in Dps brightness and abrupt decrease in DNA fluctuations to the binding of labeled Dps and compaction of the DNA. For each DNA molecule, a variable delay of 200 ± 230 s (**mean \pm SD**) was observed prior to the collapse (**Fig.4A**). In order to visualize the compaction at high time resolution, we aligned the traces at the time point of collapse (**Fig.4C**). An averaged trace for all observed molecules after alignment shows that the majority of Dps molecules bound in a 6 s window, with DNA

compaction occurring nearly simultaneously (**Fig.4D**). This sharp transition suggests a highly cooperative binding mechanism and a tight coupling between Dps binding and the compaction of DNA.

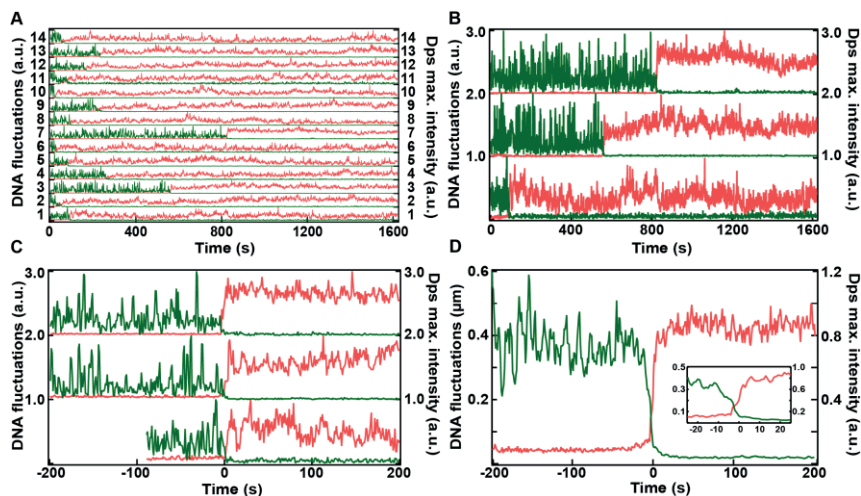


Fig.4. DNA compaction by Dps observed with fluorescence in real time. (A) Fourteen normalized traces show the abrupt decrease in DNA positional fluctuations (green) and the sharp increase in the maximum fluorescent intensity of Dps (red) that define DNA compaction. Compaction occurred rapidly after a variable wait time of 200 ± 230 s (mean \pm SD). (B) Three normalized example traces (1,3,7 from A) show the abrupt decrease in DNA positional fluctuations between frames (green) and the sharp increase in the maximum fluorescence intensity of Dps (red) that define DNA compaction. (C) Three normalized example traces (1,3,7 from A) time-shifted so that collapse in DNA positional fluctuations (green) and increase in Dps maximum fluorescence intensities (red) occurred at t=0 (trace 1,3,7 from Fig.A). (D) Individual records ($N=14$), time-shifted so that collapse occurred at t=0, were averaged. The majority of Dps (red) bound and compacted the DNA (green) in less than 6 s. All measurements are done in the reaction buffer: 50 mM NaCl, 50 mM Hepes-KOH pH 7.3.

Taking into account the labelling efficiency of Dps, the concentrations used, and the penetration depth of the evanescent wave we calculated the fluorescent intensity per Dps dodecamer in the flow cell. Based on this calculation we estimated that 4 ± 1.6 (mean \pm SD) Dps dodecamers are bound per 1 kbp of DNA. These data, combined with our bulk gel shift assays (**Fig.1**), demonstrate that Dps indeed binds DNA in a very cooperative manner.

3.3 Reversible DNA compaction by Dps reveals hysteresis

3.3.1 Past concentrations of Dps influences DNA compaction

Once Dps has assembled on DNA, we were interested in observing the dissociation of the Dps-DNA complex as well. Therefore, we analyzed five consecutive records of DNA molecules in the absence and presence of Dps under different ionic conditions. We first measured the average fluctuations of DNA molecules in the absence of Dps (**Fig.5A, DNA only**). Addition of 0.75 μM Dps in the reaction buffer resulted in a compaction of the DNA molecules (i.e. decreased fluctuations) and an abrupt increase of the peak Dps fluorescence (**Fig.5A, Flush in Dps**). Upon flushing out Dps with 5 volumes of reaction buffer, we observed that the Dps intensity decreased but the Dps-DNA complexes remained a static structure (**Fig.5A, Flush out Dps**). Addition of 3 mM MgCl_2 to the buffer weakened the affinity of Dps for DNA. This caused a sharp drop in Dps fluorescence intensity and a marked increase in DNA fluctuations, indicating the release of Dps from the DNA (**Fig.5A, Flush in MgCl_2**). Subsequent removal of the MgCl_2 by flushing in 5 additional volumes of the reaction buffer demonstrated that the DNA remained flexible (**Fig.5A, Flush out MgCl_2**). Dps could also be released by raising the pH to 8.1 (**Fig.5B**).

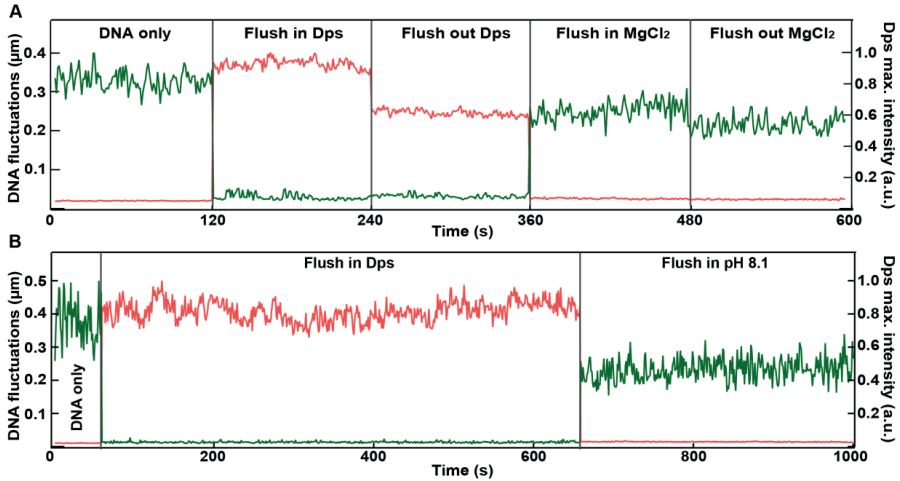


Fig.5. DNA compaction by Dps observed with fluorescence in real time. (A) Average DNA fluctuations (green) and Dps intensity (red) of a set of molecules ($N=53$) were recorded under five successive buffer conditions: DNA in reaction buffer without Dps (0-120 s); addition of $0.75 \mu\text{M}$ Dps (120-240 s); flushing with reaction buffer to remove Dps (240-360 s); addition of 3mM MgCl_2 (360-480 s); flushing with reaction buffer to remove MgCl_2 (480-600 s). (B) Average DNA fluctuations (green) and Dps intensity (red) of a set of molecules ($N=23$) were recorded under three successive buffer conditions: DNA in reaction buffer (pH 7.3) without Dps (0-60 s); addition of $0.45 \mu\text{M}$ Dps (60-660 s); flushing with reaction buffer at pH 8.1 to remove Dps (660-1000 s). All measurements are done in the reaction buffer: 50 mM NaCl, 50 mM Hepes-KOH pH 7.3.

In these experiments, preformed Dps-DNA complexes remain stable even after we lowered the Dps concentration to below $0.075 \mu\text{M}$ by flushing the flow cell with buffer (this estimation was made based on the reduction in the fluorescent background). In contrast, initially bare DNA did not collapse even after the addition of up to $0.1 \mu\text{M}$ Dps. These experiments establish that DNA compaction by Dps is history-dependent rather than being a simple function of the current Dps concentration. In order to probe this hysteresis in more detail, we decided to use tension to perturb Dps-DNA assemblies.

3.3.2 Tracking Dps binding to DNA under tension

We developed a magnetic tweezer assay (17-19) that allowed us to modulate the force applied to individual DNA molecules in the presence of Dps (see

chapter 2). By applying a slowly decreasing force (from 15 to 0.01 pN over >40 min) followed by a slowly increasing force (from 0.01 to 15 pN over >40 min) we probed for hysteresis between the assembly and disassembly of Dps-DNA complexes.

First, we consider the force-extension curves when the force is gradually decreased. For DNA molecules without Dps in the solution (**black solid line, Fig.6A**), the measured extension at a given force can be approximated by the worm-like chain (WLC) model (**grey solid line, Fig.6A**) (20). In contrast, for DNA molecules in the presence of 8 μM Dps, a sharp compaction of the DNA is observed. Three example DNA traces (**blue, orange and green solid lines, Fig.6A**) show an abrupt collapse that occurs at a critical force $F_1 \approx 1.5$ pN. This result demonstrates that the Dps molecules can perform work on the magnetic bead to compact DNA.

Next, we consider the force-extension curves when the force is gradually increased. Without Dps present, the DNA extension (**black dashed line, Fig.6A**) again follows the WLC model (**grey solid line, Fig.6A**), as expected. However, in the presence of Dps the DNA extension follows a new pattern. The DNA molecules remain highly compacted until they reach a second critical force $F_2 \approx 6$ pN. At this force, the Dps-DNA complex breaks, and the DNA returns to the extension predicted by the WLC model (**blue, orange and green dashed lines, Fig.6A**). We define F_1 and F_2 as the forces that correspond to a DNA extension of half the contour length ($\sim 3.5 \mu\text{m}$) (**Fig.6A**).

Plotting the average of multiple force-extension curves ($N=11$), we observe that the DNA extension is roughly homogeneous among the different molecules with a reproducible hysteresis (**Fig.6B**). The variation of F_1 and F_2 between molecules ranged from 10-25% in different conditions. We attribute this variation to experimental uncertainty, since the actual force applied to beads across the field of view can vary by as much as 24% (21).

To illustrate this behavior further, we replot the decreasing force-extension data from **Fig.6A** near the critical force F_1 as a function of time (**Fig.6C**). We observe that around F_1 the DNA extension decreased monotonically until it reached a fully compact state. We also replot the increasing force-extension

data near the second critical force F_2 (**Fig.6D**). The DNA extension exhibits an almost monotonic increase in extension until it is fully extended, indicating that DNA compaction is reversible. This result demonstrates that outside of the critical force region, the DNA extension converges to a single equilibrium fairly rapidly, with hundreds of Dps dodecamers binding or releasing over the course of 200-300 s. We also note that on short timescales (~ 1 s) the DNA extension can exhibit small (<50 nm) reversible fluctuations (**Fig.6C inset and 6D inset**).

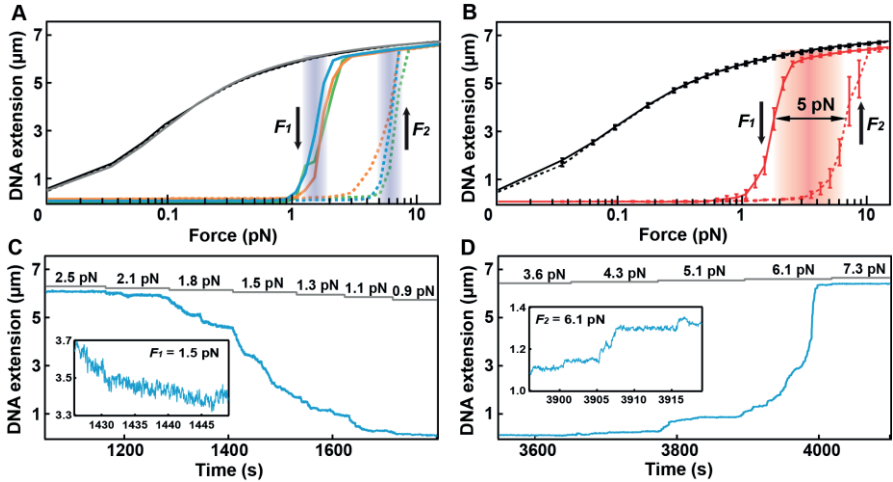


Fig.6. DNA force-extension cycles show hysteresis. (A) Force-extension curves for a DNA tether without Dps (black) and for three DNA tethers in the presence of 8 μM Dps (blue, orange, green). The force-extension relationship of bare DNA is compared to the worm-like chain model (grey) (20). Solid lines correspond to decreasing force and dashed lines to increasing force. (B) Average DNA extension ($N=11$, mean, SEM) in the absence (black) and presence (red) of 8 μM Dps. Solid lines correspond to decreasing force and dashed lines to increasing force. Hysteresis is demonstrated by the 5 pN gap between critical forces F_1 and F_2 . (C) Extension of a single DNA molecule (blue) plotted as a function of time as the force is decreased near the critical force F_1 . Reversible fluctuations in the extension were limited to less than 100 nm (inset). The WLC extension (grey) is also plotted at each force. (D) Extension of the same DNA molecule plotted while the force is increased near the critical force F_2 . The WLC extension (grey) is also plotted at each force. All measurements are done in the reaction buffer: 50 mM NaCl, 50 mM Hepes-KOH pH 7.3.

3.3.3 Hysteresis remains extremely stable over hour-long timescales

Interestingly, in every recorded force-extension cycle in the presence of Dps we observe a distinct hysteresis in the DNA extension, with $F_2 > F_1$. In principle, this hysteresis could be a function of the pulling rate, as has been observed for RNA hairpins and other two-state systems near equilibrium (22, 23). However, additional experiments demonstrate that the observed hysteresis in our system is nearly independent of the pulling rate. First, we repeated the measurement with both a four-fold increase and a two-fold decrease in the pulling rate and observed essentially no change in the amount of hysteresis defined by F_1 and F_2 (**Fig.7A**). Second, we performed experiments where we shifted from a high force ($F_{high} > F_2$) directly to an intermediate force ($F_1 < F_{int} < F_2$) and did not observe collapse of the DNA extension over the course of 30 min. Similarly, when we shifted from a low force ($F_{low} < F_1$) directly to the same intermediate force, the DNA remained stably collapsed for 30 min (**Fig.7B**). Therefore, we conclude that under identical conditions the Dps-DNA complex can be trapped in one of two stable conformations, even on time scales exceeding the doubling time of bacteria.

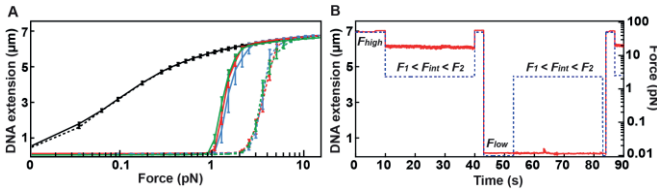


Fig.7. Hysteresis in Dps-DNA complexes is stable over many timescales. (A) Repeated force-extension cycles with 2μM Dps present in the reaction buffer were performed at the standard pulling rate (95 min, red) as well as a 4x increase (24 min, green) or 2x decrease (190 min, blue) in the pulling rate. Force-extension curves are compared to the force-extension curve without Dps (black). Each curve is generated from the mean of 10 to 20 molecules and the bars correspond to standard errors in the mean. (B) A time-trace of DNA extension was measured with 8 μM Dps (red) present in the reaction buffer. First, the force (dashed blue) was raised above the critical range ($F_{high} > F_2$), then brought to an intermediate force ($F_1 < F_{int} < F_2$) for 30 minutes. Second, the force was lowered below the critical range ($F_{low} < F_1$), then brought back to an intermediate force ($F_1 < F_{int} < F_2$) for 30 minutes. All measurements are done in the reaction buffer: 50 mM NaCl, 50 mM Hepes-KOH pH 7.3.

3.3.4 Artificial point mutation changes Dps cooperativity

Previously, it has been proposed that interactions between Dps and DNA is at major role attributed to the N-terminal lysine residues (24). Therefore, in the Dps-DNA complex, DNA is assumed to be threaded to interact with the lysine residues (15). In accordance with this hypothesis, based on agarose gel mobility assays (14), those members of the Dps family that do not possess a positively charged N-terminus do not appear to bind DNA.

In this section using magnetic tweezers assay we tested the binding affinity for DNA of Dps mutant K5A with replaced lysine residue in the disordered N-terminal tail (kindly provided by Dr. Anne Meyer). The K5A Dps mutant almost could not bind to DNA under the tension even at concentration twice higher than the wild type Dps (**Fig.8**). However, it still showed a small hysteresis loop, indicating presence of very weak Dps-Dps and Dps-DNA interactions. It is intriguing in this connection that an artificial point mutation changes Dps from cooperative to non-cooperative and non-binding protein. Therefore, cooperativity in a multisubunit Dps protein depends on a delicate balance between many forces and configurations. It seems likely that a small change in amino acid mutation can change the cooperative and binding properties of the whole enzyme. Then, it becomes apparent how difficult it is for evolution to obtain the appropriate cooperativity.

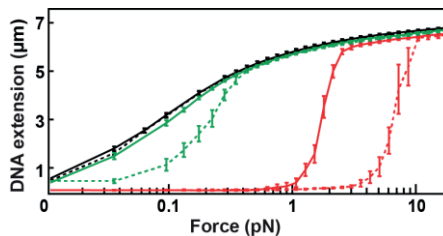


Fig.8. Point mutation in the N-terminal Dps tail changes affinity for DNA binding. Force-extension curves for DNA without Dps (*black*), in the presence of 8 μM Dps (*red*) and in the presence of 16 μM K5A Dps mutant (*green*). Solid lines correspond to decreasing force and dashed lines to increasing force. All measurements are done in the reaction buffer: 50 mM NaCl, 50 mM Hepes-KOH pH 7.3.

3.4 Standard cooperativity models

We considered several possible models to explain the history-dependent mechanism of complex formation between a long, flexible polymer and a large number of self-interacting proteins. Cooperative binding is frequently modeled with the Hill equation (16). The resulting binding curve shows a characteristic sigmoidal shape that transitions sharply from low to high occupancy compared to a non-cooperative binding curve. The Hill equation has been used to characterize Dps binding previously (14), and it reasonably fits our own bulk experimental data (**Fig.1**). However, the Hill model assumes that the system can equilibrate to find the global minimum in free energy, which precludes hysteresis. Other standard models of cooperativity, such as the Koshland-Némethy-Filmer (KNF) (25), Monod-Wyman-Changeux (MWC) (26), and Conformational Spread (CS) (27) models, can potentially be used to model hysteresis, although almost all of the current literature focuses on their predictions at equilibrium. To better understand how a system can be trapped in non-equilibrium states, we turned to the Ising model of ferromagnetism.

3.5 A modified Ising model of cooperativity predicts hysteresis

3.5.1 Ising model from ferromagnetism

The Ising model was first developed to describe interactions between magnetic dipoles that are arranged in an array and placed in an external magnetic field, giving rise to ferromagnetism (28). A ferromagnet is a lattice of coupled dipoles that without an applied magnetic field are equally likely to point up or down (**Fig.9A**). In the Ising model, a cooperative interaction between adjacent dipoles lowers each of their energies when both dipoles have the same sign (29). Consequently, neighboring dipoles tend to align with each other (**Fig.9B**). The magnetic properties of the array of dipoles depend on the magnitude of the coupling energy. Below the critical value, the array is paramagnetic (i.e. magnetized only when an external field is applied). Close to the critical point, the propagation of nearest-neighbor interactions causes one

dipole to influence other dipoles over a wide range. Then, a weak external field gives rise to a strong magnetization. Above a critical value, a high proportion of the dipoles all point in the same direction, and the array is ferromagnetic (i.e. magnetized without an external field is applied). Therefore, in an idealized ferromagnetic system, a strong magnetic field can lock the dipoles predominantly in a single orientation, creating a stable magnetization that persists when the magnetic field is reduced.

Inspired by the Ising model of ferromagnetism, we make an analogy to our observations that Dps can lock DNA in a stable complex that persists when the concentration of Dps is reduced or the tension is increased. Below we describe hysteresis in Dps-DNA system as a consequence of cooperative binding in the limit of large complexes. Further, we provide a method to relate the amount of hysteresis to the strength of the neighboring interactions between bound proteins and DNA.

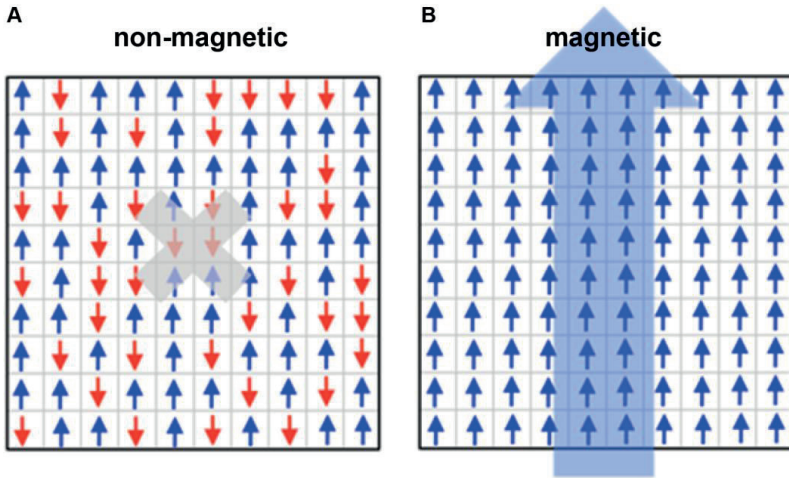


Fig.9. Representation of the Ising model of a ferromagnet. (A) Without magnetic field an isolated magnetic dipole is equally likely to point up (blue) or down (red). **(B)** When magnetic field is applied, the dipole tends to point in the direction of the field in order to have a lower energy.

3.5.2 Derivation of the binding probability of non-cooperative ligands

To apply the Ising model to Dps-DNA interactions we posit that a DNA strand contains N Dps binding sites that can exist in an empty or occupied state. Further, we assume that Dps binding and DNA compaction at the binding site are tightly coupled, so that the number of occupied binding sites is proportional to the DNA extension. The protein at concentration $[A]$ in solution quickly adopts a thermodynamic equilibrium with the binding sites. The free energy of an unoccupied site is set as zero. First, we derive a standard equation for the probability of a binding site being occupied in order to simplify comparisons between the models. Second, we extend this derivation to understand the effects of the Hill model (16) and Ising model (28)

The probability of binding on DNA is a function of the protein concentration $[A]$. This enters into the expression for the chemical potential of the system $\mu = \mu_0 + k_B T \ln([A]/c_0)$, where μ_0 is the potential at a standard concentration c_0 , k_B is Boltzmann's constant, and T is the absolute temperature. The binding of one Dps protein reduces the free energy of the system by $\Delta G = (\epsilon - \mu)$, where ϵ accounts for interactions between the protein and DNA. The probabilities of a given site having a bound protein depends on the free energy difference between the two states:

$$P = \frac{e^{-\Delta G/k_B T}}{1 + e^{-\Delta G/k_B T}} = \frac{e^{-(\epsilon - \mu)/k_B T}}{1 + e^{-(\epsilon - \mu)/k_B T}} = \frac{1}{1 + e^{(\epsilon - \mu)/k_B T}}. \quad [1]$$

The dissociation constant K_D (the protein concentration at which the binding probability is 0.5) can be defined by the concentration where $(\epsilon - \mu)=0$:

$$K_D = c_0 e^{(\epsilon - \mu_0)/k_B T}. \quad [2]$$

The non-cooperative probability of occupying a binding site on a DNA molecule is then given by the familiar equation:

$$P_{NC} = \frac{1}{1 + \frac{K_D}{[A]}}. \quad [3]$$

The binding curve for non-cooperative protein binding to DNA has a hyperbolic shape (**Fig.10**).

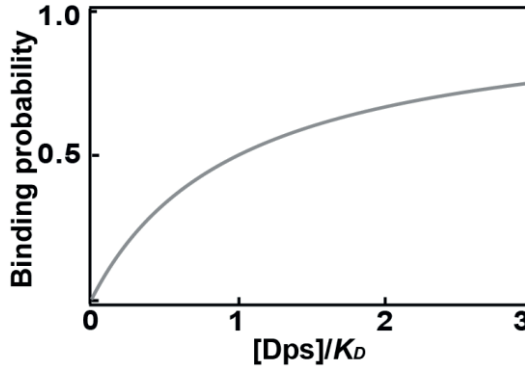


Fig.10. The binding probability of non-cooperative ligands. The probability of occupying a binding site on DNA as a function of the effective Dps concentration in the case of no cooperativity (grey) (eq.[3]).

3.5.3 Derivation of the binding probability using the Hill model

The binding curve of a cooperative protein has a sigmoidal shape (**Fig.11**). This curve can be obtained if we assume that groups of N_H binding sites can only alternate between a completely occupied or completely unoccupied state. The probability of N_H binding sites being occupied is then given by the equation:

$$P_{Hill} = \frac{e^{-N_H \Delta G / k_B T}}{1 + e^{-N_H \Delta G / k_B T}} = \frac{1}{1 + \left(\frac{K_D}{[A]}\right)^{N_H}}, \quad [4]$$

where N_H is the Hill coefficient.

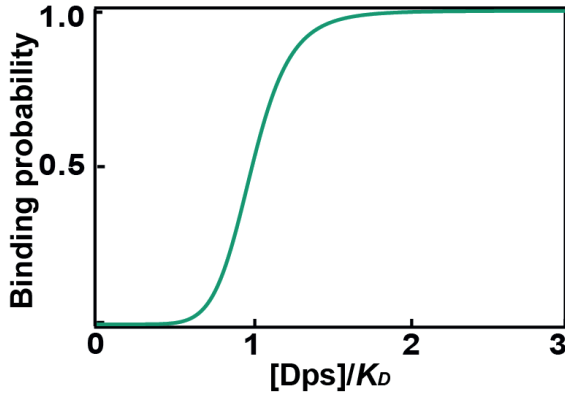


Fig.11. The binding probability using the Hill model. The probability of occupying a binding site on DNA as a function of the effective Dps concentration in the case of Hill cooperativity ($N_H = 8$, green) (eq.[4]).

3.5.4 Derivation of the binding probability using the Ising model

The Ising model considers the contribution of an additional energy term – the interaction energy between nearest neighbor proteins – in the overall binding probability (**Fig.12**). We model these interactions by adding the cooperativity parameter $I = \frac{\gamma}{k_B T}$, where γ is the energy constant that characterizes sum of the neighboring interactions between Dps proteins in the completely compact state. The free energy difference between the occupied and unoccupied states for a given binding site depends on how many neighboring sites are already occupied by Dps. When no neighboring sites are occupied by Dps, the free energy difference is identical to the non-cooperative case, or $\Delta G/k_B T = \ln\left(\frac{K_D}{[A]}\right)$. If all the neighboring sites are occupied then the free energy difference shifts to become $\Delta G/k_B T = \ln\left(\frac{K_D}{[A]}\right) - I$. When an intermediate number of neighboring sites are occupied, the free energy difference adopts a value intermediate between these two limits.

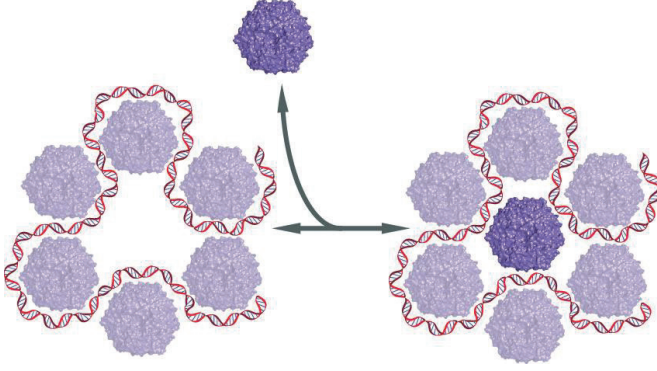


Fig.12. Dps dodecamer interacting with neighboring Dps and DNA. A cartoon representation of the possible interactions between a Dps dodecamer (*dark purple*), and neighboring Dps (*light purple*), and DNA.

In principle, we could enumerate all the possible intermediate binding configurations to calculate the binding probability. However, this would require us to make numerous assumptions about what intermediate states can exist and what energy to assign each of these states. Instead of this approach, we choose to make the model more general and more computationally tractable by using the mean field approximation (30). In the mean-field approximation, we assume the shift in energy is proportional to the probability that the neighboring sites are occupied so that $\Delta G/k_B T = \ln\left(\frac{K_D}{[A]}\right) - P \cdot I$. The probability of Dps occupying a given binding site on the DNA would then be given by equation (Fig.13, red):

$$P_{Ising} = \frac{e^{-\Delta G/k_B T}}{1 + e^{-\Delta G/k_B T}} = \frac{1}{1 + \frac{K_D}{[A]} e^{-PI}}. \quad [5]$$

Note that the Hill model predicts that the higher the cooperativity (i.e. as N_H increases), the more steeply $P([A])$ increases near the concentration $[A] = K_D$. As N_H approaches ∞ (i.e. as cooperativity is maximized) the curve has a vertical slope near $[A] = K_D$. In the Ising model, the concentration where half the binding sites are occupied occurs not at K_D but at $[A] = K_D e^{-I/2} = K_{eff}$. In contrast to the Hill model, the slope of the curve can be positive, infinite, or

negative depending on the strength of the parameter I . When the slope is negative, the system exhibits hysteresis.

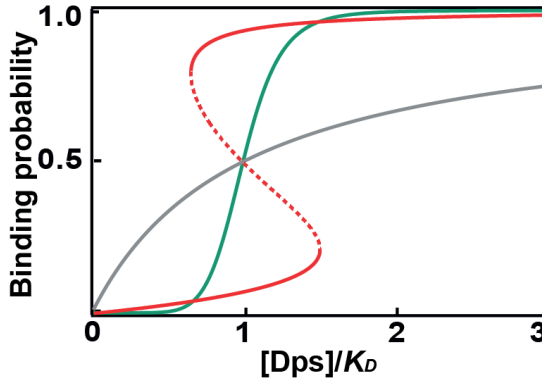


Fig.13. An Ising model describes hysteresis in DNA compaction by Dps. The probability of occupying a binding site on DNA as a function of the effective Dps concentration in the case of: no cooperativity (*grey*) (eq.[3]), Hill cooperativity ($N_H = 8$, *green*) (eq.[4]) and Ising cooperativity ($I = 8$, *red*) (eq.[5]).

In a non-cooperative binding curve ($I = 0$), only one local equilibrium exists and P smoothly increases as a function of Dps concentration (**Fig.13, grey**). In a cooperative binding curve where the system can globally equilibrate, we expect P to increase sharply as a function of concentration (**Fig.13, green**). However, our Ising model predicts that there is a region where three solutions for P exist for a given Dps concentration (**Fig.13, red**). In this region, the high and low solutions represent stable local equilibria of the system. The intermediate solution is an unstable equilibrium that corresponds to the energetic barrier between the stable solutions. Therefore, our model predicts that Dps-DNA complexes can exist in either a highly compact or extended conformation depending on the path used to bring the concentration into the critical region.

3.5.5 The effects of DNA tension in each binding model

Next, we consider the effects of a changing tension applied to the Dps-DNA complex. When DNA is under tension we must include another parameter

when calculating the binding probability: the applied force F . To model the effects of force, we set the size of each binding site to 60 base pairs of DNA based on titration measurements of Dps dodecamers (15). Compaction of these 60 base pairs by Dps decreases the DNA extension by a distance $\delta(F)$ that is dependent on the force applied to the DNA molecule. At a given force F , this translates to a reduction in the DNA extension of $\delta(F)$ which we calculate using the worm-like chain model (WLC) (20):

$$X(F) = X_{WLC}(F)(1 - P(F)), \quad [6]$$

where X_{WLC} is the DNA extension predicted by the WLC, $X(F)$ is the reduced DNA extension.

If now we define the constant $D = \frac{\delta(F)}{k_B T}$, the free energy change upon binding Dps shifts by an additional amount $\Delta G/k_B T = \ln\left(\frac{K_D}{[A]}\right) - P \cdot I + FD$. Then, the probability of occupying a binding site is a function of the protein concentration and applied force. For each model, the probabilities become (Fig.14):

$$P_{NC} = \frac{1}{1 + \frac{K_D}{[A]} e^{FD}}, \quad [7]$$

$$P_{Hill} = \frac{1}{1 + \left(\frac{K_D}{[A]}\right)^{N_H} e^{FD}}, \quad [8]$$

$$P([A], F) = \frac{1}{1 + \frac{K_D}{[A]} e^{FD - PI}} = \frac{1}{1 + \frac{K_{eff}}{[A]} e^{FD - (P - 0.5)I}}. \quad [9]$$

Here, $K_{eff} = K_D e^{-I/2}$ is the Dps concentration associated with 50% occupancy of the binding sites at zero force. The dimensionless parameter I is analogous to the Hill coefficient and serves a measure of cooperativity, while K_D describes how tightly Dps binds bare DNA. Summarizing, all of these parameters give rise to a transcendental equation for the probability P of a given DNA binding site being occupied by a Dps dodecamer [eq.9] that defines our model.

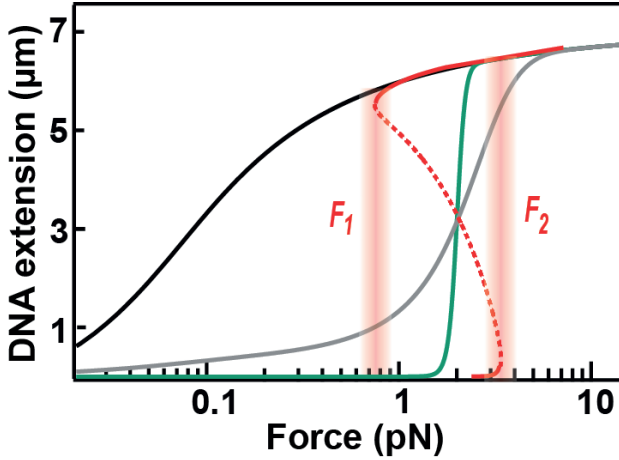


Fig.14. Force-extension curves measure cooperativity and hysteresis. Force-extension predictions for Dps binding on DNA with different cooperative models: no binding (*black*), non-cooperative (*grey*) (eq.[6], [7]), Hill (*green*) (eq.[6],[8]) and Ising (*red*) (eq.[6], [9]). Sharp transitions can occur at critical forces F_1 (compaction) and F_2 (decompaction).

Similar to the case without tension, our model predicts the existence of two highly stable local equilibria and one unstable equilibrium within a critical range of forces between F_1 and F_2 . The path used to bring the DNA into the critical force range determines which equilibrium is adopted. Above F_2 the DNA has an extended conformation. As the force is decreased below F_2 , the DNA remains trapped at the extended local equilibrium. However, below F_1 no extended equilibrium exists. Therefore, when the force is then dropped below F_1 the Dps-DNA complex rapidly transitions to a compact conformation. Similarly, a compact DNA molecule suddenly transitions to an extended conformation only when the force is increased above F_2 . In terms of the global free energy calculations, critical forces F_1 and F_2 correspond to the forces where the energetic barrier between the stable equilibria vanishes.

3.5.6 Derivation of inflection points for Ising model

From eq.[9] we cannot write the probability P explicitly in terms of the force F . However, at each critical force F_1 and F_2 , a Dps dodecamer that binds DNA

performs a fixed amount of work $W = F \cdot \delta(F)$ that we can write as an explicit function of P :

$$\begin{aligned}\frac{K_D}{[A]} e^{\frac{W}{k_B T}} e^{-PI} &= \frac{1-P}{P} \\ e^{\frac{W}{k_B T}} &= \frac{1-P}{P} e^{PI} \frac{[A]}{K_D} \\ \frac{W}{k_B T} &= PI - \ln(P) + \ln(1-P) + \ln\left(\frac{[A]}{K_D}\right).\end{aligned}$$

If $P(W)$ contains inflection points (**Fig.14**), slope of $W(P)$ must go to zero at these points. Setting the slope of $W(P)$ to zero and solving for the inflection probabilities P_{inf} gives:

$$\begin{aligned}\frac{\partial\left(\frac{W}{k_B T}\right)}{\partial P} &= I - \frac{1}{P_{inf}} - \frac{1}{1-P_{inf}} = 0 \\ 0 &= IP_{inf}^2 - IP_{inf} + 1.\end{aligned}$$

Solving quadratic equation:

$$P_{inf} = \frac{1}{2} \pm \frac{\sqrt{1-\frac{4}{I}}}{2}. \quad [10]$$

The derivation for P_{inf} shows that the total energetic contribution of the nearest neighbor interactions around one Dps dodecamer must be greater than $I = 4$ in order to observe hysteresis. Below this value there are no real solutions for the inflection points.

Next, using the formula for $W(P)$ we can relate P_{inf} to the two corresponding critical forces F_1 and F_2 (**Fig.14**):

$$F_1 D = \left(\frac{1}{2} - \frac{\sqrt{1-\frac{4}{I}}}{2} \right) I - \ln \left(\frac{1 - \sqrt{1-\frac{4}{I}}}{1 + \sqrt{1-\frac{4}{I}}} \right) + \ln \left(\frac{[A]}{K_D} \right)$$

$$F_2 D = \left(\frac{1}{2} + \frac{\sqrt{1-\frac{4}{I}}}{2} \right) I - \ln \left(\frac{1 + \sqrt{1-\frac{4}{I}}}{1 - \sqrt{1-\frac{4}{I}}} \right) + \ln \left(\frac{[A]}{K_D} \right).$$

We define W_{diff} as the difference in work performed by Dps at the two critical forces F_1 and F_2 and show that it is a function of the parameter I :

$$\frac{W_{diff}}{k_B T} = F_2 D - F_1 D = I \sqrt{1 - \frac{4}{I}} - 2 \ln \left(\frac{1 + \sqrt{1-\frac{4}{I}}}{1 - \sqrt{1-\frac{4}{I}}} \right). \quad [11]$$

We see that W_{diff} depends only on the nearest neighbor interactions I and not on K_D . Therefore, W_{diff} can be used to quantify the strength of the hysteresis. Further, we expect that changes in Dps concentration should not affect work difference.

We can also define W_{ave} , the average of the work performed by Dps at the two critical forces F_1 and F_2 , and show that it is given by:

$$\frac{W_{ave}}{k_B T} = \frac{(F_1 \cdot D + F_2 \cdot D)}{2} = \frac{I}{2} + \ln \left(\frac{[A]}{K_D} \right) = \ln \left(\frac{[A]}{K_{eff}} \right). \quad [s12]$$

We see that W_{ave} depends on the nearest neighbor interactions I , Dps-DNA interactions K_D , and the Dps concentration $[A]$. A change in Dps concentration is predicted to cause a logarithmic increase in the average work.

3.6 Conclusions

We performed real-time *in vitro* measurements to study the biophysical properties of Dps-DNA complex formation at the single-molecule level. We find that a rate-limiting nucleation event stimulates the rapid incorporation of multiple Dps dodecamers on DNA, resulting in extensive compaction (**Fig.4**). Moreover, the degree of DNA compaction by Dps is influenced by past concentrations of Dps (**Fig.5**), i.e. the system exhibits hysteresis. By changing the tension applied to Dps-DNA complexes, we show that hysteresis is also observed in force-extension curves and can be characterized by the critical forces F_1 and F_2 , which define the onset of DNA compaction and decompaction, respectively (**Fig.6**). This hysteresis is nearly independent of the pulling rates

(**Fig.7A**). Instead, we find that within the range of forces between F_1 and F_2 the DNA is trapped in one of the two stable local equilibria, i.e. compact or extended (**Fig.7B**). These data, combined with bulk gel shift assays (**Fig.1**), demonstrate that Dps binds DNA cooperatively. Further, we successfully applied a modified Ising model to explain observed phenomenon of hysteresis in the complex Dps-DNA system.

We find that long-lived hysteresis arises naturally as a consequence of strong protein cooperativity in the limit of large complexes. This feature provides a useful mechanism for cells to adopt unique epigenetic states and is likely to be observed in other systems as well. For example, other proteins that condense DNA could exhibit similar dynamics, providing a new mechanism for epigenetic regulation. Alternately, replication of some eukaryotic viruses requires many copies of self-interacting proteins to assemble into large viral factories (9). Cooperative hysteresis could provide a useful gating mechanism to prevent premature assembly of these replication factories. More generally, any large protein complex could exhibit hysteresis in assembly, especially when a 2D or 3D lattice can be identified. This provides a framework for modeling other biological systems involving large assemblies of macromolecules.

References

1. Koshland DE, Jr. & Hamadani K (2002) Proteomics and models for enzyme cooperativity. *J Biol Chem* 277(49):46841-46844.
2. Kaizuka Y, Douglass AD, Varma R, Dustin ML, & Vale RD (2007) Mechanisms for segregating T cell receptor and adhesion molecules during immunological synapse formation in Jurkat T cells. *Proc Natl Acad Sci U S A* 104(51):20296-20301.
3. Ben-Jacob E, Coffey DS, & Levine H (2012) Bacterial survival strategies suggest rethinking cancer cooperativity. *Trends in microbiology* 20(9):403-410.
4. Whitty A (2008) Cooperativity and biological complexity. *Nat Chem Biol* 4(8):435-439.
5. Bohr C, Hasselbalch K, & Krogh A (1904) About a new biological relation of high importance that the blood carbonic acid tension exercises on its oxygen binding. *Skand Arch Physiol* 16:402-412.
6. Shank EA, Cecconi C, Dill JW, Marqusee S, & Bustamante C (2010) The folding cooperativity of a protein is controlled by its chain topology. *Nature* 465(7298):637-U134.
7. Courey AJ (2001) Cooperativity in transcriptional control. *Curr Biol* 11(7):R250-R252.

8. Narlikar GJ, Fan HY, & Kingston RE (2002) Cooperation between complexes that regulate chromatin structure and transcription. *Cell* 108(4):475-487.
9. de Castro IF, Volonte L, & Risco C (2013) Virus factories: biogenesis and structural design. *Cell Microbiol* 15(1):24-34.
10. den Boon JA, Diaz A, & Ahlquist P (2010) Cytoplasmic viral replication complexes. *Cell Host Microbe* 8(1):77-85.
11. Almiron M, Link AJ, Furlong D, & Kolter R (1992) A novel DNA-binding protein with regulatory and protective roles in starved *Escherichia coli*. *Genes & development* 6(12B):2646-2654.
12. Wolf SG, et al. (1999) DNA protection by stress-induced biocrystallization. *Nature* 400(6739):83-85.
13. Ganguly A, Rajdev P, Williams SM, & Chatterji D (2012) Nonspecific Interaction between DNA and Protein allows for Cooperativity: A Case Study with *Mycobacterium* DNA Binding Protein. *J Phys Chem B* 116(1):621-632.
14. Karas VO, Westerlaken I, & Meyer AS (2015) The DNA-Binding Protein from Starved Cells (Dps) Utilizes Dual Functions To Defend Cells against Multiple Stresses. *J Bacteriol* 197(19):3206-3215.
15. Ceci P, et al. (2004) DNA condensation and self-aggregation of *Escherichia coli* Dps are coupled phenomena related to the properties of the N-terminus. *Nucleic Acids Res* 32(19):5935-5944.
16. Barcroft J & Hill AV (1910) The nature of oxyhaemoglobin, with a note on its molecular weight. *J Physiol-London* 39(6):411-428.
17. Yu Z, et al. (2014) A force calibration standard for magnetic tweezers. *Review of scientific instruments* 85(12):123114.
18. Velthuis AJWT, Kerssemakers JWJ, Lipfert J, & Dekker NH (2010) Quantitative Guidelines for Force Calibration through Spectral Analysis of Magnetic Tweezers Data. *Biophys J* 99(4):1292-1302.
19. Cnossen JP, Dulin D, & Dekker NH (2014) An optimized software framework for real-time, high-throughput tracking of spherical beads. *Review of Scientific Instruments* 85(10):103712
20. Bustamante C, Marko JF, Siggia ED, & Smith S (1994) Entropic Elasticity of Lambda-Phage DNA. *Science* 265(5178):1599-1600.
21. De Vlaminck I, Henighan T, van Loenhout MT, Burnham DR, & Dekker C (2012) Magnetic forces and DNA mechanics in multiplexed magnetic tweezers. *PLoS One* 7(8):e41432.
22. Liphardt J, Onoa B, Smith SB, Tinoco I, & Bustamante C (2001) Reversible unfolding of single RNA molecules by mechanical force. *Science* 292(5517):733-737.
23. Collin D, et al. (2005) Verification of the Crooks fluctuation theorem and recovery of RNA folding free energies. *Nature* 437(7056):231-234.
24. Grant RA, Filman DJ, Finkel SE, Kolter R, & Hogle JM (1998) The crystal structure of Dps, a ferritin homolog that binds and protects DNA. *Nat Struct Biol* 5(4):294-303.

25. Koshland DE, Nemethy G, & Filmer D (1966) Comparison of Experimental Binding Data and Theoretical Models in Proteins Containing Subunits. *Biochemistry-U S A* 5(1):365-385.
26. Monod J, Wyman J, & Changeux JP (1965) On Nature of Allosteric Transitions - a Plausible Model. *J Mol Biol* 12(1):88-118.
27. Bray D & Duke T (2004) Conformational spread: the propagation of allosteric states in large multiprotein complexes. *Annu Rev Biophys Biomol Struct* 33:53-73.
28. Ising E (1925) Report on the theory of ferromagnetism. *Z Phys* 31:253-258.
29. Duke TA & Bray D (1999) Heightened sensitivity of a lattice of membrane receptors. *Proc Natl Acad Sci U S A* 96(18):10104-10108.
30. Tome T & de Oliveira MJ (1990) Dynamic phase transition in the kinetic Ising model under a time-dependent oscillating field. *Phys Rev A* 41(8):4251-4254.

Chapter 4

Kinetics of Dps binding to DNA



4.1 Introduction

Enzymes are biologically active proteins that speed up (catalyze) biochemical reactions in the cells. The properties of enzymes have been intensively studied for almost a century, starting with the demonstration of alcoholic fermentation as a chemical process (1). The overall regulation of cellular metabolism can also be understood from a chemical point of view. By studying the kinetic behavior of individual enzymes, we can gain insights into an enzyme's mechanism of action and its significance in the overall metabolic pattern. Further, these knowledges can be used in performing research, clinical diagnosis, food analysis and also serve as a prerequisite for the design of inhibitors (drugs) directed against a certain enzyme. Therefore, establishing enzyme kinetics is a first step towards our understanding of the chemistry of life.

In addition to enzymes, kinetic equations can be useful for studying the binding of macromolecules like proteins and DNA. Recent progress in experimental techniques, particularly at single-molecule level, makes it possible to collect information about the binding rates of proteins and their local dynamical activities. Here, fluorescent microscopy and magnetic-tweezers techniques that can provide these data become irreplaceable. Using these techniques, it is possible to measure microscopic forces of interactions between the molecules, characterize the kinetics of biomolecular association and detect structural intermediates. These experiments provide additional information about equilibrium and non-equilibrium thermodynamics and kinetics of biomolecular processes.

Little is understood about the intrinsic kinetic properties of Dps binding to DNA, since only static structures of Dps-DNA complexes have been documented and previous studies have focused on the equilibrium behavior (2, 3). However, characterization of Dps kinetics will shed a light on the role that this protein occupies in the metabolic processes of bacteria.

In the previous chapter we defined a key activity of Dps: its ability to bind to DNA, to self-interact (i.e. cooperativity) and to induce conformational changes

to the DNA. We established the phenomenon of hysteresis in the process of DNA compaction by Dps and derived a model to fit experimental data by modifying an Ising model. In this chapter we examine these processes from a kinetics perspective by following DNA compaction dynamics and tuning various factors that affect Dps activity.

Utilizing fluorescent assays, in **section 4.2**, we compare how different amounts of monovalent salt change the affinity of Dps for DNA. We find elevated ionic strengths greatly slow the arrival of Dps dodecamers to the DNA. Applying magnetic tweezers in **section 4.3**, we then measure the mechanical forces that characterize the interactions between Dps and DNA and test how tension applied to the DNA molecule modulates binding and dissociation rates of Dps. In order to understand phenomenon of hysteresis in the process of DNA compaction by Dps and why our model gives rise to it, in **section 4.4** we discuss hysteresis in a scope of kinetics by plotting global free energy diagram. Since hysteresis might also rise from several other models of cooperativity we show why our model is the most convenient for a Dps-DNA system by comparing energy diagrams for these models in **section 4.5**. Concluding remarks are represented in **section 4.6**.

4.2 Salt modulates cooperativity of Dps

Using our single-molecule fluorescence assay (chapter 2) we were able to observe Dps binding to DNA at two salt concentrations and the resultant transition from a long, flexible DNA molecule into a compact Dps-DNA complex. To induce DNA compaction, a reaction buffer with various concentrations of monovalent salt and labeled Dps was added into the flow cell. Initially, the DNA molecule moved freely around the attachment point. The binding of Dps to the DNA resulted in a co-localization of these two molecules and a smaller, immobile Dps-DNA complex. We measured the transition of the DNA into an immobile state by recording the fluctuations of the mean DNA position between frames and we measured the arrival of Dps by recording the maximum fluorescence intensity of the Dps signal in individual complexes. We note that active compaction was only observed in a very narrow range of Dps concentrations for each buffer condition. Lower

concentrations produced no observable compaction events and higher concentrations resulted in complete compaction during the buffer exchange.

Below we focus on the DNA compaction process recorded in high salt reaction buffer (1.5 μ M Dps, 70 mM NaCl, 50 mM Hepes-KOH pH 7.3). For each DNA molecule, a variable delay of 192 ± 169 s (mean \pm SD) was observed prior to a rapid collapse (Fig.1A). In order to visualize the compaction at high time resolution, we aligned the traces at the time point of collapse (Fig.1B). An averaged trace for all observed DNA molecules shows that the majority of Dps bound in a ~ 20 s window, with DNA compaction occurring concurrently (Fig.1C). We attribute the sharp increase in Dps intensity and the abrupt decrease in DNA fluctuations to the cooperative nature of Dps binding. Once the rapid binding phase was finished, little additional Dps bound to the complex. We followed the maximum fluorescence intensity of the preformed Dps-DNA complexes for 30 additional minutes and did not observe significant changes (data not shown).

This concurrent transition to compacted DNA is much slower at 70 mM NaCl in comparison with the transition observed at lower salt (0.2 μ M Dps, 50 mM NaCl). There Dps bound in a ~ 6 s window (Fig.1D). This is consistent with our previous estimates that high salt weakens Dps-DNA interactions as well as Dps-Dps interactions and lowers Dps cooperativity. Therefore, even with an elevated Dps concentration, increased salt makes the Dps binding mechanism slower. We also tried to measure Dps compaction at higher salt concentrations (80 mM), but at this ionic strength we could not observe compaction at the highest Dps concentrations we could test (2.5 μ M).

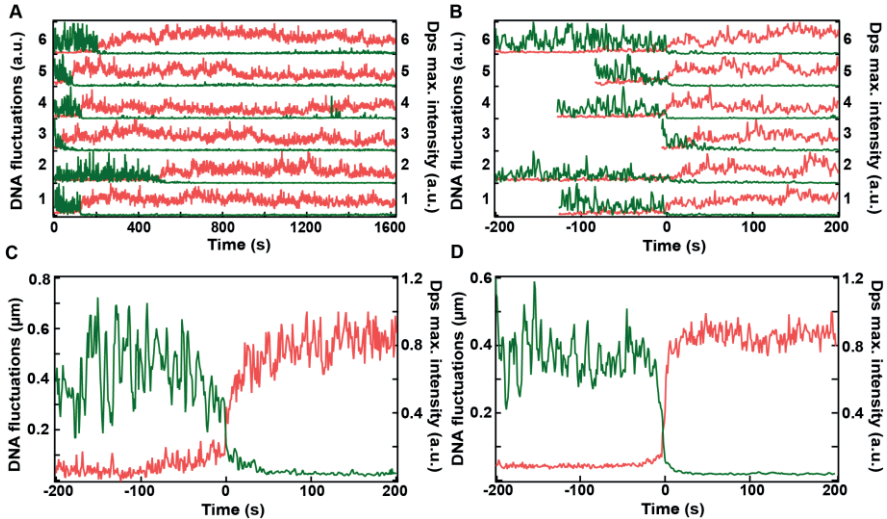


Fig.1. DNA compaction by Dps observed with fluorescence in real time. (A) Six normalized traces show the decrease in DNA positional fluctuations (*green*) and the increase in the maximum fluorescent intensity of Dps (*red*) that define DNA compaction. Compaction occurred rapidly after a variable wait time of 192 ± 169 s (mean \pm SD). (B) Six normalized example traces time-shifted so that collapse in DNA positional fluctuations (*green*) and increase in Dps maximum fluorescence intensities (*red*) occurred at $t=0$. (C) Individual records ($N=6$), time-shifted so that collapse occurred at $t=0$, were averaged. The majority of Dps (*red*) bound and compacted the DNA (*green*) in about 60 s. The measurements are done in the reaction buffer: 1.5 μ M Dps, 70 mM NaCl, 50 mM Hepes-KOH pH 7.3. (D) Individual records ($N=14$), time-shifted so that collapse occurred at $t=0$, were averaged. The majority of Dps (*red*) bound and compacted the DNA (*green*) in less than 6 s. The measurements are done in the reaction buffer: 0.2 μ M Dps, 50 mM NaCl, 50 mM Hepes-KOH pH 7.3.

Taking into account the labelling efficiency of Dps, the concentrations used, and the penetration depth of the evanescent wave we calculated the fluorescent intensity per Dps dodecamer in the flow cell. Based on this calculation we estimated that at 1.5 μ M Dps and 70mM NaCl, Dps dodecamers bound at 14 ± 7 (mean \pm SD) per 1 kbp of DNA. This estimate is 3.5-fold higher than the one made at 0.2 μ M Dps and 50 mM NaCl, where 4 ± 1.6 (mean \pm SD) Dps dodecamers are bound per 1 kbp of DNA. Therefore, at high salt more Dps molecules are needed in order to compact the same amount of DNA. Because Dps does not require a fixed stoichiometry to compact DNA, we conclude that

Dps-DNA complexes can exhibit heterogeneity over different buffer conditions.

4.3 Tension modulates the affinity of Dps for DNA

Previously, we established that tension offers a complimentary parameter to Dps concentration that can be used to modulate the compaction of DNA. Here we again turn to our magnetic tweezers assay (see chapter 2) in order to resolve the dynamics of DPS compaction in detail. In order to determine the critical forces associated with compaction and decompaction at 1 μM Dps, we recorded time-traces of DNA extension as the force was gradually lowered and then increased again (**Fig.2**). Having identified the critical forces F_1 and F_2 , we then focused on Dps-DNA dynamics near these forces.

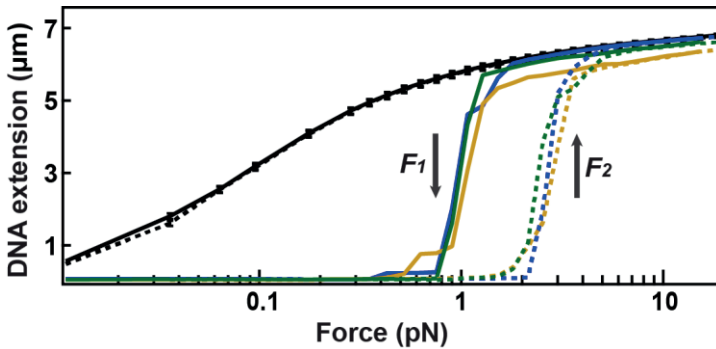


Fig.2. DNA force-extension cycle defines critical forces. Force-extension curves for a DNA without Dps (black) and for three DNA tethers in the presence of 1 μM Dps (blue, green and yellow). Solid lines correspond to decreasing force and dashed lines to increasing force.

We developed a new force-jump assay to follow compaction and decompaction. Using this assay, we have plotted time-traces for DNA compaction mediated by 1 μM Dps (**Fig.3A**) in a window of 2 min. Prior to applying the force of interest we stretch the DNA molecule to its full length at 40 pN to remove bound Dps. Next, we lower the force to the values where we expect to observe DNA compaction. We observe that around critical force $F_1 \approx 1$ pN the DNA extension undergoes a monotonic decrease until it reaches a fully compact conformation. However, we can clearly detect that full DNA

compaction by Dps occurs at different time point depending on applied force. The speed of wrapping changes noticeably even with 0.2 pN differences in tension. The lower the tension applied to the DNA molecule the faster Dps compacts it.

We also plot time-traces for the DNA decompaction process mediated by 1 μ M Dps on the same traces (**Fig.3B**) in a widow of 2 min. Prior to applying the force of interest we lower the tension to 0.01 pN to assure full DNA compaction. Next, we increase the force to the values where we expect to observe DNA decompaction. We show that around the critical force $F_2 \approx 3$ pN, the DNA extension exhibits an almost monotonic increase until it is fully stretched. Here, we can also clearly detect a dependency of the speed of Dps dissociation on the applied force. The higher the tension applied to the DNA molecule, the faster the Dps-DNA complex breaks apart.

These results demonstrate that outside of the critical force region, the DNA extension converges to a single equilibrium fairly rapidly, but slowly enough to observe the dynamics of the process. To completely condense the DNA hundreds of Dps dodecamers must bind or release DNA over a timescale of seconds to a few minutes. We also note that on short timescales (~ 1 s) the DNA extension can exhibit small (< 50 nm) reversible fluctuations, but the overall processes are nearly monotonic.

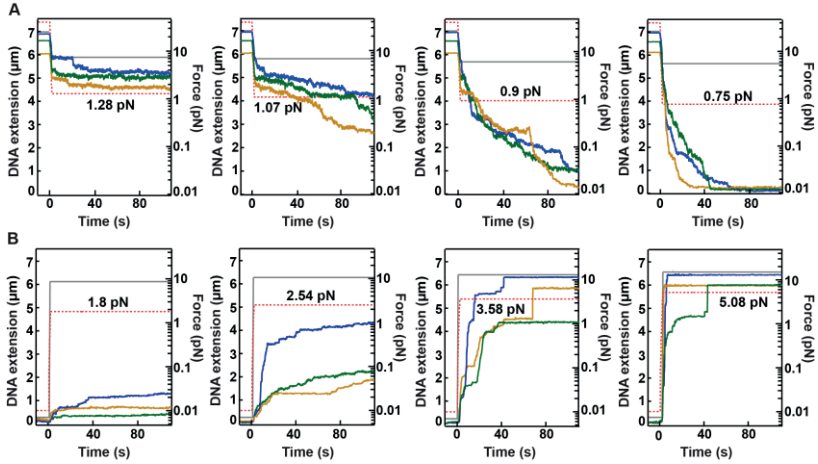


Fig.3. Force-jump experiments reveal dynamics of DNA compaction and decompaction. (A) Three DNA tethers (*blue, green and yellow*) undergo compaction as a function of time. Extension was recorded at constant tensions (*dashed line*) near the critical force F_1 (from left to right): 1.28 pN, 1.07 pN, 0.9 pN and 0.75 pN. Reversible fluctuations in the extension were limited to less than 100 nm. The WLC extension (*grey*) is also plotted at each force. **(B)** Three example DNA tethers initially in a fully compacted state (*blue, green and yellow*) undergo decompaction as a function of time. Extension was recorded at constant tensions (*dashed line*) near the critical force F_2 . The WLC extension (*grey*) is also plotted at each force. All measurements are done in the reaction buffer: 1 μ M Dps, 50 mM NaCl, 50 mM Hepes-KOH pH 7.3.

Having identified a narrow range of forces where we are able to detect the speed of DNA compaction and decompaction, we now examine how force influences the velocity. Further, we characterize these processes by calculating velocities for different Dps concentrations as a function of force (Fig.4).

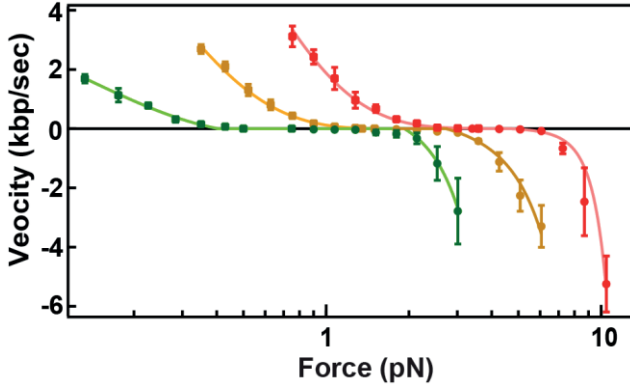


Fig.4. Velocity of DNA compaction and decompaction. Velocities (mean $N=15$, SE) are calculated as a function of force for different Dps concentrations: 0.5 μM Dps (green circles), 1 μM Dps (yellow circles) and 8 μM Dps (red circles). Velocity of decompaction are fit to eq.[1] (solid lines).

The velocity of DNA compaction can be fit with truncated exponential function:

$$V(F) = \max(V_0 e^{-FD} - V_{floor}, 0). \quad [1]$$

Here, V_0 is the velocity of compaction without applied force, F is the applied force, $D = \frac{\delta(F)}{k_B T}$ is the normalized change in DNA extension, and V_{floor} is the threshold. We assume that because the DNA starts in a fully compact or fully extended state, any net negative velocity will be measured as zero. The hysteresis of the Dps-DNA system creates a zero velocity plateau between the critical forces at each Dps concentration.

By fitting DNA compaction velocities with eq.[1] we can extract an average step size of wrapping characterized by $\delta(F)$ for different Dps concentrations: 29.4 ± 11.5 bp (0.5 μM Dps), 18.6 ± 1.2 bp (1 μM Dps) and 9.5 ± 0.5 bp (8 μM Dps). By fitting DNA decompaction velocities with eq.[1] we can extract an average step size of unwrapping characterized by $\delta(F)$ for different Dps concentrations: 4.4 ± 11.8 bp (0.5 μM Dps), 2.0 ± 0.8 bp (1 μM Dps) and 3.2 ± 0.4 bp (8 μM Dps). The weighted average of these distance parameters for wrapping and unwrapping were calculated as 37.5 bp and 8.4 bp respectively.

4.4 Kinetic interpretation of the hysteresis

4.4.1 Global free energy diagram for an Ising mechanism

In this section we develop our model further (see chapter 3), using the new information on the dynamics of the Dps-DNA system. Experimental results described above show that kinetics of Dps-induced compaction vary depending on ionic strength and tension applied to DNA. Ionic strength affects cooperativity by changing the interaction between neighboring Dps dodecamers and tension affects affinity of Dps for DNA. Moreover, we find that tension affects Dps association and dissociation rates differently, suggesting the transition state for individual Dps dodecamers lies close to the fully wrapped state. Ionic strength and tension also modulate two critical forces F_1 and F_2 that establish the amount of hysteresis. Therefore, hysteresis is a great part of Dps-DNA system's kinetics. Here we show why our model gives rise to the kinetic phenomenon of hysteresis and what role tension and ionic strength plays in this system. Below we derive an equation for the change in the global free energy of the system as a function of bound protein and the cooperativity parameter.

In chapter 3 we derived a transcendental equation for the probability P of a given DNA binding site being occupied by a Dps dodecamer that defines our model:

$$P([A], F) = \frac{1}{1 + \frac{K_D}{[A]} e^{FD - PI}} = \frac{1}{1 + \frac{K_{eff}}{[A]} e^{FD - (P - 0.5)I}}. \quad [2]$$

Here, $[A]$ is the concentration of Dps, F is the applied force, $D = \frac{\delta(F)}{k_B T}$ is the normalized change in extension, and $K_{eff} = K_D e^{-1/2}$ is the Dps concentration associated with 50% occupancy of the binding sites at zero force. The dimensionless parameter I is analogous to the Hill coefficient and serves a measure of cooperativity, while K_D describes how tightly Dps binds bare DNA.

Therefore, our model contains only two free parameters, which are defined in limiting cases:

1. the DNA is fully extended and the affinity of Dps for DNA is characterized by a dissociation constant K_D
2. the DNA is fully compacted, the sum of all the energetic interactions between one dodecamer and its neighbors defines the cooperativity parameter I .
3. for intermediate conformations some binding sites are empty, so the number of interactions between bound dodecamers will be lower than in the fully compacted conformation.

Because the DNA can fold in many possible conformations, we cannot predict the exact number of interactions stabilizing a specific bound dodecamer. Instead, we use a mean-field approximation (4) to estimate that this number scales with the mean probability of Dps occupying the other binding sites. While the Ising model and the mean-field approximation have been applied to study cooperative binding in other systems (5), our approach focuses specifically on how these assumptions can give rise to hysteresis.

To understand why our model gives rise to hysteresis from the point of kinetics, we examine a concentration where the binding sites are equally likely to be occupied or empty ($[A] = K_{eff}e^{FD}$). When no cooperativity exists ($I = 0$), the occupancies of the binding sites are independent of each other, much like individual coin tosses. Then for a DNA molecule containing N -binding sites, there are 2^N possible binding configurations. We can group these configurations based on the total number of occupied binding sites, n . Here n can take any value from 0 to N . The number of configurations that correspond to a given value of n is given by the binomial coefficient, $\binom{N}{n}$. When writing the global free energy as a function of n , these configurations translate to an entropic contribution to the free energy proportional to $S(n) = k_B \ln \binom{N}{n}$. The global free energy predicted by our Ising model then becomes:

$$\mathcal{G}_{global}(n)/k_B T = \mathcal{G}(n)/k_B T - S(n)/k_B. \quad [3]$$

Here $\mathcal{G}(n)$ is the sum of $\Delta\mathcal{G}$ from 0 to n . If we set $P = \frac{n}{N}$, then we can approximate $\mathcal{G}(n)$ as an integral:

$$\mathcal{G}(n) = \int_0^n \Delta\mathcal{G}(n) dn. \quad [4]$$

For our Ising model, this becomes:

$$\begin{aligned} \mathcal{G}(n)/k_B T &= \int_0^n \left(\ln\left(\frac{K_D}{[A]}\right) - \left(\frac{n}{N}\right) \cdot I + FD \right) dn \\ &= n \left(\ln\left(\frac{K_D}{[A]}\right) + FD \right) - n^2 \left(\frac{I}{2N} \right). \end{aligned} \quad [5]$$

This leads to a formula for the global free energy:

$$\mathcal{G}_{global}(n)/k_B T = n \left(\ln\left(\frac{K_D}{[A]}\right) + FD \right) - n^2 \left(\frac{I}{2N} \right) - \ln\binom{N}{n}. \quad [6]$$

It is instructive to consider the case when $\mathcal{G}(0) = \mathcal{G}(N)$, i.e. when the DNA is equally likely to be completely empty of completely bound. This occurs at the Dps concentration $[A] = K_{eff} e^{FD}$, giving us a global free energy that is purely a function of n, N , and I :

$$\mathcal{G}_{global}(n)/k_B T = \left(n - \frac{n^2}{N} \right) \left(\frac{I}{2} \right) - \ln\binom{N}{n} = (P - P^2) \left(\frac{IN}{2} \right) - \ln\binom{N}{n}. \quad [7]$$

This equation is plotted for $N = 360$ and $I = 0, 4, 8$, and 12 in **Fig.5**. We have added small peaks to the curve to represent the barriers related to the binding and dissociation rates of individual Dps dodecamers, k_{on} and k_{off} . In the limit of zero cooperativity, the system reaches equilibrium at a rate of $k_{eq} = k_{on} + k_{off}$. From these curves, it is clear that the global free energy can become bi-stable if the cooperativity is strong. If we substitute $x = \frac{N}{2} - n$ and expand around $x = 0$, we obtain:

$$\begin{aligned} \mathcal{G}_{global}(x)/k_B T &= \left(\frac{N}{2} + x - \frac{1}{N} \left(\frac{N}{2} + x \right)^2 \right) \left(\frac{I}{2} \right) - \ln\left(\frac{N}{\frac{N}{2} + x} \right) \\ &\approx \left(\frac{NI}{8} \right) - \left(\frac{x^2 I}{2N} \right) + N * \ln(2) - \frac{1}{2} * \ln\left(\frac{N\pi}{2} \right) + \frac{2x^2}{N} \end{aligned}$$

$$= \left(\left(\frac{NI}{8} \right) - N * \ln(2) - \frac{1}{2} * \ln \left(\frac{N\pi}{2} \right) \right) + \frac{x^2}{2N} \left(1 - \left(\frac{I}{4} \right) \right). \quad [8]$$

Therefore, if we plot the global free energy as a function of the number of bound dodecamers, it scales with the logarithm of the binomial distribution, creating an entropic minimum at $P = 0.5$ (**Fig.5; eq.[8]**).

When $I > 0$, a quadratic term is added to the global free energy proportional to $\frac{1}{2}IP(1 - P)$, penalizing states near $P = 0.5$. At the critical value of $I = 4$ the solution at $P = 0.5$ switches from a stable equilibrium to an unstable equilibrium. For values of $I > 4$ a global energetic barrier arises between the majority bound/unbound states, and the Dps-DNA complex behaves collectively as a two-state system.

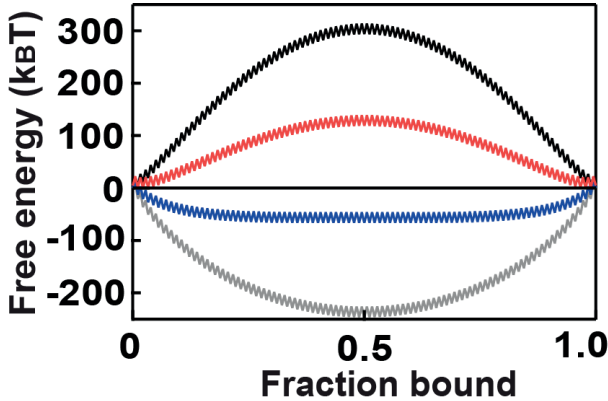


Fig.5. Kinetic interpretation of the hysteresis for an Ising mechanism. Global free energy ΔG_{global} (**eq.[8]**) plotted as a function of bound Dps for various values of cooperativity parameter G demonstrates that high cooperativity creates two local equilibria: no cooperativity $I=0$ (grey), $I = 4$ (blue), $I = 8$ (red), and $I = 12$ (black).

Before this transition to a two state system, the Dps-DNA complex reaches equilibrium at a rate of roughly $k_{eq} = k_{on} + k_{off}$, where k_{on} and k_{off} are the individual binding and dissociation rates of Dps dodecamers (represented by the small saw-tooth peaks in **Fig.5**). After the transition, for values of $I > 4$, we see the global free energy function is peaked at $n = \frac{N}{2}$ and two stable local equilibria arise. When the function is peaked, the binding transition closest to

the peak becomes rate limiting for transitions between the local equilibria. The system equilibrates at a timescale of $k_{eq} = e^{-H}(k_{on} + k_{off})$, where H is the height of the global barrier in units of $k_B T$. For $I \gg 4$, the height of this barrier scales with both the number of binding sites N and with cooperativity I :

$$H \approx \left(\frac{NI}{8}\right) - N * \ln(2) - \frac{1}{2} * \ln\left(\frac{N\pi}{2}\right)$$

When the barrier at $P = 0.5$ is very high, we are unlikely to observe transitions over the barrier so the positions of the local equilibria become more important than the global equilibrium. Therefore, for large Dps-DNA complexes (e.g. kilobases of DNA) even small changes in the cooperativity dramatically increase the barrier height. For the $\sim 300k_B T$ barrier shown in **Fig.4**, k_{eq} will be approximately 10^{130} times slower than k_{on} and k_{off} .

4.4.2 Tilting the global free energy with force and ionic strength

Further, if $[A] \neq K_{eff}e^{FD}$, then we can define an energy difference $U = \ln \frac{K_{eff}}{[A]} + FD$. The global free energy can then be rewritten as:

$$\mathcal{G}_{global}(n)/k_B T = \left(n - \frac{n^2}{N}\right)\left(\frac{I}{2}\right) - \ln\binom{N}{n} + nU. \quad [9]$$

Therefore, change in the force or concentration of Dps adds a linear term to the global free energy. For large positive or negative values of dU this term can remove one of the two stable solutions from the global free energy diagram. This corresponds to the inflection points in F_1 and F_2 . If we define the force $F_{ave} = (F_1 + F_2)/2$, then for $F = F_{ave}$ we find $U(F_{ave}) = 0$. In **Fig.6** we calculate the global free energy for forces spanning between F_{ave} and F_1 with $I = 12$. Note that the model predicts the barrier to vanish at $U(F_1)$, which is equal to $F_{ave}D - F_1D = 2.61$ when $I = 12$.

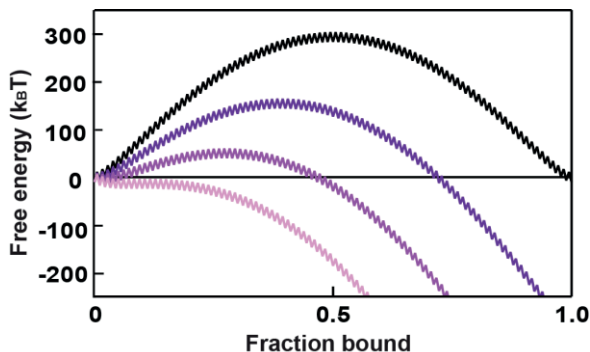


Fig.6. Tilting the global free energy with force. The global free energy curves G_{global} as a function of the number of bound Dps dodecamers at different forces (eq.[9]): $\frac{F_1+F_2}{2}$ (black), $\frac{2F_1+F_2}{3}$ (dark purple), $\frac{5F_1+F_2}{6}$ (purple), and F_1 (light purple).

In an Ising mechanism this tilt of global free energy induced by force is similar to the tilt induced by ionic strength since it weakens Dps-Dps and Dps-DNA interactions. Therefore, high monovalent salt also creates a barrier for Dps binding and much more Dps is needed to overcome it. This is consistent with data experimentally observed in section 3.4.

4.5 Hysteresis in other models of cooperativity.

4.5.1 Ising and KNF mechanisms of hysteresis

To examine whether hysteresis is unique to an Ising mechanism, we compare our model to other models of cooperativity. The Koshland-Némethy-Filmer (KNF) model (6), like our model, assumes a tight coupling between the occupancy of the DNA binding site and its conformation. Unlike our model, the KNF model assumes cooperative interactions are mediated through the conformation of neighboring DNA binding sites rather than through Dps-Dps contacts. However, given that occupancy and conformation are tightly coupled, these two interpretations produce equivalent energetic predictions. Therefore, our model can be viewed as a modification of the KNF model tailored to the flexible geometry of the Dps-DNA system.

4.5.2 Global free energy diagram for an MWC mechanism.

The Monod-Wyman-Changeux (MWC) model makes a very different physical assumption, requiring a concerted switch between a completely extended and a completely compacted DNA molecule (7). This concerted switching is not a physically realistic model of DNA dynamics, which should be uncorrelated over distances larger than the persistence length. Nevertheless, like our model the MWC model would give rise to a large global energetic barrier between two local binding equilibria and, therefore, to hysteresis.

In the MWC model (7), at a given value of the occupied binding sites n we must consider all the possible states in the relaxed (i.e. extended) conformation and all the possible states in the tight (i.e. compact) conformation of the DNA when calculating the free energy. Each conformation is governed by a different dissociation constant, K_R or K_T . By convention we define $C = \frac{K_R}{K_T}$. We also define L , the ratio of time spent in the compact versus extended conformations when no ligand is bound. With these parameters, we can calculate the global free energy exactly:

$$\mathcal{G}_{MWC}(n)/k_B T = -\ln \left(\left(\frac{CK_T}{[A]} \right)^{-n} + L \left(\frac{K_T}{[A]} \right)^{-n} \right) + \ln \binom{N}{n}. \quad [10]$$

The three free parameters of the MWC model give us one more degree of freedom than the two free parameters used in the Ising model. To compare the models, we can constrain the value of L and the concentration $[A]$ to ensure the function is symmetric about $n = \frac{N}{2}$. This gives us $[A] = K_T \sqrt{C}$ and $L = (C)^{-N/2}$, and the global free energy function becomes:

$$\mathcal{G}_{MWC}(n)/k_B T = -\ln \left((C)^{-\frac{n}{2}} + (C)^{\frac{n-N}{2}} \right) + \ln \binom{N}{n}. \quad [11]$$

For $n \ll N$, \mathcal{G}_{MWC} approaches the Ising free energy if we set $C = e^I$. In **Fig.7**, we plot \mathcal{G}_{MWC} for $C = e^0, e^4, e^8$, and e^{12} . For all values of $C > 1$ we find that the function is peaked at $n = \frac{N}{2}$.

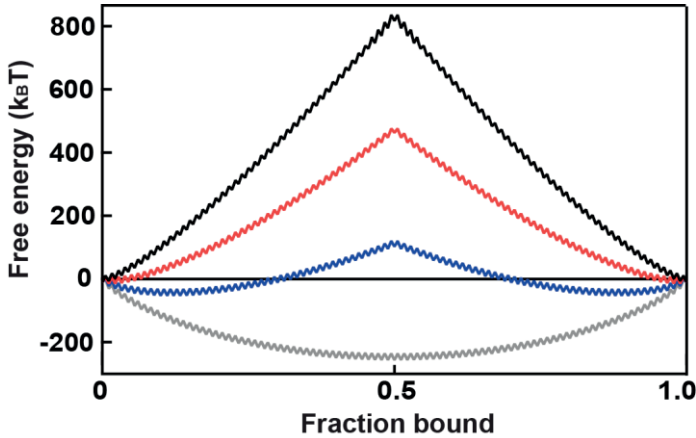


Fig.7. Hysteresis in MWC cooperative model. The MWC model is characterized by the three parameters C , L , and K_T (eq.[10]). The model predicts a sharp barrier in the global free energy for large N . The strength of the cooperativity is set by $C = K_R/K_T$: $C = 1$ (grey), $C = e^4$ (blue), $C = e^8$ (red) and $C = e^{12}$ (black). $N = 360$.

4.5.3 Global free energy diagram for a CS mechanism

The Conformational Spread (CS) model (8) is also derived from the Ising model, but it contains as many as five free parameters (9) compared to the two used in our model. With these additional parameters, CS model can approximate the KNF model, the MWC model, or our own model when applied to a fixed lattice. The CS model assumes that the binding substrate exists in an explicit geometry, such as a 1D ring or a 2D lattice (9). Traditionally the CS model avoids a mean-field approximation, so for 2D and 3D lattices the global free energy and binding probability must be computed numerically rather than by deriving explicit equations (e.g. eq.[2]). In our system, there is no fixed lattice since the DNA can fold in many potential conformations. Therefore, an exact comparison of our model to the CS model is not possible. Instead we consider below a fixed 3D lattice (27 binding sites) and demonstrate that both models predict hysteresis.

The CS model is characterized by up to five parameters (9). If we impose a symmetry condition about $n = \frac{N}{2}$, we can reduce this to three parameters,

E_j, E_A , and E_L . Like the KNF model (6), the CS model posits that cooperativity arises from repulsive interactions between DNA binding sites that are not in the same conformation. As such, the CS model is a less physically realistic model for our specific system. However, in the limiting case when DNA conformation and Dps binding are tightly coupled ($E_A \gg 0$), the CS model produces equivalent energetic predictions to our model. In this limit, $\frac{E_j}{k_B T} = \frac{I}{2j}$, where j is the number of nearest neighbor contacts. For a 1D ring $j=2$, for a square lattice $j=4$, and for a cubic lattice $j=6$. We can also relate the ligand binding energy to our effective dissociation constant as $\frac{E_L}{k_B T} = \ln\left(\frac{[A]}{K_{eff}}\right)$. However, in order to write an explicit formula for the global free energy for a substrate with N binding sites, we must perform a sum of the Boltzmann factors over all $\binom{N}{n}$ possible states. This becomes impractical for large N . Therefore, we performed a Markov Chain Monte Carlo (MCMC) algorithm (10) to derive the global free energy on a 3x3x3 cubic lattice. The results are compared with the free energy predicted by our model in **Fig.8**.

Below the critical coupling energy $\left(\frac{2jE_j}{k_B T} = I = 4\right)$ we find that the models are in close agreement. At higher coupling energies, the CS model predicts that a barrier arises with a height that is smaller than the barrier predicted by our model. The difference comes from the fact that CS model allows the system to find favorable clusters of bound sites rather than assuming the occupancy of neighboring binding sites should be uncorrelated (i.e. the mean field approximation). While the exact height of the barrier is more accurately approximated on a cubic lattice using the CS model, both models qualitatively predict the existence of a large energetic barrier. The transition to a regime dominated by hysteresis occurs at nearly the same coupling energy for 3D and 2D lattices. On a 1D lattice, the mean field approximation is less accurate, and the critical coupling energy begins to scale with $\ln(N)$ (8).

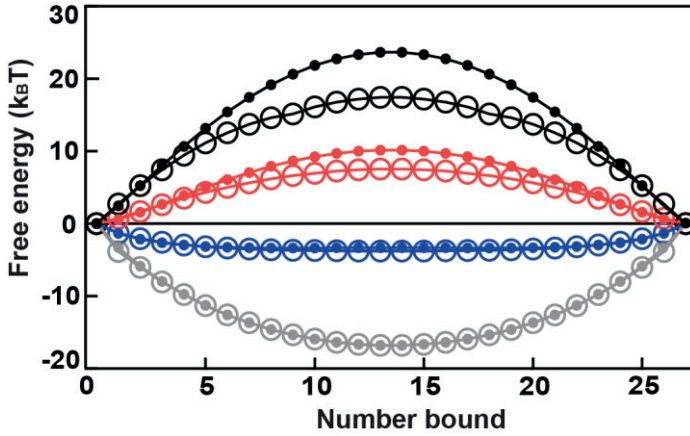


Fig.8. Hysteresis in CS cooperative model. The global free energy is estimated for the CS model using a Markov Chain Monte Carlo algorithm on a $3 \times 3 \times 3$ lattice (*open circles*). For comparison we plot our mean field approximation for $N = 27$ (*solid circles*). $I = 0$ (*grey*), $I = 4$ (*blue*), $I = 8$ (*red*), and $I = 12$ (*black*).

4.6 Conclusions

The overall regulation of cellular metabolism can only be understood through the kinetic study of proteins that represent working parts of the metabolic machine and define its performance. Dps is known for its ability to initiate a massive change in the chromosome and, therefore, in the metabolic processes of the cell during life-threatening conditions. In this chapter we characterized the kinetic properties of Dps and defined limits of its activity depending on ionic strength of the buffer and DNA tension. We demonstrated that Dps compacts DNA by reducing the amount of energy that is needed to overcome an energy barrier between two local equilibria. We show how ionic strength and DNA tension may tilt this energy barrier by affecting cooperativity of Dps or its binding affinity for DNA. These findings help us to understand hysteresis as a kinetic biological phenomenon that monitors time for the cell adaptation when it undergoes stress.

Also, we conclude that cooperativity can lead to hysteresis for a variety of mechanistic assumptions. However, we find our modified Ising model is particularly well-suited for modeling Dps-DNA complexes: it directly accounts

for Dps-Dps interactions that are implied by the crystal structure (11), it provides an explicit prediction of the free energies and equilibria using a minimal set of free parameters, and it allows for partially collapsed states. Further, the mean field approximation allows our model to be applied easily to a range of systems that might also be fit with a KNF or CS model while remaining agnostic about the exact geometry of the lattice. This makes our model particularly attractive when the lattice structure is undefined or too complex to precisely calculate the intermediate states.

References

1. E. B (1897) Alkoholische Ghrung ohne Hefezellen. *Berichte der deutschen chemischen Gesellschaft* 30(3):2668-2678.
2. Kim J, et al. (2004) Fundamental structural units of the Escherichia coli nucleoid revealed by atomic force microscopy. *Nucleic Acids Res* 32(6):1982-1992.
3. Frenkiel-Krispin D, et al. (2001) Regulated phase transitions of bacterial chromatin: a non-enzymatic pathway for generic DNA protection. *Embo J* 20(5):1184-1191.
4. Tome T & de Oliveira MJ (1990) Dynamic phase transition in the kinetic Ising model under a time-dependent oscillating field. *Phys Rev A* 41(8):4251-4254.
5. Agliari E, Barra A, Burioni R, Di Biasio A, & Uguzzoni G (2013) Collective behaviours: from biochemical kinetics to electronic circuits. *Sci Rep* 3:3458.
6. Koshland DE, Nemethy G, & Filmer D (1966) Comparison of Experimental Binding Data and Theoretical Models in Proteins Containing Subunits. *Biochemistry-U.S.* 5(1):365-385.
7. Monod J, Wyman J, & Changeux JP (1965) On Nature of Allosteric Transitions - a Plausible Model. *J Mol Biol* 12(1):88-118.
8. Bray D & Duke T (2004) Conformational spread: the propagation of allosteric states in large multiprotein complexes. *Annu Rev Biophys Biomol Struct* 33:53-73.
9. Duke TA, Le Novere N, & Bray D (2001) Conformational spread in a ring of proteins: a stochastic approach to allostery. *J Mol Biol* 308(3):541-553.
10. Geyer CJ (1992) Practical Markov Chain Monte Carlo. *Statistical Science* 7(4):473-483.
11. Grant RA, Filman DJ, Finkel SE, Kolter R, & Hogle JM (1998) The crystal structure of Dps, a ferritin homolog that binds and protects DNA. *Nat Struct Biol* 5(4):294-303.

Chapter 5

Electrostatics drives Dps-DNA interactions



5.1 Introduction

All molecules inside of the cell have a charge. Therefore, electrostatics play a major role in protein-protein complex formation, DNA binding mechanisms, conformational adaptabilities, protein movements and many others. The electrostatic properties are evolutionally selected by a protein to perform a specific function. In general rigid regions of the protein have stronger electrostatic interactions rather than functional hinges or flexible regions. Increase in binding specificity and affinity of certain protein involve optimization of electrostatics. For instance, monovalent salt and magnesium concentrations control structure of the bacterial chromosome by changing binding modes of many nucleoid-associated proteins (1-3). These changes substantially contribute to the regulation of gene expression in bacteria.

The affinity of Dps for DNA is also electrostatically dependent. Dps is known to be very sensitive to buffer conditions. Like many DNA-binding proteins, Dps binds DNA more weakly in the presence of higher salt concentrations. Less typically, divalent cations such as Mg^{2+} can substantially weaken the affinity of Dps for DNA (4, 5). It has been proposed that fluctuations in divalent cation concentrations act as a trigger for biocrystal assembly *in vivo* (5, 6). Dps dodecamers have an overall negative surface charge that electrostatically repels the DNA backbone, while positively charged lysine residues located in the disordered N-termini play an important role in DNA binding (4, 7, 8). Any additional knowledges of how Dps-DNA complex formation is controlled by electrostatic changes in the intracellular environment, can shed a light on motifs of cellular stress response in energy limited conditions.

In the previous chapters, we established hysteresis in the process of DNA compaction by Dps and derived the model that predicts this phenomenon. In this chapter we address the significance of electrostatic interactions in DNA compaction mediated by Dps and its link to hysteresis. In **section 5.2** we explore the effects of salinity, magnesium, crowding, and pH on this process utilizing magnetic tweezers assay. In **section 5.3** we report that these physiological states can influence critical forces and change amount of

hysteresis. Further, we demonstrate how to determine the model parameters: cooperativity and dissociation constant of Dps, based on amount of hysteresis measured experimentally. Lastly, in **section 5.4**, we discuss possible implications of cooperative hysteresis as a cellular mechanism for survival. Concluding remarks are represented in **section 5.5**.

5.2 Dps-induced compaction of DNA is influenced by salt, magnesium, pH, and crowding conditions

In order to compact DNA, Dps must do work on the bead and in order to break Dps-DNA complex, bead must do work on the Dps. The amount of work done in each case is a function of the strength of the Dps-DNA and Dps-Dps interactions. To explore what role electrostatics play in these interactions how they can be altered, we measured the compaction of DNA molecules exposed to Dps under a variety of buffer conditions. We performed force-extension cycles with the same pulling rate paying particular attention to the total width of the hysteresis loop, defined as the difference between critical forces F_1 and F_2 and shifts in the average of F_1 and F_2 .

We recorded the compaction and decompaction of DNA at several Dps concentrations (2, 4, 8 μM). Surprisingly, varying the Dps concentration over this range yielded relatively minor changes in the mean values of F_1 and F_2 , and in the width of the hysteresis loop (**Fig.1A**). Increasing the concentration of monovalent salts from 50 to 150 mM destabilized the Dps-DNA complex, as demonstrated by the progressive reduction of F_1 and F_2 and the narrowing of the width of the hysteresis loop (**Fig.1B**). The addition of magnesium (2 mM) to the buffer caused a similar destabilization of the Dps-DNA complex (**Fig.1C**). We also tested whether crowding can affect DNA compaction. Interestingly, the addition of PEG 8K caused a sharp increase in the stability of the Dps-DNA complex (**Fig.1D**). Finally, we observed that increasing the pH weakened the Dps-DNA complex (**Fig.1E**).

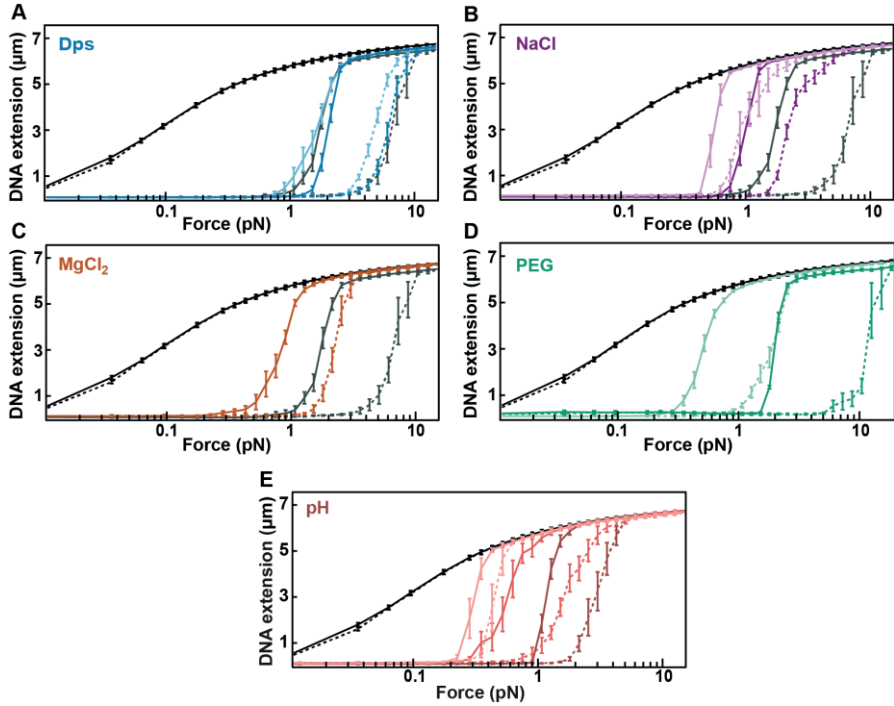


Fig.1. Buffer conditions affect DNA-Dps stability. Decreasing and increasing force records are represented by solid and dashed lines respectively. **(A)** Force-extension cycles with different Dps concentrations in the buffer: 2 μM (light blue), 4 μM (dark blue) and 8 μM (dark grey) (50 mM NaCl, pH 7.3). **(B)** Force-extension cycles with different NaCl concentrations in the buffer: 50 mM (dark grey), 100 mM (dark purple), and 150 mM (light purple) (8 μM Dps, pH 7.3). **(C)** Force-extension cycles with different MgCl_2 concentrations in the buffer: 0 (dark grey) and 2 mM (orange) (8 μM Dps, 50 mM NaCl, pH 7.3). **(D)** Force-extension cycles with different 8K PEG concentrations (w/v) in the buffer: 0 (light green) and 5% (dark green) (0.5 μM Dps, 50 mM NaCl, pH 7.3). **(E)** Force-extension cycles in the buffer at different pH levels: pH 6.9 (dark pink), 7.3 (pink), and 8.1 (light pink) (2 μM Dps, 100 mM NaCl, 50 mM Hepes-KOH). For all conditions we also recorded force-extension curves for bare DNA (black), which did not vary significantly. Each curve is generated from the mean of 10 to 20 molecules and the error bars correspond to standard errors of the mean.

Overall, our results revealed that Dps-induced compaction and decompaction of DNA is strongly influenced by tension applied to the DNA, ionic strength, magnesium, macromolecular crowding, and pH. These results are consistent

with the trends observed in a recent single-molecule study of Dps-DNA interactions (9).

5.3 Compare an Ising model to empirical data

In this section we provide a method to relate the amount of hysteresis to the strength of the neighboring interactions between bound proteins and DNA. In chapter 3 we derived a transcendental equation for the probability P of a given DNA binding site being occupied by a Dps dodecamer that defines our model:

$$P([A], F) = \frac{1}{1 + \frac{K_D}{[A]} e^{FD - PI}} = \frac{1}{1 + \frac{K_{eff}}{[A]} e^{FD - (P - 0.5)I}}. \quad [1]$$

Here, $[A]$ is the concentration of Dps, F is the applied force, $D = \frac{\delta(F)}{k_B T}$ is the normalized change in extension, and $K_{eff} = K_D e^{-I/2}$ is the Dps concentration associated with 50% occupancy of the binding sites at zero force. The dimensionless parameter I is analogous to the Hill coefficient and serves a measure of cooperativity, while K_D describes how tightly Dps binds bare DNA.

From eq.[2] we cannot write the probability P explicitly in terms of the force F . However, at each critical force F_1 and F_2 , a Dps dodecamer that binds DNA performs a fixed amount of work $W = F \cdot \delta(F)$ that we can write as an explicit function of P :

$$\frac{W}{k_B T} = PI - \ln(P) + \ln(1 - P) + \ln\left(\frac{[A]}{K_D}\right). \quad [2]$$

We estimate F_1 and F_2 by identifying where the DNA reaches 50% of its full extension ($\sim 3.5 \mu\text{m}$) in the decreasing and increasing force-extension curves. At each critical force, a Dps dodecamer that binds DNA performs a fixed amount of work $W = F \cdot \delta(F)$. We define W_{diff} as the difference in work performed by Dps at the two critical forces F_1 and F_2 and show that it is a function of the parameter I :

$$\frac{W_{diff}}{k_B T} = (F_2 \cdot D - F_1 \cdot D) = I \sqrt{1 - \frac{4}{I}} - 2 \ln \left(\frac{1 + \sqrt{1 - \frac{4}{I}}}{1 - \sqrt{1 - \frac{4}{I}}} \right). \quad [3]$$

We can also define W_{ave} , the average of the work performed by Dps at the two critical forces F_1 and F_2 , and show that it is given by:

$$\frac{W_{ave}}{k_B T} = \frac{(F_1 \cdot D + F_2 \cdot D)}{2} = \frac{I}{2} + \ln \left(\frac{[A]}{K_D} \right) = \ln \left(\frac{[A]}{K_{eff}} \right). \quad [4]$$

Next, we compare this model to our empirical findings. When we change the concentration of Dps, W_{diff} remains roughly constant, as predicted by eq.[3]. However, if we change the ionic strength of the buffer, we observe large changes in W_{diff} , indicating that I is influenced by electrostatic interactions between neighboring Dps molecules (**Fig.2A**). We also find that W_{ave} can be roughly fit to a logarithmic function of Dps concentration as predicted by eq.[4] and exhibits a strong dependence on electrostatic interactions (**Fig.2B**). The magnitude of the change in W_{ave} relative to W_{diff} requires that both I and K_D are dependent on salt concentration. Low salt leads to tighter binding on bare DNA and strengthens neighboring interactions between Dps dodecamers.

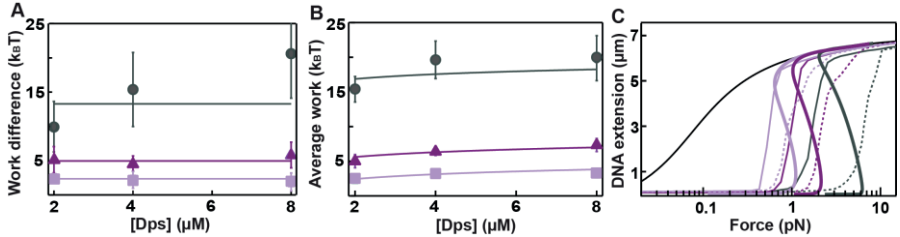


Fig.2. Ising model fits empirical data. (A) Work difference as a function of Dps concentration for different NaCl concentrations (mean, SD): 50 mM (dark grey circles), 100 mM (dark purple triangles) and 150 mM (light purple squares). These values were fit to eq.[3] (solid lines). (B) Average work as a function of Dps concentration for different NaCl concentrations (mean, SD): 50 mM (dark grey circles), 100 mM (dark purple triangles), and 150 mM (light purple squares). These values were fit to eq.[4] (solid lines). (C) Ising model force-extension curves (bold solid lines) are superimposed on the experimental data (thin solid and dashed lines) for different NaCl concentrations: 50 mM (dark grey), 100 mM (dark purple), and 150 mM (light purple) at 8 μM Dps.

Having determined the model parameters I and K_D at each salt concentration, we compare three experimental force-extension curves (**Fig.2C, dashed lines**) to the predictions of our model (**Fig.2C, solid lines**). Within the critical region between F_1 and F_2 , we observe that the experimental curves track one of the two stable solutions. Outside this critical region, we find the experimental curves converge to the single stable solution.

A quantitative summary of the interaction parameters I and K_D (as derived from W_{diff} and W_{ave}) for all buffer conditions tested is presented in **Table 1**.

We find that the neighboring interactions are weakened dramatically by salt, magnesium, and increasing pH. This result emphasizes that electrostatics play an important role in the binding of Dps dodecamers to each other. Conversely, the addition of crowding agents strengthens the neighboring interactions. Given that macromolecular crowding favors complexes with a smaller exposed surface area (10) this finding supports the idea that Dps dodecamers form a compact geometry on the DNA. The affinity of Dps for extended DNA, as measured by $\ln(K_D)$, is affected by buffer conditions in a similar manner to the neighboring interactions. Therefore the overall stability of the complex, as measured by W_{ave} , correlates with the amount of hysteresis, as measured by W_{diff} (**Fig.3**).

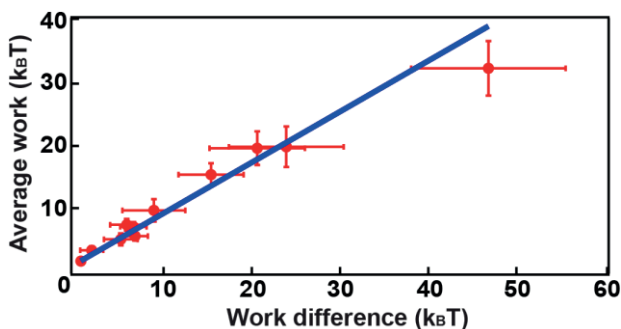


Fig.3. Correlation between work difference and average work. Work difference (W_{diff}) and average work (W_{ave}) performed by Dps dodecamers in order to bind DNA were derived at various buffer conditions. These values are plotted against each other (*red*) and a linear regression was applied (*blue*). The two variables exhibit a strong correlation (Pearson's $r=0.89$). Bars correspond to standard deviations, as shown in Table 1.

Table 1. List of values for W_{diff} , W_{ave} , I , and $\ln(K_D)$ derived from the Ising model for different buffer conditions (mean, SD).

| | | Work difference, $K_B T$ | Work average, $K_B T$ | Cooperativity, I | $\ln(K_D)$ | Buffer condition |
|------------------------|-----|-----------------------------|--------------------------|-----------------------|------------------|---|
| Dps, μM | 2 | 15.38 \pm 3.69 | 15.38 \pm 1.84 | 23.62 \pm 4.05 | -2.88 \pm 1.84 | NaCl=50 mM; MgCl ₂ =0; PEG=0; pH=7.3 |
| | 4 | 20.61 \pm 5.41 | 19.63 \pm 2.70 | 29.30 \pm 5.83 | -3.59 \pm 2.70 | |
| | 8 | 23.91 \pm 6.49 | 19.87 \pm 3.25 | 32.83 \pm 6.94 | -1.37 \pm 3.25 | |
| NaCl, mM | 50 | 23.91 \pm 6.49 | 19.87 \pm 3.25 | 32.83 \pm 6.94 | -1.37 \pm 3.25 | Dps=8 μM ; MgCl ₂ =0; PEG=0; pH=7.3 |
| | 100 | 5.82 \pm 1.87 | 7.34 \pm 0.93 | 12.74 \pm 2.26 | 1.11 \pm 0.93 | |
| | 150 | 1.86 \pm 1.31 | 3.25 \pm 0.66 | 7.61 \pm 1.97 | 2.63 \pm 0.66 | |
| MgCl ₂ , mM | 0 | 23.91 \pm 6.49 | 19.87 \pm 3.25 | 32.83 \pm 6.94 | -1.37 \pm 3.25 | Dps=8 μM ; NaCl=50 mM; PEG=0; pH=7.3 |
| | 2 | 6.59 \pm 1.50 | 7.02 \pm 0.75 | 13.66 \pm 1.78 | 1.88 \pm 0.75 | |
| PEG, % | 0 | 6.77 \pm 1.45 | 5.52 \pm 0.73 | 13.87 \pm 1.72 | 0.72 \pm 0.73 | Dps=0.5 μM ; NaCl=50 mM; MgCl ₂ =0; pH=7.3 |
| | 5 | 46.83 \pm 8.76 | 32.46 \pm 4.38 | 56.87 \pm 9.09 | -4.72 \pm 4.38 | |
| pH | 6.9 | 8.90 \pm 3.57 | 9.65 \pm 1.78 | 16.36 \pm 4.12 | -0.78 \pm 1.78 | Dps=2 μM ; NaCl=100 mM; MgCl ₂ =0; PEG=0 |
| | 7.3 | 5.15 \pm 1.91 | 5.01 \pm 0.95 | 11.92 \pm 2.35 | 1.65 \pm 0.95 | |
| | 8.1 | 0.63 \pm 0.26 | 1.50 \pm 0.13 | 5.64 \pm 0.49 | 2.01 \pm 0.13 | |

5.4 Biological implication of cooperative hysteresis

The hysteresis described here for Dps-DNA complexes could be advantageous to bacterial survival for several reasons. First, this novel form of protein cooperativity and cooperative hysteresis allows cells to create a binary response to small changes in external conditions. This property makes it possible for the bacteria to maintain a subcritical concentration of Dps without substantial DNA compaction. Small alterations in the pH, crowding, salinity, or magnesium concentration in the cell could then greatly increase the overall affinity of Dps for DNA, quickly inducing compaction and protecting the chromosome. Cooperative hysteresis allows cells to maintain a memory of past conditions, therefore, cells may tailor their response to current stress conditions. For example, a previous report suggests that Dps mediates a phase transition allowing starved cells to guard against additional stresses more effectively (5). Further, a population of cells could engage in bet-hedging strategies through hysteresis, allowing otherwise identical cells to become locked into different states. The variety of responses of these cells to new stress conditions would be more robust than adopting a single response.

5.5 Conclusions

In this chapter we identified electrostatic interactions that drive DNA compaction by Dps. We found that Dps affinity for DNA is strongly affected by salinity, magnesium, crowding, and pH. By fitting experimental data with our model we demonstrate that these intracellular conditions influence the strength of the neighboring interactions between bound Dps proteins and DNA. Therefore, it leads to the change in the amount of hysteresis. Based on this relation for each tested condition we define cooperativity parameter and dissociation constant of Dps. We note that this type of cooperative hysteresis might be used by biological systems as a relatively simple mechanism of protein binding to DNA that can readily and very fast be achieved, maximizing the cell's ability to grow and minimizing energy consumption. However, there is still much to understand and there are some basic questions about

consequence of this type of cooperativity for cellular metabolism. These questions provides a framework for modeling other biological systems involving large assemblies of macromolecules.

References

1. Bonnefoy E, Takahashi M, & Yaniv JR (1994) DNA-binding parameters of the HU protein of *Escherichia coli* to cruciform DNA. *J Mol Biol* 242(2):116-129.
2. Lin J, Chen H, Droge P, & Yan J (2012) Physical organization of DNA by multiple non-specific DNA-binding modes of integration host factor (IHF). *PLoS One* 7(11):e49885.
3. Liu Y, Chen H, Kenney LJ, & Yan J (2010) A divalent switch drives H-NS/DNA-binding conformations between stiffening and bridging modes. *Genes & development* 24(4):339-344.
4. Ceci P, et al. (2004) DNA condensation and self-aggregation of *Escherichia coli* Dps are coupled phenomena related to the properties of the N-terminus. *Nucleic Acids Res* 32(19):5935-5944.
5. Frenkiel-Krispin D, et al. (2001) Regulated phase transitions of bacterial chromatin: a non-enzymatic pathway for generic DNA protection. *Embo J* 20(5):1184-1191.
6. Minsky A, Shimoni E, & Frenkiel-Krispin D (2002) Stress, order and survival. *Nat Rev Mol Cell Bio* 3(1):50-60.
7. Karas VO, Westerlaken I, & Meyer AS (2015) The DNA-Binding Protein from Starved Cells (Dps) Utilizes Dual Functions To Defend Cells against Multiple Stresses. *J Bacteriol* 197(19):3206-3215.
8. Grant RA, Filman DJ, Finkel SE, Kolter R, & Hogle JM (1998) The crystal structure of Dps, a ferritin homolog that binds and protects DNA. *Nat Struct Biol* 5(4):294-303.
9. Lee SY, Lim CJ, Droge P, & Yan J (2015) Regulation of Bacterial DNA Packaging in Early Stationary Phase by Competitive DNA Binding of Dps and IHF. *Sci Rep* 5:18146.
10. Zhou HX, Rivas G, & Minton AP (2008) Macromolecular crowding and confinement: biochemical, biophysical, and potential physiological consequences. *Annu Rev Biophys* 37:375-397.

Chapter 6

How does DNA supercoiling affect Dps affinity?

Authors: N. Vtyurina & M. Ganji



6.1 Introduction

Supercoiling of the DNA molecule is a major force driving the compaction of bacterial genome (1-4). DNA supercoiling occurs in a topologically closed DNA when the helix undergoes over- or under-winding due to increased writhe. While over-winding leads to positive supercoiling, under-winding leads to negative supercoiling. Additionally, supercoiled DNA may form three possible structures: a plectoneme, a toroid, or a combination of both. Plectonemes are more common in nature and take part in shaping most bacterial chromosomes.

Bacterial genomes consist of a single circular DNA molecule that is negatively supercoiled contributing to the one thousand-fold compaction of the chromosome inside the cell (5). Additionally, the chromosome is constrained by different nucleoid associated proteins (NAPs) into topological domains of 10-100 kbp size (1, 2). By binding to multiple DNA sites, NAPs stabilize particular supercoil-dependent structures of the DNA, and also create different local conformations through twisting, bridging, and DNA bending (1).

Despite the complex bacterial genome packaging, regulatory sites of the DNA that are essential for life processes must be made accessible to the transcription and replication machineries. Because of the interplay between supercoiling and genome packaging, any large variations in the supercoiled state of DNA can affect gene expression with severe consequences for the bacterium (3). Therefore, DNA supercoiling should be recognized as a vitally important component of chromosome packaging and the regulation of the cellular processes.

It was found that the extent to which each of the NAPs contributes to DNA supercoiling depends on the growth phase and physiological state of the cell (4, 5). This feature makes the level of DNA supercoiling very dynamic and environmentally regulated (4, 6). For instance, in response to environmental stresses, the physiological states of the bacterial cell change for the sake of survival and adaptation. One of the responses includes an upregulation of one

of the NAPs, Dps, that compacts DNA yet keeps the genome accessible for life sustaining processes like transcription. Another response includes a change in DNA supercoiling state and, subsequently, was found to influence expression of genes (7-9).

As both DNA supercoiling and Dps contribute to the physiological response of bacteria on the environmental changes, a detailed understanding of interplay between DNA supercoiling and Dps protein is required. These findings can shed a light on the mechanisms that modulate transcription during challenging conditions for bacterial survival and provide insights on overall metabolic regulation. We therefore developed two new assays to examine how Dps-DNA complexes are influenced by supercoiling and topology. The first is a fluorescence-flow assay that traps DNA in curved or plectonemic topologies while Dps binds. The second is a magnetic tweezers assay that allows us to measure Dps-induced compaction of DNA as the linking number is increased or decreased by rotating the magnetic bead. The assays demonstrate Dps preferentially binds to plectonemes and enhances the torsional compaction of DNA.

In the previous chapters, we demonstrated that torsionally relaxed DNA is compacted by Dps through a cooperative Ising mechanism. In this chapter, we focus on the affinity of Dps for other DNA conformations, paying particular attention to plectonemic DNA as one of the DNA supercoiling states. Using fluorescence microscopy, we test preferences of Dps in binding to different DNA shapes in **section 6.2**. Additionally, we show in **section 6.3** that preformed Dps-DNA complexes are able to engulf more DNA and accommodate it inside these complexes. With magnetic tweezers in **section 6.4** we examine how presence of Dps influences DNA coiling under constant tension. Further, we extend our force-extension measurements on stretched DNA at zero twist (described in the chapter 2) to similar studies but on supercoiled DNA. Thus, in **section 6.5** we explore how preformed supercoiled DNA state influences Dps activity. We summarize our observations with the model presented and make conclusion remarks in **section 6.6**.

6.2 Affinity of Dps for DNA supercoils, U-shape and stretched DNA

In this section we stretched DNA under flow and examined Dps binding to several different conformations of DNA molecules: DNA plectonemes, U-shaped and linear DNA molecules. To visualize the various DNA conformations and subsequent Dps binding on a single-molecule level, we developed the fluorescence assay described below.

We introduced a linear 20.6 kbp DNA biotinylated at both ends (**Fig.1A**) into a streptavidin-coated flow cell at a flow rate of 30 $\mu\text{l}/\text{min}$. After one end of the DNA attached to the surface the molecules became stretched in the direction of applied flow. While the flow continued, the other end of the DNA attached to the surface at different location. Thus, in the field of view we observed DNA molecules variously tethered to the surface and visualized them along its length using epi-fluorescence. We choose the intercalating dye SYTOX orange (Invitrogen) for DNA labeling due to the high quantum yield of this dye coupled with high binding and unbinding rates (10) that ensured a rapid equilibrium of DNA-dye complexes and reduced the photo-induced damage of DNA molecules.

We found that some of the DNA molecules attached to the surface became U-shaped upon application of flow (**Fig.1B**). We conclude that these molecules were nicked or tethered via only a single biotin at one end, allowing them to torsionally relax. The relative location of the two DNA attachments points also varied among the molecules, creating a range of broader and narrower U-shaped DNA under flow. In the same field of view we also observed DNA molecules that simply stretched in the direction of applied flow (**Fig.1C**). Presumably, these were attached to the surface at one end only due to the lack of one of the biotin handles.

Lastly, we observed that on some fraction of the DNA molecules plectonemes spontaneously formed (**Fig.1D**). These DNA molecules were tethered with both biotin handles to the surface forming topologically closed molecules. Binding of many intercalating dye molecules to topologically closed DNA

locally introduced changes in the base stacking of double helix. This resulted in decrease in the sum of number of helical turns of the DNA (T_w) due to partial unwinding of the of two neighboring bases by an angle of around 30° as well as additional separation of around ~ 0.3 nm (11). These effects were compensated by the increase in the number of spatial crossings of DNA to itself (W_r). Increase in W_r corresponds to plectoneme formation, while the sum of T_w and W_r remained fixed giving the linking number $L_k = T_w + W_r$ (12, 13). Upon an applied flow, plectonemic DNA stretched in the direction of the flow but remained intertwined.

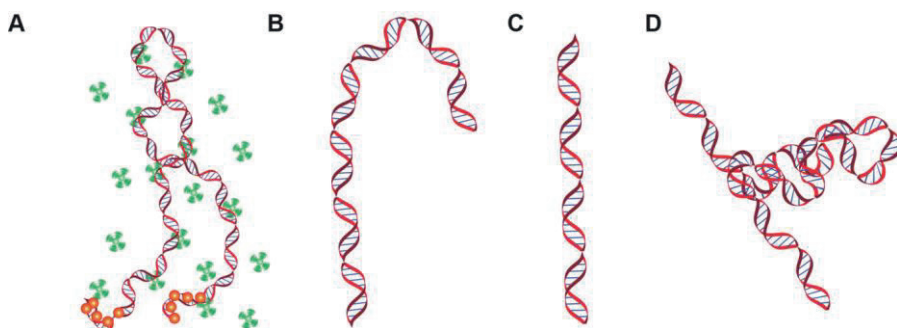


Fig.1. DNA shapes and design of the construct for the fluorescence assay. (A) Cartoon of the DNA construct with biotin handles (orange circle) at both ends designed for the fluorescence assay. The construct is labeled with intercalating fluorescent dye SYTOX orange (green stars). (B,C,D) Cartoon of the DNA shapes obtained upon applied flow: plectonemic DNA, U-shape and linear DNA.

In this experiment we recorded a movie with the acquisition rate of 10 Hz before and after injection of 200 nM of Cy5-labelled Dps in a buffer containing 40 mM Tris-HCl, 50 mM NaCl, pH 7.3. Thus, during the flow the central part of the DNA molecules adapted one of three conformations: U-shaped, linear DNA and plectonemic DNA (**Fig.1B, C and D**).

While reducing the flow (frame 50-275) we observed Dps binding to DNA and compacting U-shaped DNA faster than linear DNA but slower than plectonemic DNA. Qualitatively the distinction in time of the DNA compaction by Dps for various DNA shapes can be seen if we focus on the alternate snapshots of DNA molecules at different time points (**Fig.2**). The binding of Dps to

U-shaped DNA was detected at frame 175 (**Fig.2A**), while Dps binding to plectonemic DNA was detected already at frame 125 (**Fig.2C**). At last stretched DNA was compacted by Dps when the flow was reduced almost completely at frame 275 (**Fig.2B**)

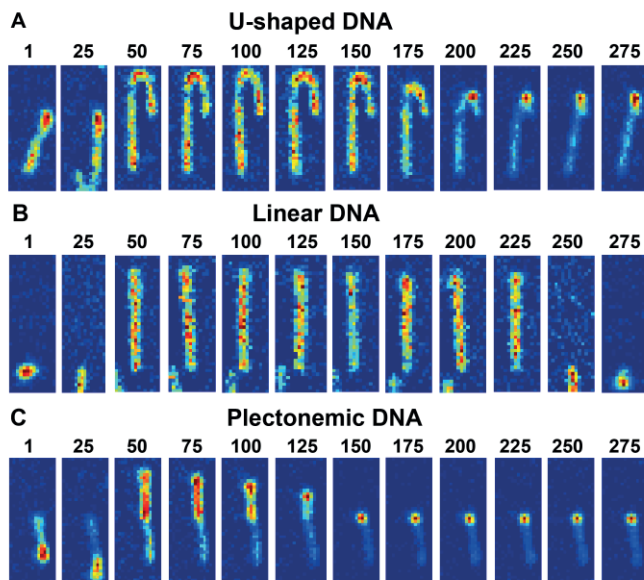


Fig.2. Real-time observation of Dps interacting with U-shape and plectonemic DNA. All the images were acquired at 100 msec intervals simultaneously for all molecules. The frame number is indicated on each snap-shot. **(A)** Snap-shots showing DNA compaction due to binding of Dps to U-shaped DNA formed during the flow as both ends were anchored to the surface. Full compaction of the DNA occurred at frame number 225. **(B)** Snap-shots showing DNA compaction due to binding of Dps to linear DNA formed during the flow as one end was anchored to the surface. Full compaction of the DNA occurred at frame number 275. **(C)** Snap-shots DNA compaction due to binding of Dps to plectonemic DNA. Plectonemes can be seen as a tip pointing out during the flow in frames 75 and 100. Full compaction of the DNA occurred at frame 150.

By the time the flow was completely stopped (frames after 275), we did not observe any fluctuations across the DNA length that are typical to a doubly tethered DNA without Dps, meaning all the DNA molecules were tightly compacted by Dps. The DNA-Dps complexes can be readily seen as a bright fluorescence spots on image obtained by overlapping fluorescence from DNA

and Dps channels (**Fig.3A**). Strikingly, Dps was not detected along the entire length of stretched DNA except of the binding site where it nucleated, stabilized and compacted DNA.

To demonstrate this further, we performed quantitative analysis of the distribution of Dps along DNA molecules. An example molecule for analysis is shown in rectangular on **Fig.3A**. The average fluorescence intensities of DNA and Dps were calculated along the length of the DNA molecules and plotted on the same graph for comparison (**Fig.3B**). This result clearly indicated that Dps is only bound to one site of the DNA.

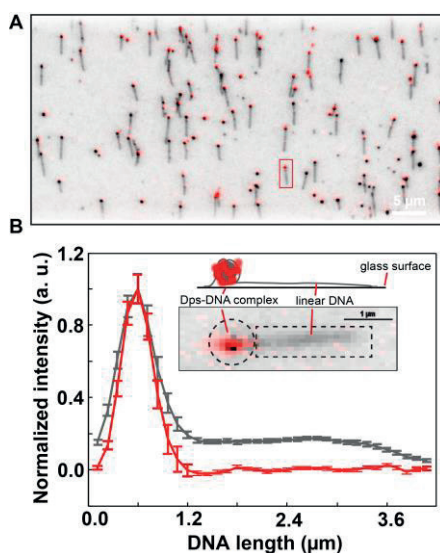


Fig.3. Distribution of Dps molecules along stretched DNA. (A) Overlaid fluorescence signals obtained from DNA labelled with SYTOX orange (*comet like structures in grey color*) and Cy5-labelled Dps (*bright spots in red color*) after the formation of Dps-DNA complexes. An example of stretched DNA molecule with Dps-DNA complex formed on one sight (*shown in rectangular*). (B) Plot showing the intensity distribution of Cy5-Dps (*red*) along labelled DNA with SYTOX orange (*grey*) obtained by averaging the intensity of Cy5 and SYTOX orange from 90 different structures. Inset represents an example molecule from (A) illustrating direction of pixels used in the plot.

Therefore, this fluorescence assay not only facilitated to observe DNA compaction mediated by Dps but also provided insights into the nucleation of

Dps on DNA of various conformational states in real time. Overall, our results strongly suggest that Dps binds and makes a complex with DNA only if two DNA strands are close to each other. Thus, the preferential for Dps DNA conformation is plectoneme or a kinked DNA. Additionally, Dps has no affinity for stretched DNA.

6.3 Dps-DNA complex accommodates excess of the DNA

Above we observed and quantified the process of Dps-DNA complex formation. However, it remains unclear whether Dps-DNA complexes have an amount of Dps proportional to the amount of wrapped DNA. Here we hypothesized that stable Dps-DNA complexes can form at various ratios of Dps to DNA. Thus, we tested if the preformed Dps-DNA complexes can bind an additional amount of free DNA in the absence of additional Dps.

Before adding free DNA to the flow cell containing preformed Dps-DNA complexes, we performed buffer exchange (~50 times the volume of the flow cell) to make sure that there is no free Dps diffusing in the solution. After this step Dps-DNA complexes remained in completely stable and compacted conformation. Then, while recording, we added 100 μ l of ~100 fM 20.6 kbp DNA plasmid labelled with SYTOX orange.

Before binding to the Dps-DNA complex, plasmid DNA remained flexible with no Dps bound (shown in red circle in **Fig.4A**). A difference in fluorescence intensities detected for Dps-DNA complexes before and after addition of plasmid DNA demonstrates that some of the complexes bound freely moving DNA plasmid and incorporated it inside of them. Thus, on the plotted time trace of the intensity of those Dps-DNA complexes that engulfed additional DNA plasmids, a sharp intensity increase is observed (**Fig.4 B**). These time traces with single step fluorescent increment confirmed the binding of plasmid DNA inside of the preformed Dps-DNA complexes.

The ability of a fixed amount of Dps to integrate various amounts of DNA into a complex suggests that rather than adopting a single rigid structure, the Dps-

DNA complex is flexible and can adopt multiple geometries. This might allow enzymes moving along the DNA, such as RNAP, to actively rearrange Dps-DNA complexes, providing access to hidden sequences. Further investigation of this possibility is presented in chapter 7.

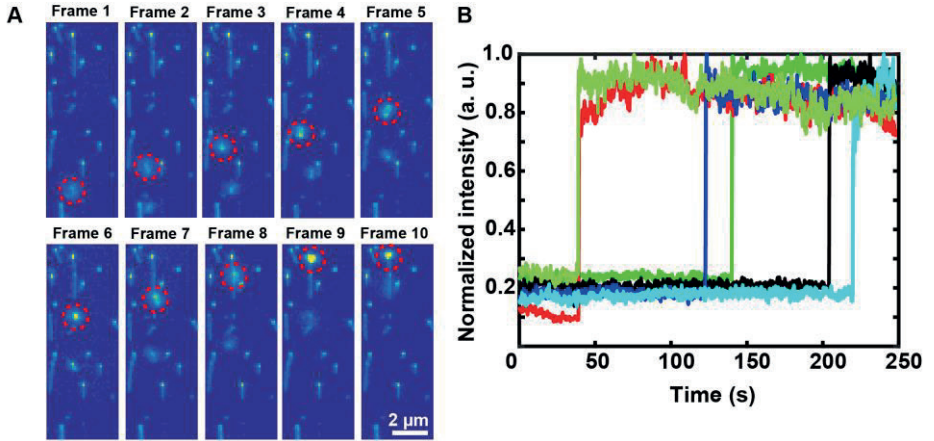


Fig.4. Binding of DNA plasmid to preformed Dps-DNA complex. (A) DNA plasmid (shown in red circle) freely moving towards preformed Dps-DNA complex (frame 1-8) and permanently binding to it (frame 9). Each frame is a snapshot taken at a 200 msec interval. (B) Normalized time traces of six events when a single step sharp increase in fluorescence intensity of the DNA-Dps complex indicated binding of extra DNA plasmid.

6.4 Coiling of DNA at constant stretching forces and presence of Dps

6.4.1 Rotation-extension DNA curves are influenced by Dps

Many enzymes can over- and under-wind DNA dynamically in the cell. It is therefore interesting to see how Dps interacts with DNA molecules with different linking numbers. In order to examine this behavior, we developed a magnetic tweezer assay (14-16) that allowed us to perform experiments on rotationally constrained single DNA molecules (**Fig.5A**). By rotating a pair of small vertically aligned permanent magnets, we modulated the supercoiling

state of the 20.6 kbp DNA under constant tension (**Fig.5B**). In all the experiments, we generated positive plectonemes on the DNA molecules (from 0 to +310 turns and back over 16 min) followed by generating negative plectonemes (from 0 to -310 turns and back over 16 min). Further, we compare DNA rotation-extension curves measured for the same range of stretching forces in the absence and in the presence of Dps. Based on this comparison we analyze how presence of Dps influences DNA coiling under constant tension.

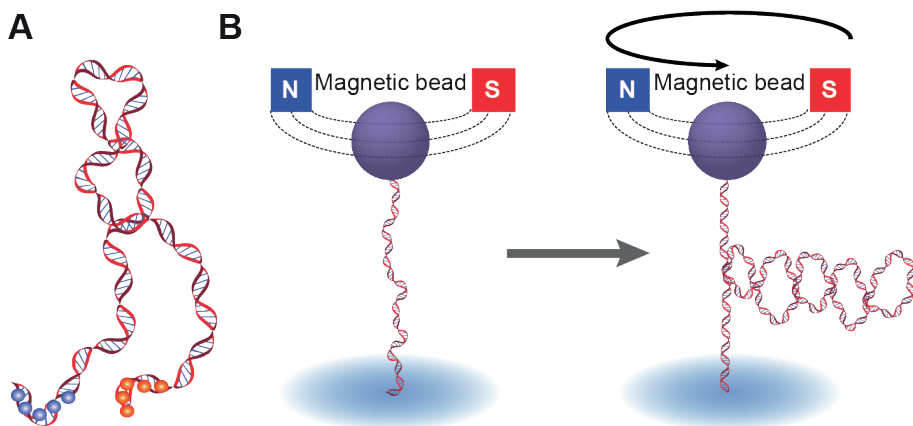


Fig.5. DNA construct for rotation-extension experiments. (A) Cartoon of the DNA construct with a digoxigenin handle (blue circles) at one end and a biotin handle (orange circle) at another end designed for the rotation assay performed with magnetic tweezers. **(B)** Cartoon of the magnetic tweezers assay showing a DNA molecule attached by one end to a microscope coverslip and by the other end to a magnetic bead. Rotation of a pair of small vertically aligned permanent magnets controls plectonemes formation.

To visualize experimentally measured DNA rotation-extension curves, we plot the DNA extension as a function of applied turns for the range of stretching forces between 0.5 and 7 pN (**Fig.6A**). First, we consider rotation-extension curves measured in the absence of Dps as DNA is gradually twisted towards +310 turns. Consistent with previous reports, no compaction due to plectoneme formation is observed at 7 pN stretching forces (**Fig.6A, top curve**). At such a high force, overwound DNA instead forms an alternative conformation termed P-DNA (17), and overall the rotation-extension curve

looks nearly flat. However, we clearly detect a linear decrease in the DNA extension indicating the formation of positive plectonemes at lower stretching forces (5, 2.5 and 0.5 pN) (**Fig.6A, three lowest curves**). When we return the DNA to its natural linking number (0 turns), the extension follows exactly the same values with no observed hysteresis. These results are consistent with the trends observed in other single-molecule studies of DNA coiling (13, 17, 18).

Second, we consider the rotation curves without Dps measured when DNA is gradually twisted towards -310 turns (**Fig.6A**). We observe that in this regime at high stretching forces (7, 5 and 2.5 pN) (**Fig.6A, three top curves**) DNA does not form negative plectonemes but denatures locally instead, consistent with previous reports (17, 19). This results in the absence of a significant decrease of the tether length and overall the rotation-extension curves look almost flat. At a low stretching force of 0.5 pN (**Fig.6A, lowest curve**), rotation-extension curves exhibit a linear decrease in the extension and a buckling transition occurs at the same amount of turns as when positively twisted. Therefore, at low forces we observe a symmetric pattern in the DNA rotation-extension curve. When we bring DNA back to its natural twist, the extension again follows the same values. To summarize all observed topological patterns of the rotation-extension curves measured on bare DNA, we plot them in correspondence with the range of tested stretching forces and predicted DNA extensions without twist (**Fig.6B**).

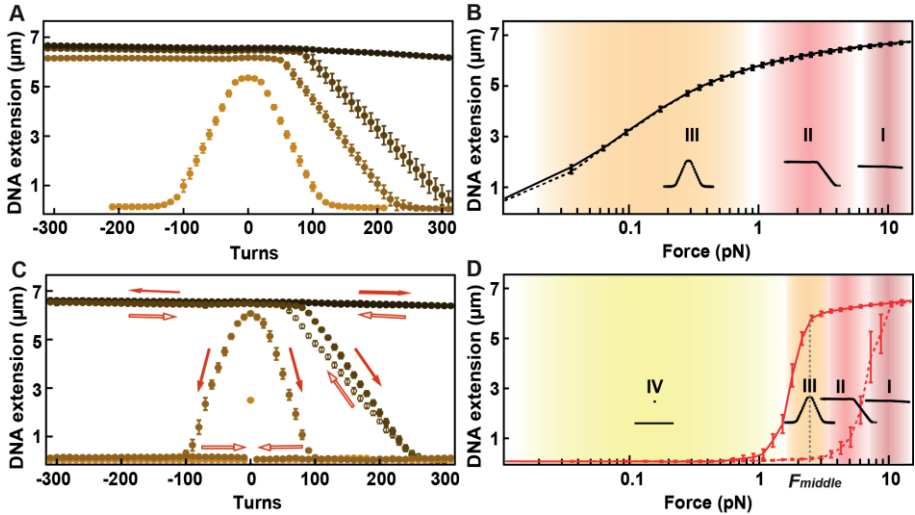


Fig.6. Effect of Dps on the DNA rotation-extension cycles. (A) Average DNA extension ($N=10$, mean, SE) without Dps as a function of turns at different stretching forces (top to bottom): 7 pN, 5 pN, 2.5 pN and 0.5 pN. (B) All observed DNA rotation-extension curves without Dps are classified in accordance to their patterns and plotted together with the force-extension curve (black) in three force regions: I (flat: $F > 7$ pN), II (plectonemes are limited to positive supercoiling: 1 pN $< F < 7$ pN), and III (symmetric plectoneme formation: $F < 1$ pN). (C) Average DNA extension ($N=6$, mean, SE) with $2 \mu\text{M}$ Dps as a function of turns at different stretching forces (top to bottom): 7 pN, 5 pN, 2.5 pN, and 0.5 pN. The direction of rotation is depicted by arrows (blue): increasing turns (closed arrow) and decreasing turns (open arrow). (D) All observed DNA rotation-extension curves with Dps are classified in accordance to their patterns and plotted together with the force-extension curve (red) in four force regions: I (flat extended $F > 7$ pN), II (only positive coiling 3 pN $< F < 7$ pN), III (symmetric coiling $F = F_{\text{middle}} = 2.5$ pN), and IV (flat compacted $F < 2$ pN). All measurements are performed in the reaction buffer: 50 mM NaCl, 50 mM Hepes-KOH pH 7.3.

Next, we consider the rotation-extension curves in the presence of $2 \mu\text{M}$ Dps measured when DNA is gradually twisted towards $+310$ turns or -310 turns (Fig.6C). Similar to the absence of Dps, at stretching forces around 7 pN we did not detect the formation of neither positive nor negative plectonemes (Fig.6C, top curve). At such a high force, the DNA rotation-extension curve is flat. When we return DNA back to its natural twist, the extension follows exactly the same values. This result suggests that Dps is unable to compact DNA at such a high force and no plectonemes formed on the DNA.

At 5 pN stretching force in the presence of Dps, we detect a linear decrease in the DNA extension under positive supercoiling, consistent with the formation of plectonemes. Under negative supercoiling no plectonemes are formed (**Fig.6C, second from the top**). Qualitatively, this curve looks similar to the equivalent 5 pN rotation curve taken in the absence of Dps. However, while the buckling transition occurs at a similar point (~ 80 turns), Dps causes the extension to decrease by a larger amount per turn as we continue rotating (110 bp/turn with Dps compared to 78 bp/turn without Dps). As a result of this, the end-to-end extension of bare positively coiled DNA reaches zero at around 60 turns later than positively coiled DNA in the presence of Dps at the same force (**Fig.6A and C, second from the top**). These results, combined with our previous observation that Dps does not bind to extended DNA (**Fig. 3B**), imply that at tension of 5 pN Dps can bind only to plectonemic DNA. Further, bound Dps seems to alter the plectoneme structure to incorporate more DNA. Moreover, when we unwind DNA from +310 turns to its natural twist, the extension does not return to the same values observed while winding the DNA. Instead, it increases with slightly lower rate (92 bp/turn). This result is reminiscent of the hysteresis observed in DNA force-extension curves taken in the presence of Dps (**Fig.6D, red**).

We next examine a lower stretching force of about 2.5 pN in the presence of Dps. As before, the DNA extension exhibits an enhancement in the linear decrease per rotation (**Fig.6C, second from the bottom**). On bare DNA the extension first reaches zero at +220 turns compared to +120 turns in the presence of Dps. Additionally, at this force the presence of Dps enhances the linear decrease in the DNA extension for both positive and negative rotations of the bead resulting in a nearly symmetric pattern (**Fig.6C, second from the bottom**). We note that at the same force of 2.5 pN (**Fig.6A, second from the bottom**) the rotation curve looks qualitatively different for bare DNA: it is asymmetric, with no plectonemes formed under negative supercoiling. Again, the presence of Dps leads to hysteresis in the DNA extension. When we bring return the DNA back from ± 310 turns to its natural twist, the DNA extension remains fixed at zero (**Fig.6C, shown with red arrows**). Only after the tension was briefly increased to 7 pN the DNA extension returned to its full

length. This demonstrates that twisting DNA allows Dps to bind DNA and form a stable complex that would be kinetically inaccessible when the DNA is torsionally relaxed.

Lastly, we consider the DNA rotation-extension curve at 0.5 pN stretching force and presence of Dps (**Fig.6C, lowest curve**). As soon as this force was applied, Dps compacted the DNA and we were able to detect only the average DNA extension while it was falling to collapse at zero twist. Further rotations did not result in any changes of the DNA extension. This result is consistent with DNA force-extension curves measured in the presence of Dps (chapter 3) and shows DNA rapidly enters a fully compacted state at any forces lower than 2 pN in this buffer. To summarize the observed topological patterns of the DNA rotation-extension in the presence of Dps, we plot them in correspondence with the tested stretching forces and measured DNA extension at zero twist (**Fig.6D**).

Overall, we find that Dps can readily bind to DNA plectonemes even at forces above critical in contrast to extended DNA that can be bound by Dps only below the critical force. Therefore, DNA rotation can be used to control the formation of Dps-DNA complexes on DNA under tension. Enzymes that induce supercoils in the cell could therefore trigger Dps complexes to assemble or disassemble locally.

6.4.2 Dps compensates force and stabilize plectonemes

Returning to the rotation-extension patterns observed: flat, asymmetric, and symmetric (i.e. I, II, and III, respectively) in the absence and presence of Dps (**Fig.6B and D**), we find that the presence of Dps creates qualitatively similar curves that are consistent with plectoneme formation. However, Dps seems to shift the divisions between different rotation-extension patterns to higher stretching forces (**Fig.6B and D**). To probe this idea further, we overlay rotation-extension curves measured on bare DNA with the curves measured at various forces in the presence of Dps but buckle at approximately the same amount of turns (**Fig.7**). This striking overlap between the rotation-extension

curves at different forces implies that Dps stabilizes plectonemes, allowing them to be maintained at forces ~ 2 pN higher than bare DNA at the equivalent linking number. We also note that there is the gradual rise of hysteresis between increasing and decreasing turns as we lower the stretching force, suggesting that Dps forms more stable complexes with DNA at lower forces.

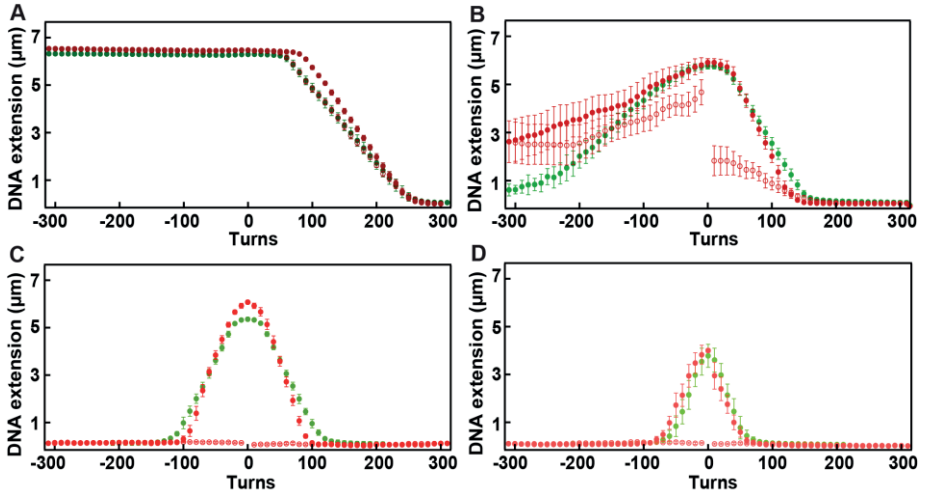


Fig.7. Dps enforces DNA plectonemes formation by compensating force. (A) Average DNA extension ($N=10$, mean, SE) measured at stretching force of 3 pN (green) without Dps compared to the average DNA extension measured at stretching force of 5 pN (red) with Dps as a function of turns. (B) Average DNA extension ($N=8$, mean, SE) measured at stretching force of 1 pN (green) without Dps compared to the average DNA extension measured at stretching force of 3 pN (red) with Dps as a function of turns. (C) Average DNA extension ($N=10$, mean, SE) measured at stretching force of 0.5 pN (green) without Dps compared to the average DNA extension measured at stretching force of 2.5 pN (red) with Dps as a function of turns. (D) Average DNA extension ($N=6$, mean, SE) measured at stretching force of 0.18 pN (green) without Dps compared to the average DNA extension measured at stretching force of 2 pN (red) with Dps as a function of turns. All measurements are done at 2 μ M Dps in the reaction buffer: 50 mM NaCl, 50 mM Hepes-KOH pH 7.3.

6.5 Force-extension curves of coiled DNA

In the bacterial cell the chromosome exists in a supercoiled state with locally preformed plectonemes. It is therefore intriguing to observe how Dps binds to

plectonemic DNA and compacts it. In this section we investigate *in vitro* how a preformed supercoiled DNA state influences Dps binding. To explore this, we extend our force-extension measurements on stretched DNA at zero twist to similar studies but on supercoiled DNA. Briefly, we stretched DNA molecules at 7 pN force, twisted them by ± 100 turns, and measured force-extension curves in the presence and absence of Dps. We applied a slowly decreasing force (from 19 to 0.03 pN over >40 min) followed by a slowly increasing force (from 0.03 to 19 pN over >40 min). For comparison we also plot force-extension curves measured at zero DNA twist without and with Dps (**Fig.8**).

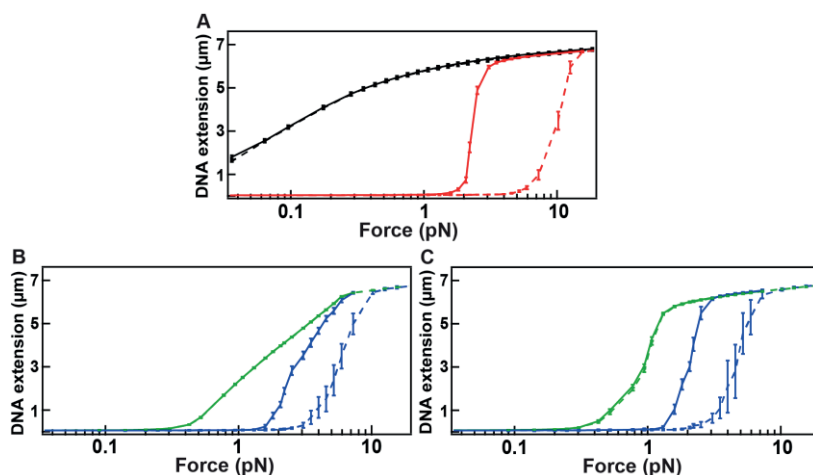


Fig.8. Dps affects force-extension curves of supercoiled DNA. (A) Average extension of relaxed DNA (0 turns) ($N=15$, mean, SE) measured as a function of force without Dps (black) and compared to the force-extension curve in the presence of 4 μM Dps (red). (B) Average extension of positively coiled DNA (+100 turns) at 7 pN ($N=6$, mean, SE) measured as a function of force without Dps (green) and compared to the force-extension curve in the presence of 4 μM Dps (blue). (C) Average extension of negatively coiled DNA (-100 turns) at 7 pN ($N=6$, mean, SE) measured as a function of force without Dps (green) and compared to the force-extension curve in the presence of 4 μM Dps (blue). All measurements are done in the reaction buffer: 50 mM NaCl, 50 mM Hepes-KOH pH 7.3.

For both positively and negatively coiled DNA, the force-extension curves reveal a similar trend (**Fig.8A and B**). We again observe hysteresis between the compaction and decompaction processes in the presence of Dps. However,

the application of either positive or negative supercoils causes the hysteresis to shrink significantly. Thus, force-extension curves of supercoiled DNA lie within the hysteresis loop measured for torsionally relaxed DNA. We also identify differences in positive and negative DNA supercoiling. When the force is decreased, the extension of positively coiled DNA collapses at higher forces in comparison with torsionally relaxed DNA. Since this effect is not observed as strongly for negatively coiled DNA, we conclude that positive plectonemes enhance DNA compaction by Dps. When we increase the force, supercoiled DNA transitions to an extended conformation at lower forces compared to torsionally relaxed molecules. This result suggests that Dps-DNA complexes formed on supercoiled DNA are not as stable as those formed on relaxed DNA.

Another interesting feature we observe on these force-extension curves is that there is no abrupt collapse of the DNA extension in the presence of Dps when it is coiled in comparison with relaxed DNA. The coiled Dps-DNA complex gradually follows the pattern of bare non-coiled DNA with a lot of intermediate points between compacted and extended DNA conformations. This shows that Dps only compacts a fraction of the DNA at a time, proportional to the number of plectonemes formed. Supercoiling can therefore be used to partition DNA into Dps-accessible plectonemes surrounded by DNA regions resistant to Dps binding under intermediate tensions. Such a partitioning could be useful *in vivo* to keep some DNA sequences accessible to other binding proteins.

6.6 Conclusions

In this chapter we investigated how different DNA conformations and supercoiling states affect Dps binding, nucleation and subsequent DNA compaction. Also we looked at influence of Dps on DNA coiling and pre-coiled DNA. Utilizing a fluorescence assay, we showed that Dps has no affinity for stretched DNA and requires two DNA strands to be close to each other in order to nucleate on DNA. We considered three different DNA shapes and found that as closer the DNA strands are, as faster Dps mediates DNA compaction. First, Dps nucleates on DNA plectonemes (**Fig.9A**), then on bent DNA (**Fig.9B**) and the last on linear DNA but only after its released from

tension (**Fig.9B and C**). Nucleation of Dps leads, therefore, to Dps-DNA complex formation (**Fig.9D**). Additionally preformed Dps-DNA complexes can accommodate excess of free DNA plasmid (**Fig.9F**).

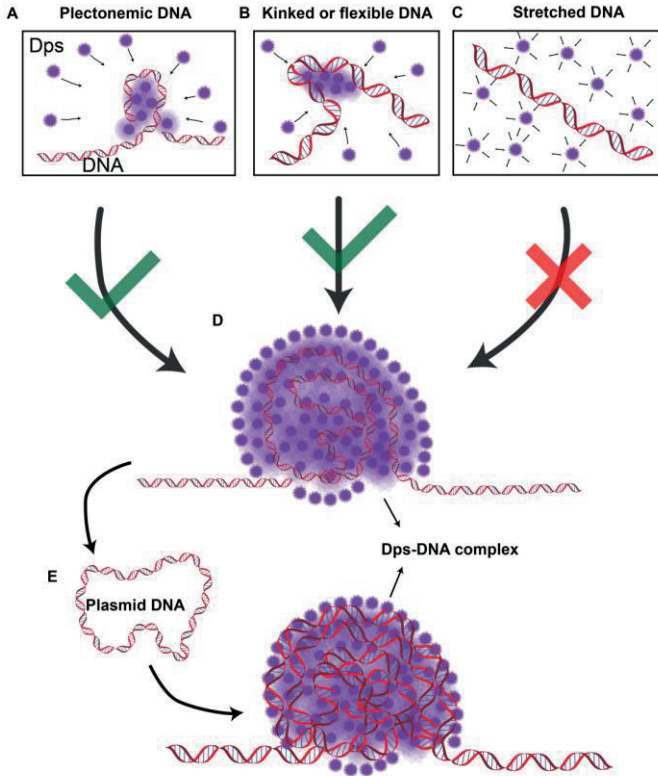


Fig.. Schematic representation of Dps nucleating on DNA and forming Dps-DNA complex. (**A**) Plectonemic DNA acts as nucleation point for formation Dps-DNA complexes. (**B**) Nucleation of Dps is favorable on a kinked or flexible DNA due to two strands located close to each other. (**C**) Dps does not bind to an inflexible or taut DNA. If the DNA is held at constant force, formation of Dps-DNA complex is hindered. (**D**) Schematic showing Dps-Dps interactions are prevalent in the initial Dps-DNA complex. (**E**) A DNA plasmid binds to preformed Dps-DNA complex.

Using magnetic tweezers assay we showed that presence of Dps also affects DNA rotation-extension curves and enhances plectoneme formation stabilizing them on the DNA. Dps-DNA complexes follow the same patterns

with gradual linear decrease in the extension as bare DNA while rotating the molecules, however, the rotation-extension curves are shifted to higher forces that compensates about 2 pN of tension. At the force located in the middle of the hysteresis loop of the force-extension curve in the presence of Dps, we observe plectonemes formation on the Dps-DNA complexes that are symmetric in regard to the number of negative and positive turns. Any shifts from the middle force generate stochasticity in plectonemes formation within Dps-DNA complexes and rotation-extension curves lose its symmetry. Dps-DNA complexes also exhibit hysteresis between increasing and decreasing turns relatively to the natural DNA twist without regard to positive or negative supercoiling DNA states. Surprisingly, under tension, the presence of preformed plectonemes on the DNA enhances rather gradual decrease in DNA extension and shrinks the hysteresis loop observed for the Dps-DNA complexes at zero twist.

The achieved results demonstrate how DNA supercoiling states can influence Dps binding and change overall affinity as well as activity of this particular protein. Overall, in the presence of DNA supercoils Dps acts less cooperatively in compare with flexible DNA, therefore, compacting DNA in the way leaving more room for free DNA strands. Perhaps, this feature allows access to proteins regulating other processes in the cell like transcription and replication. Thus, even though Dps compacts DNA extremely tightly and it is not easy to break the Dps-DNA complex afterwards, there are many mechanisms inside of the cell that can tune strongly the activity of Dps depending on physiological state of the cell. Therefore, in living cell the dynamic interplay between Dps and supercoiling DNA states must be vitally important rising curiosity to this process and can be explored much further.

References

1. Dillon SC & Dorman CJ (2010) Bacterial nucleoid-associated proteins, nucleoid structure and gene expression. *Nat Rev Microbiol* 8(3):185-195.
2. Dorman CJ (2014) Function of nucleoid-associated proteins in chromosome structuring and transcriptional regulation. *Journal of molecular microbiology and biotechnology* 24(5-6):316-331.

3. Peter BJ, et al. (2004) Genomic transcriptional response to loss of chromosomal supercoiling in *Escherichia coli*. *Genome Biol* 5(11):R87.
4. Goldstein E & Drlica K (1984) Regulation of bacterial DNA supercoiling: plasmid linking numbers vary with growth temperature. *Proc Natl Acad Sci U S A* 81(13):4046-4050.
5. Azam TA, Iwata A, Nishimura A, Ueda S, & Ishihama A (1999) Growth phase-dependent variation in protein composition of the *Escherichia coli* nucleoid. *J Bacteriol* 181(20):6361-6370.
6. Higgins CF, et al. (1988) A physiological role for DNA supercoiling in the osmotic regulation of gene expression in *S. typhimurium* and *E. coli*. *Cell* 52(4):569-584.
7. Dorman CJ (1996) Flexible response: DNA supercoiling, transcription and bacterial adaptation to environmental stress. *Trends in microbiology* 4(6):214-216.
8. Higgins NP (2007) Under DNA stress, gyrase makes the sign of the cross. *Nature structural & molecular biology* 14(4):256-258.
9. Rui S & Tse-Dinh YC (2003) Topoisomerase function during bacterial responses to environmental challenge. *Front Biosci* 8:d256-263.
10. Biebricher AS, et al. (2015) The impact of DNA intercalators on DNA and DNA-processing enzymes elucidated through force-dependent binding kinetics. *Nat Commun* 6.
11. Lee JS & Morgan AR (1978) A rapid method for the measurement of the unwinding angle of intercalating agents and the superhelix density of circular DNAs. *Nucleic Acids Res* 5(7):2425-2439.
12. White JH (1969) Self-linking and the gauss integral in higher dimensions *Am. J. Math* 91(693-728).
13. Strick TR, Allemand JF, Bensimon D, & Croquette V (1998) Behavior of supercoiled DNA. *Biophys J* 74(4):2016-2028.
14. Yu Z, et al. (2014) A force calibration standard for magnetic tweezers. *Review of scientific instruments* 85(12):123114.
15. Velthuis AJWT, Kerssemakers JWJ, Lipfert J, & Dekker NH (2010) Quantitative Guidelines for Force Calibration through Spectral Analysis of Magnetic Tweezers Data. *Biophys J* 99(4):1292-1302.
16. Cnossen JP, Dulin D, & Dekker NH (2014) An optimized software framework for real-time, high-throughput tracking of spherical beads. *Review of Scientific Instruments* 85(10):103712
17. Allemand JF, Bensimon D, Lavery R, & Croquette V (1998) Stretched and overwound DNA forms a Pauling-like structure with exposed bases. *Proc Natl Acad Sci U S A* 95(24):14152-14157.
18. Lipfert J, Klijnhout S, & Dekker NH (2010) Torsional sensing of small-molecule binding using magnetic tweezers. *Nucleic Acids Res* 38(20):7122-7132.
19. Strick TR, Croquette V, & Bensimon D (1998) Homologous pairing in stretched supercoiled DNA. *Proc Natl Acad Sci U S A* 95(18):10579-10583.

Chapter 7

RNAP transcription through Dps-DNA complexes

Authors: N. Vtyurina & R. Janissen



7.1 Introduction

All the information needed to synthesize the proteins that function inside of the cell is stored in the genome. To launch the first step in the expression of a particular protein, the sequence of the corresponding gene must be converted into messenger RNA (mRNA). This conversion process is called transcription. Subsequently, the mRNA produced is used as a template when its sequence is translated into the amino acid sequence of the protein. This principle of protein synthesis is common to all living organisms and is described in the central dogma of molecular biology (1).

In this chapter we focus on the process of transcription that takes place on the bacterial nucleoid. The transcription of genetic information stored in DNA to mRNA is carried out by molecular motor proteins called RNA polymerases (RNAP). Thus, RNAPs play a crucial role in the regulation of gene expression. Their kinetics have been studied extensively using several techniques ranging from gel electrophoresis (2-4) to single-molecule approaches (5, 6) to deep sequencing (7). It has been established that during transcription, RNAP unwinds a 14-nucleotide bubble in the double stranded DNA helix (dsDNA) and subsequently translocates along the DNA while elongating the RNA chain (8-10). The elongation phase is influenced by gene regulatory processes that synchronize transcription and translation. Therefore, it is important to characterize the transcriptional pausing dynamics during elongation.

Many previous studies have analyzed the transcriptional pauses during elongation of individual RNAPs translocating along linearly stretched dsDNA molecules (6, 9, 11-13). RNAP can pause due to sequences encoded in the DNA template (14, 15), mis-incorporation of non-complimentary nucleotides (16, 17), stochastic changes in the polymerase conformation (18), or because of protein “roadblocks” bound to the downstream DNA (19-21). Inside the bacterial cell the transcription process is also influenced by different DNA topological states that are controlled by nucleoid-associated proteins (NAPs) (22). Nevertheless, the molecular mechanism by which topological alterations on the DNA affect RNAP transcription in bacteria is poorly understood. Dps

protein is one of the NAPs that compacts the bacterial genome, particularly during stress conditions. By changing the DNA topology and promoter accessibility, Dps could influence cellular metabolism. A detailed study of how transcription occurs in the presence of Dps can therefore shed light on the coordination of gene expression with DNA topology.

In the previous chapters, we characterized the process of DNA compaction by Dps alone at the single-molecule level utilizing the magnetic tweezers assay. In this chapter, we modified a magnetic tweezers assay in order to characterize the dynamic process of RNAP transcription through preformed Dps-DNA complexes (**section 7.2**). Specifically, we focus on the RNAP dynamics e.g. change in elongation rate and pausing frequency of RNAP that occur in different tested configurations. We perform dwell time analysis (**section 7.3**) to investigate the enzyme dynamics in the presence and absence of Dps. In **section 7.4**, we apply an assisting force to the RNAP molecules and allow it to transcribe through Dps-DNA complexes located downstream of RNAP. A second configuration allows us to apply an opposing force to the RNAP while transcribing through stretched bare DNA with Dps-DNA complexes located upstream of RNAP. This second configuration enables us to test if Dps prevents backtracking of RNAP. We compare dwell-time distributions for these two configurations. In **section 7.5** we examine the degree to which RNAPs can transcribe through completely compacted Dps-DNA complexes at very low opposing force. Concluding remarks are represented in **section 7.6**.

7.2 Methods for tracking RNAP translocation along the DNA

In this magnetic tweezers assay, dsDNA molecules were tethered at one end to the surface of the flow cell via a digoxigenin handle (**Fig.1A**). A streptavidin-coated superparamagnetic bead was attached to the singly biotinylated RNAP stalled near the promoter region of the dsDNA forming the RNAP:DNA ternary complex. The magnetic beads and thus the RNAP:DNA complexes were manipulated by a pair of vertically aligned permanent neodymium-iron-boron

magnets (SuperMagne) separated by a distance of 1 mm that controlled the applied magnetic force (**Fig.1B**).

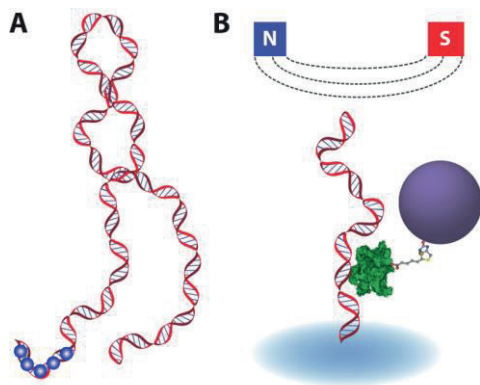


Fig.1. DNA and RNAP labeling for magnetic tweezers assay. (A) Schematic representation of the DNA construct with digoxigenin handle (blue circles) at one end and used in the magnetic tweezers assay. (B) Cartoon of RNAP (green) labeled with a single biotin molecule (grey) and attached to the streptavidin-coated magnetic bead (purple).

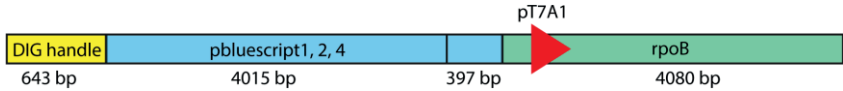
7.2.1 DNA constructs and RNAP labeling for magnetic tweezers assay

For the assisting force (AF) configuration, a double-stranded DNA 9.5 kbp linear construct was designed to contain a digoxigenin-enriched DNA handle, a random 4bk spacer sequence of pbluescript plasmid, a *rpoB* coding sequence, a T7A1 promoter sequence with the *RpoB* sequence and its transcription terminator (**Fig.2A**). The fragments were prepared by PCR and linearly ligated together. Further, this linear dsDNA was at one end ligated to a digoxigenin-labelled DNA handle of 643 base pairs. The other end was ligated to a 4.5 kb DNA *rpoB*-encoding fragment containing a T7A1 promoter.

For the opposing force (OF) configuration, a 7.5 kbp linear double-stranded DNA construct was designed to contain a digoxigenin-enriched DNA handle and a T7A1 promoter sequence with the *RpoB* sequence (**Fig.2B**). The fragments were prepared by PCR and ligated together. The sequence was generated by amplification of a 5143 bp fragment containing a T7A1

promoter. Further, this linear double-stranded DNA was at one extremity ligated to a digoxigenin-labelled DNA handle of 643 base pairs and a spacer sequence of 1268 bp. The constructs were made by Theo van Laar (TU Delft, the Netherlands).

A



B



Fig.2. DNA constructs for assisting and opposing force configurations. (A) Schematic of the 9.5 kbp linear DNA construct used in the AF configuration visualizing the lengths and the positions of the different DNA segments. **(B)** Schematic of the 7.5 kbp linear DNA construct used in the OF configuration visualizing the lengths and the positions of the different DNA segments.

Wild-type *E. Coli* RNA polymerase holoenzyme containing transcription factor σ^{70} and a biotin-modification at the β' -subunit was kindly supplied by Prof. Dr. Irina Artsimovitch (Ohio State University, USA). Approximately 60 % of elongation complexes formed by this holoenzyme showed activity (23).

7.2.2 Flow cell preparation

The flow cell preparation protocol used in this study has been described in detail elsewhere (9, 24-27). In short, polystyrene reference beads of 1.5 μm in diameter (Polysciences GmbH, Germany) were diluted 1:4000 in PBS buffer (pH 7.4; Sigma Aldrich) and then adhered to the nitrocellulose (Invitrogen) surface of the flow cell. Further, digoxigenin antibodies (Roche Diagnostics) at concentration of 0.5 mg/ml were incubated for 4-5 hours within the flow cell, following overnight incubation of 10 mg/ml BSA (New England Biolabs) diluted in preparation buffer containing 20 mM TRIS, 100 mM KCl and 10 mM MgCl_2 adjusted to pH 7.9.

7.2.3 RNAP transcription assay

A mixture of 31 nM RNAP and 3 nM DNA was prepared in the buffer containing 20 mM TRIS, 100 mM KCl, 10 mM MgCl₂, 1 mM DTT, pH 7.9 and left to incubate for 10 min at 37 °C. Further, 50 μM ATP, CTP, GTP (GE Healthcare Europe) were added to the solution and left to incubate for additional 10 min at 30 °C. Presence of the initiation factor σ^{70} and ATP, CTP, GTP ribonucleoside triphosphates enabled RNAP binding to the T7A1 promoter and initiated elongation and transcription. The elongation proceeded until the adenosine base A29 on the DNA sequence is reached and then transcription stopped due to the lack of the complementary nucleotide uracil. This reaction resulted in the formation of a DNA:RNAP ternary complex with RNAP stalled at the position A29 after the promoter sequence. In the last step, the solution was diluted with 250 μl of preparation buffer to obtain a 0.25 nM RNAP:DNA ternary complex. The complex was introduced into the flow cell and incubated for 30 min. Addition of 400 times diluted streptavidin-coated superparamagnetic beads (MyOne Dynabeads, Invitrogen/Life Technologies) with a diameter of 1 μm resulted in the attachment of the beads to biotinylated RNAP stalled on the DNA (**Fig.1B**).

Before the re-initiation of transcription for tracking, we exchanged the preparation buffer for a transcription buffer containing 50 mM Hepes, 100 mM KCl, 4 mM MgCl₂, pH 7.3 and 5 % PEG 8K (Promega). At this step, for the experiments with Dps, we added 1 μM of Dps protein to the transcription buffer while DNA is stretched to its full length at force of 5 pN. This force prevents compaction of the DNA by Dps in the region between RNAP and the surface attachment point. Further, we re-initiate transcription by adding all nucleotides - including uracil triphosphate (IBA Lifesciences GmbH)- at concentration of 1 mM to the stalled ternary complexes and instantly starting the measurements with a sampling frequency of 25 Hz. Since transcription re-initiates in a fraction of all the stalled ternary complexes, we define the efficiency of transcription re-initiation as the ratio between the number of transcribing tethers and the number of all the stalled ternary complexes that were tracked.

7.3 Analyzing RNAP translocation along the DNA

7.3.1 RNAP transcription traces

The number of magnetic beads that we are able to track in the field of view in an individual experiment ranges from 100 to 250. By tracking the bead z-position, we are able to observe the upward translocation of RNAP on the DNA during the transcription process for the assisting force configuration and downward translocation for the opposing force configuration. For all performed transcription experiments, we observe that RNAP re-initiation efficiencies usually surpass 30 %. Each transcription trace corresponds to the activity of a single RNAP and reflects the transcription dynamics of a single enzyme (**Fig.3**). The transcription traces were processed using custom-written Igor pro v6.39 (Wavemetrics, USA) based scripts.

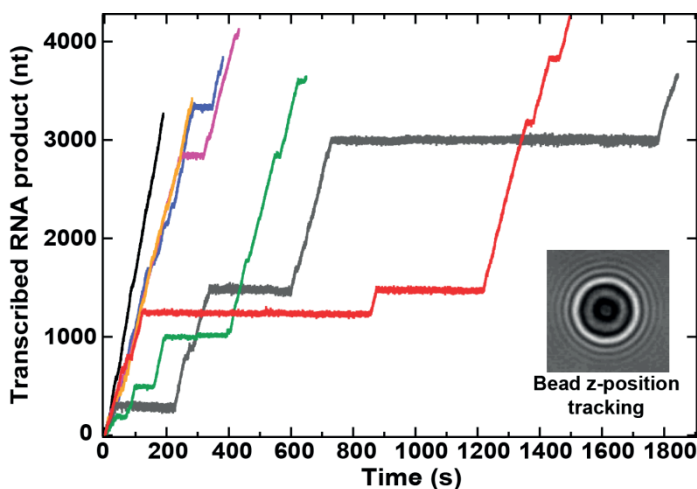


Fig.3. RNAP transcription traces. Example bead z-position traces as a function of time during elongation measured at assisting force of 7.5 pN and rNTP concentration of 1 mM. Each trace corresponds to the transcription activity of a single RNAP.

All the transcription traces consist of elongation interrupted by pauses of different durations, ranging from few tenths of a second to up to an hour. RNAP traces exhibit extremely heterogeneous dynamics with different pause

durations and pause frequencies during transcription, in agreement with previous studies (5, 6, 12). Therefore, the traces were examined for potential transcription activity and only those were further used in the dwell-time analysis.

7.3.2 Dwell time analysis

To quantitatively assess the transcription dynamics of *E. coli* RNAP, we conduct a statistical analysis of elongation and transcriptional pausing. An accurate and robust evaluation of pause distributions is performed using unbiased dwell time analysis, a method employed previously for the characterization of RNA-dependent RNA polymerases (9, 28, 29). This technique provides more statistical pause distribution data than the method using numerical derivation of the velocity slope which led to biasing the data by omission of shorter pauses (12, 30).

7.4 RNAP transcription at assisting and opposing forces in the presence of Dps

We use two configurations in order to track RNAPs transcribing along the DNA in the absence and presence of Dps. First, in the assisting force (AF) configuration, the generated force facilitates RNAP translocating along the Dps-DNA complex while no Dps is bound behind it (**Fig.4**). Second, in the opposing force (OF) configuration the generated force opposes the transcription of RNAP on the DNA while the Dps-DNA complex is formed behind (**Fig.5**). Further, we perform dwell time analysis on measured traces and compare them between all the tested configurations in the absence and presence of Dps (**Fig.6**).

7.4.1 RNAP transcription at assisting force in the presence of Dps

In this section we consider configuration with assisting force applied to RNAP during transcription in the absence and presence of 1 μ M Dps (**Fig.4A**). The experiment was performed for 1.5 h at a constant force of 5 pN. Then the

measured traces were analyzed by applying the dwell time algorithm described above and plotted in **Fig.4B**.

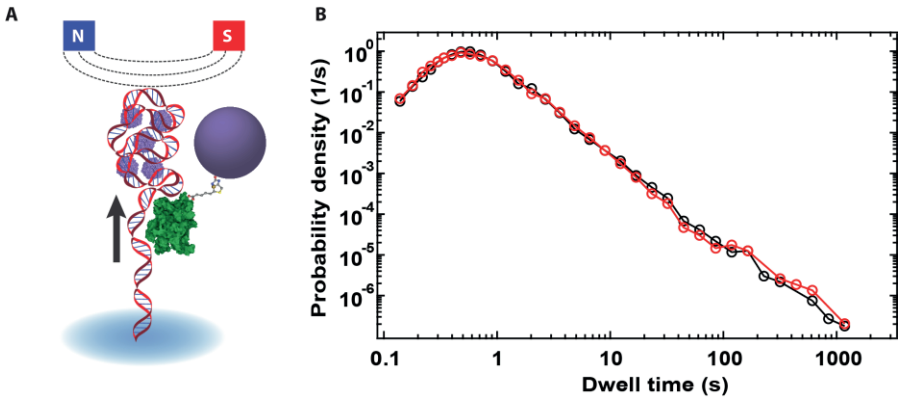


Fig.4. RNAP transcription measured at assisting force. (A) In the assisting force (AF) configuration, the magnetic force applied on the RNAP:DNA ternary complex has the same direction as the translocation of the RNAP (green) during transcription. The Dps-DNA complex (purple and red) is located in front of RNAP. (B) Dwell time analysis performed on the traces measured in the absence (black) and presence of 1 μ M Dps (red). Constant assisting force of 5 pN was applied during the whole measurement. Filtering was performed to 0.5 Hz and dwell time analysis with dwell time window (DTW) size of 10 nt.

Comparing dwell time analysis performed on the traces measured in the presence and absence of Dps at assisting force applied to RNAP:DNA complex, we do not observe any alterations in RNAP dynamics during transcription. Both curves apparently completely overlap, meaning there is no shift of the elongation peak, no changes in transcriptional pauses and no significant changes in the probability of the pause densities that corresponds to backtracking region. Therefore, DNA compaction by Dps has no influence on RNAP transcription if we apply assisting force to RNAP:DNA ternary complex.

7.4.2 RNAP transcription at opposing force in the presence of Dps

In this section we consider configuration with opposing force applied to RNAP during transcription in the absence and presence of 1 μ M Dps (**Fig.5A**). The

experiment was performed for 1.5 hours at constant force of 5 pN. Then the measured traces were analyzed by applying dwell time algorithm described above and plotted in **Fig.5B**.

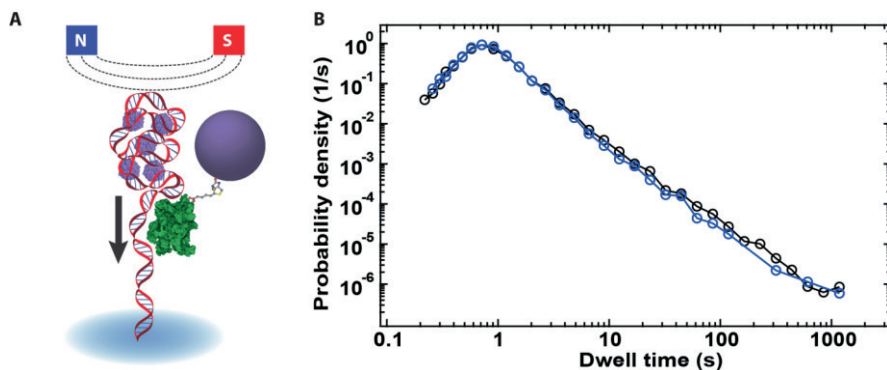


Fig.5. RNAP transcription measured at opposing force. (A) In the opposing force (OF) configuration, the magnetic force applied on the RNAP:DNA ternary complex opposes the translocation of the RNAP (green) on the DNA. The Dps-DNA complex (purple and red) is located behind RNAP. (B) Dwell time analysis performed on the traces measured in the absence (black) and presence of 1 μM Dps (blue). Constant assisting force of 5 pN was applied during the whole measurement. Filtering was performed to 0.5 Hz and dwell time analysis with DTW size of 10 nt. Filtered was performed at 0.5 Hz with DTW size of 10 nt.

Comparing dwell time analysis performed on the traces measured in the presence and absence of Dps at opposing force applied to RNAP:DNA complex we do not observe any alterations in RNAP dynamics during transcription. Both curves apparently overlap, meaning there is no shift of the elongation peak, no increase in transcriptional pauses and no changes in the probability of the pause densities that corresponds to backtracking region. Therefore, DNA compaction by Dps has almost no influence on RNAP transcription if we apply opposing force to RNAP:DNA ternary complex.

7.4.3 Comparison of assisting and opposing force configurations

In this section we compare the dwell time analysis performed on the traces measured in the presence of 1 μM Dps at two different configurations:

assisting and opposing (**Fig.6**). Both experiments were carried out for 1.5 hours at constant force of 5 pN.

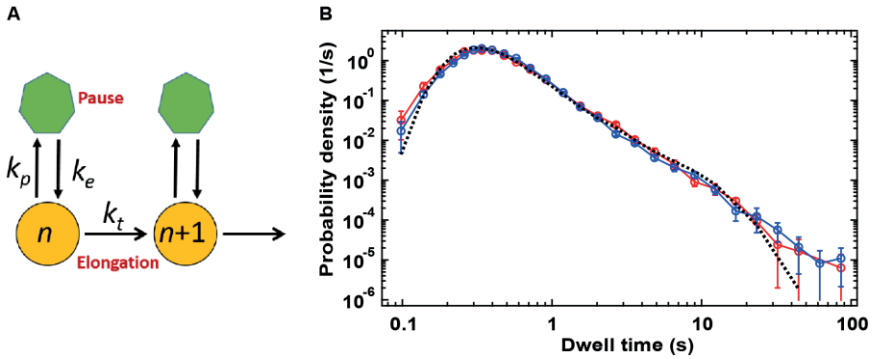


Fig.6. Comparison of RNAP transcription measured at assisting and opposing forces applying stochastic stepper model. (A) Model of stochastic stepper with elongation rate k_t , pausing entry rate k_p and exit rate k_e . **(B)** Dwell time analysis performed on the traces measured in the presence of 1 μ M Dps in assisting (red) and opposing (blue) configurations. Constant assisting force of 5 pN was applied during the whole measurement. Filtering was performed at 0.5 Hz and dwell time analysis with DTW size of 5 nt. Simulation performed with the stochastic stepper model for assisting and opposing configurations resulted in completely overlapping curves (grey dashed line). The extracted kinetic parameters from the model are: elongation rate $k_t=30$ Hz, elongation exit rate $k_p=2$ Hz, pause exit rate $k_e=0.2$ Hz, elongation probability $P = 0.12$ and pause probability $P = 0.01$.

Comparing the dwell time analyses performed on the traces measured in the presence of Dps at assisting and opposing force configurations applied to RNAP:DNA complexes we do not observe any substantial difference in RNAP elongation rates and pauses densities during transcription (**Fig.4B** and **Fig.5B**). To determine the kinetic parameters of RNAP in both experimental conditions, we apply a stochastic stepper model (**Fig.6A**) to the dwell time distributions. In this model, the motor can either step forward with a rate k_t , or enter into a pause with a rate k_p . When the motor is in a pause state, it can return to the active state with a rate k_e . The probability of pausing is then given by $P = \frac{k_p}{k_t + k_p}$. Applying this model, we performed simulations for assisting and opposing configurations and co-plotted them with the according experimental DWT distributions (**Fig.6B**). The simulations apparently overlap

with both experimental data, indicating that the transcription dynamics of RNAP is unaffected by Dps.

7.5 Tracking RNAP transcription in fully compacted Dps-DNA complexes

At the high forces used above, we are able to measure the RNAP position quickly and accurately by preventing Dps from compacting either the upstream or downstream DNA. However, Dps can compact both portions of the DNA *in vivo*. We therefore designed an assay to observe transcription on fully compacted DNA. We used the OF configuration and lowered the force to 0.7 pN, allowing Dps to bind to the entire DNA molecule (**Fig.7A**). To measure the overall progress of RNAP, we briefly extended the downstream portion of the DNA every 400 s by applying 8 pN force (**Fig.7B**). A substantial amount of traces showed a decrease in the length of the downstream DNA during these 8 pN stretching events, indicating RNAP had advanced forward. For instance, a decrease in the z-position for an example trace shown in **Fig.7B** was detected 4 times after 8, 16 and 30 min. The overall decrease of $\Delta z = 0.6 \mu\text{m}$ was measured over 80 min.

Evidence of RNAP transcription could also be detected in the fully compacted DNA. Compacted Dps-DNA complexes without active RNAP form stable configurations with Brownian fluctuations on the order of 20 nm but little long-term drift (**Fig.7C**). However, compacted Dps-DNA complexes with active RNAP are more dynamic. Slow excursions in the bead height by up to 120 nm are periodically observed after re-initiation of transcription (**Fig.7D**). We attribute these events to RNAP translocation along the DNA molecule within the Dps-DNA complex forcing the complex to rearrange. These results demonstrate that even on fully compacted DNA RNAP is capable of transcription. The Dps-DNA complex must accommodate this motion by breaking and reforming contacts between Dps and DNA, but the overall level of compaction is only transiently perturbed.

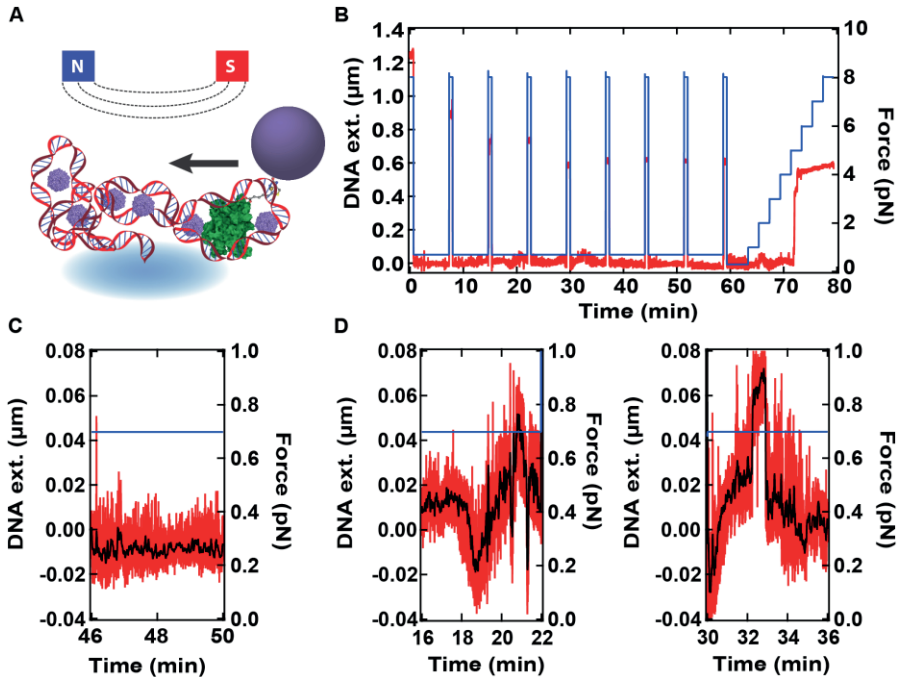


Fig.7. RNAP transcription measured in fully compacted by Dps DNA. (A) The magnetic force applied on the RNAP:DNA ternary complex opposing the translocation of the RNAP (green) through fully compacted Dps-DNA complex (purple and red). The Dps-DNA complex is located as behind as well as in front of RNAP. (B) Example time trace (red) show change in RNAP position in compare with zero time point after RNAP:DNA complex was compacted at low force (blue) and decompacted at high force every 200 sec. (C) Magnified region from example time trace (red) demonstrate stability in noise of condensed Dps-DNA complex at constant force (blue). Filtering was performed at 0.5 Hz (black). (D) Magnified regions from example time trace (red) demonstrate RNAP activity thorough condensed Dps-DNA complex at constant force (blue). Filtering was performed at 0.5 Hz (black).

7.6 Conclusions

A magnetic tweezers assay was successfully applied for the study of the *E. coli* RNA polymerase (RNAP) transcription in the presence of Dps at the single-molecule level. Several experimental configurations were designed and optimized specifically for this study. First, a force assisting RNAP translocation

was applied to study transcription through downstream Dps-DNA complexes leaving unbound DNA behind RNAP. Second, a force opposing RNAP translocation was applied in the presence of Dps, creating unbound DNA downstream of the RNAP but allowing the upstream DNA to be compacted by Dps. Lastly, the RNAP transcription was tested in a fully compacted Dps-DNA complex. The performed dwell time analysis allowed us to characterize the enzymatic behavior by examining the elongation rate and pause distributions for dwell times ranging from 0.1 s to more than 1000 s.

Surprisingly, these *in vitro* experimental results show that the presence of Dps does not cause any detectable changes in transcriptional dynamics. RNAP is capable to transcribe DNA without substantial perturbation through the compacted Dps-DNA complex. This result is unexpected due to our previous observations showing an extremely tight compaction that Dps forms on the DNA at low or zero forces. Intuitively, we expected that Dps would act as a roadblock resulting in decreased elongation rates, increased pause densities, or backtracking.

However, this finding suggests an important feature of Dps is that it allows RNAP transcription through compacted DNA molecules, keeping stressed cells metabolically active. In this way, bacteria can protect DNA with Dps during periods of high stress while independently regulating transcription. This makes Dps more useful as a general stress response factor. This strategy stands in marked contrast to the function of nucleosomes in eukaryotes, which both compact DNA and block transcription on that region of DNA (31).

References

1. B. Alberts AJ, J. Lewis, M. Raff, K. Roberts and P. Walter (2002) Molecular Biology of the Cell. Garland Science, New York, USA, 4th edition.
2. Kolb KE, Hein PP, & Landick R (2014) Antisense Oligonucleotide-stimulated Transcriptional Pausing Reveals RNA Exit Channel Specificity of RNA Polymerase and Mechanistic Contributions of NusA and RfaH. J Biol Chem 289(2):1151-1163.
3. Artsimovitch I & Landick R (2000) Pausing by bacterial RNA polymerase is mediated by mechanistically distinct classes of signals. P Natl Acad Sci USA 97(13):7090-7095.
4. Wassarman KM & Saecker RM (2006) Synthesis-mediated release of a small RNA inhibitor of RNA polymerase. Science 314(5805):1601-1603.

5. Bai L, Santangelo TJ, & Wang MD (2006) Single-molecule analysis of RNA polymerase transcription. *Annu Rev Biophys Biomol Struct* 35:343-360.
6. Larson MH, Landick R, & Block SM (2011) Single-molecule studies of RNA polymerase: one singular sensation, every little step it takes. *Molecular cell* 41(3):249-262.
7. Churchman LS & Weissman JS (2011) Nascent transcript sequencing visualizes transcription at nucleotide resolution. *Nature* 469(7330):368-+.
8. Skinner GM, Baumann CG, Quinn DM, Molloy JE, & Hoggett JG (2004) Promoter binding, initiation, and elongation by bacteriophage T7 RNA polymerase. A single-molecule view of the transcription cycle. *J Biol Chem* 279(5):3239-3244.
9. Dulin D, et al. (2015) Elongation-Competent Pauses Govern the Fidelity of a Viral RNA-Dependent RNA Polymerase. *Cell Rep* 10(6):983-992.
10. Steitz TA (2004) The structural basis of the transition from initiation to elongation phases of transcription, as well as translocation and strand separation, by T7 RNA polymerase. *Curr Opin Struc Biol* 14(1):4-9.
11. Davenport RJ, Wuite GJ, Landick R, & Bustamante C (2000) Single-molecule study of transcriptional pausing and arrest by *E. coli* RNA polymerase. *Science* 287(5462):2497-2500.
12. Galbur EA, Grill SW, & Bustamante C (2009) Single molecule transcription elongation. *Methods* 48(4):323-332.
13. Wang MD, et al. (1998) Force and velocity measured for single molecules of RNA polymerase. *Science* 282(5390):902-907.
14. Herbert KM, et al. (2006) Sequence-resolved detection of pausing by single RNA polymerase molecules. *Cell* 125(6):1083-1094.
15. Larson MH, et al. (2014) A pause sequence enriched at translation start sites drives transcription dynamics in vivo. *Science* 344(6187):1042-1047.
16. Joshua W. Shaevitz^{1*} EAA, Robert Landick⁴ & Steven M. Block^{2,3} (2003) Backtracking by single RNA polymerase molecules observed at near-base-pair resolution. *Letters to nature*.
17. Herbert KM, et al. (2010) *E. coli* NusG inhibits backtracking and accelerates pause-free transcription by promoting forward translocation of RNA polymerase. *J Mol Biol* 399(1):17-30.
18. Ishihama A (2000) Functional modulation of *Escherichia coli* RNA polymerase. *Annu Rev Microbiol* 54:499-518.
19. Vassilyev DG (2009) Elongation by RNA polymerase: a race through roadblocks. *Curr Opin Struc Biol* 19(6):691-700.
20. Mohanty BK, Sahoo T, & Bastia D (1998) Mechanistic studies on the impact of transcription on sequence-specific termination of DNA replication and vice versa. *J Biol Chem* 273(5):3051-3059.
21. Epshtein V, Toulme F, Rahmouni AR, Borukhov S, & Nudler E (2003) Transcription through the roadblocks: the role of RNA polymerase cooperation. *Embo J* 22(18):4719-4727.

22. Dillon SC & Dorman CJ (2010) Bacterial nucleoid-associated proteins, nucleoid structure and gene expression. *Nat Rev Microbiol* 8(3):185-195.
23. Svetlov V & Artsimovitch I (2015) Purification of bacterial RNA polymerase: tools and protocols. *Methods in molecular biology* 1276:13-29.
24. Cnossen JP, Dulin D, & Dekker NH (2014) An optimized software framework for real-time, high-throughput tracking of spherical beads. *Review of Scientific Instruments* 85(10):103712
25. Yu Z, et al. (2014) A force calibration standard for magnetic tweezers. *Review of scientific instruments* 85(12):123114.
26. Velthuis AJWT, Kerssemakers JWJ, Lipfert J, & Dekker NH (2010) Quantitative Guidelines for Force Calibration through Spectral Analysis of Magnetic Tweezers Data. *Biophys J* 99(4):1292-1302.
27. Janissen R, et al. (2014) Invincible DNA tethers: covalent DNA anchoring for enhanced temporal and force stability in magnetic tweezers experiments. *Nucleic Acids Res* 42(18):e137.
28. Elio A. Abbondanzieri^{1*} WJG, Joshua W. Shaevitz^{2†}, Robert Landick⁴ & Steven M. Block^{1,3} (2005) Direct observation of base-pair stepping by RNA polymerase. *Nature*.
29. Galburt EA, et al. (2007) Backtracking determines the force sensitivity of RNAP II in a factor-dependent manner. *Nature* 446(7137):820-823.
30. Shaevitz JW, Abbondanzieri EA, Landick R, & Block SM (2003) Backtracking by single RNA polymerase molecules observed at near-base-pair resolution. *Nature* 426(6967):684-687.
31. Hodges C, Bintu L, Lubkowska L, Kashlev M, & Bustamante C (2009) Nucleosomal Fluctuations Govern the Transcription Dynamics of RNA Polymerase II. *Science* 325(5940):626-628.

Summary

Each confined cell created by nature and containing DNA molecule falls into the category of “alive organism”. All information about this organism is encoded in DNA molecule in genes, except of fate only. Along with the DNA molecule that represents genetic carrier, the organism neither the genome could function without proteins. Proteins are the building blocks from which cells are assembled and capable of activating or disabling particular genes playing a crucial role in DNA replication, repair and protection. In order to understand the function of each singular protein and its role in the overall cellular metabolism, we need to characterize it from different perspectives. Without this knowledge, we do not possess a complete picture of the vitally important processes in the cell and might be losing a very promising pipeline for a treatment of many diseases.

In this thesis, we focused on characterization of the particular type of DNA-binding protein Dps (DNA-binding protein from starved cells) that physically interacts with the DNA under conditions of bacterial cell stress and starvation, playing a major role in DNA protection and chromosome compaction. However, existing knowledge of Dps mediated DNA compaction does not fully describe the kinetic features and biophysical parameters of Dps-DNA complex formation. Thus, this thesis examined how Dps compacts DNA into a complex *in vitro* revealing dynamics of the complex formation in real time and biophysical properties of the Dps-DNA interaction.

We developed two single-molecule assays to resolve the process of DNA compaction by Dps: fluorescent microscopy and magnetic-tweezers measurements. In **Chapter 2** we described experimental techniques and methods that were used in the research. The chemical modification protocols on DNA and Dps molecules were designed practically for the single-molecule measurements. The activity of the Dps protein after performed modifications was validated with control experiments.

Chapter 3 was devoted to the nature of the interactions between Dps and DNA that was probed by fluorescent microscopy and magnetic-tweezers. Probing the binding activity of Dps to DNA, we found that Dps is a highly cooperative protein that abruptly collapses the DNA extension, even under

applied tension. Moreover, we surprisingly discovered a reproducible hysteresis in the process of compaction and decompaction of the Dps-DNA complex. In this chapter we provided a detailed view of Dps binding transitions and showed that the observed hysteresis is extremely stable over timescales ranging from seconds to hours. Further, we pointed out that this process cannot be fit to standard cooperativity models. Inspired by the Ising model of ferromagnetism, we described the observation of cooperative Dps binding that exhibits hysteresis with a modified Ising model of cooperativity and found that long-lived hysteresis arises naturally as a consequence of strong protein cooperativity in the limit of large complexes.

The obtained data on Dps binding and unbinding processes provided us with kinetic features of Dps-DNA complex formation. In **Chapter 4** we examined these processes from a kinetics perspective by following DNA compaction dynamics and tuning various factors that affect Dps activity. Utilizing fluorescent assays, we compared how different amounts of monovalent salt change the affinity of Dps for DNA. We found that elevated ionic strengths greatly slow the arrival of Dps to the DNA.

Applying magnetic tweezers, we measured the mechanical forces that characterize the interactions between Dps and DNA. By testing different tension applied to the DNA molecule we modulated binding and dissociation rates of Dps. Based on this data we estimated speed and average step size of DNA wrapping and unwrapping in the presence of Dps.

In order to understand phenomenon of hysteresis in the process of DNA compaction by Dps in a scope of kinetics we plotted global free energy diagram for our modified Ising model and other models of cooperativity. We concluded that cooperativity can lead to hysteresis for a variety of mechanistic assumptions. However, we found that our modified Ising model is particularly well-suited for modeling the mechanisms of Dps-DNA complex formation.

In **Chapter 5**, utilizing magnetic-tweezers, several buffer variations that mimic changes in the cellular environment upon a stress were used in order to probe electrostatic interactions between Dps and DNA. We found that Dps affinity for DNA is strongly affected by salinity, magnesium, crowding, and pH.

With the modified Ising model for Dps-DNA complex we related the amount of hysteresis to each of the tested conditions. By fitting experimental data with our model we demonstrated that these intracellular conditions influence the strength of the neighboring interactions between bound Dps proteins and DNA. Therefore, it leads to the change in the amount of hysteresis. Based on this relation for each tested condition we defined the cooperativity parameter and dissociation constant of Dps.

In the previous chapters, we demonstrated that torsionally relaxed DNA is compacted by Dps through a cooperative Ising mechanism. However, DNA supercoiling is a vitally important component of chromosome packaging and the regulation of the cellular processes. In **Chapter 6**, we focused on the affinity of Dps for other DNA conformations, paying particular attention to plectonemic DNA as one of the DNA supercoiling states. Using fluorescence microscopy, we tested preferences of Dps in binding to different DNA shapes and found that Dps has no affinity for stretched DNA but requires two DNA strands to be close to each other in order to nucleate on DNA. First, Dps nucleates on DNA plectonemes, then on bended DNA and the last on linear DNA but only after its released from tension. Nucleation of Dps leads, therefore, to Dps-DNA complex formation. Additionally preformed Dps-DNA complexes can accommodate excess of free DNA plasmid.

Applying magnetic tweezers we examined how presence of Dps influences DNA coiling under constant tension. We showed that presence of Dps affects DNA rotation-extension curves by enhancing plectoneme formation and stabilizing them on the DNA. Dps-DNA complexes also exhibited hysteresis between increasing and decreasing turns with no regard to positive or negative supercoiling DNA states. Further, we extended our force-extension measurements on stretched DNA at zero twist (described in chapter 2) to similar studies but on supercoiled DNA in the presence of Dps. Surprisingly, under decreasing and increasing tension, presence of preformed plectonemes on the DNA resulted in rather gradual change in the DNA extension than abrupt that was previously observed for torsionally relaxed DNA. Also, preformed supercoiled DNA state caused the hysteresis loop to shrink in comparison to the hysteresis loop measured for the Dps-DNA complexes at

zero twist. This suggests, that Dps acts less cooperatively when DNA is in the supercoiled state than compared to flexible DNA. Overall, the achieved results demonstrated how DNA supercoiling states can influence Dps binding and change affinity of this particular protein.

Due to Dps compacts bacterial chromosome very tightly upon a stress, RNAP must transcribe hyper-condensed nucleoid. However, how RNAPs translocate through the Dps-DNA complex remains elusive. Knowing biophysical parameters and kinetics of the Dps-DNA complex formation allowed us to design the experiments that enabled us to track the process of RNAP transcription through these complexes. In **Chapter 7** we reported direct measurements of individual *Escherichia coli* RNAPs as they transcribed DNA compacted by Dps. Surprisingly, this *in vitro* experimental results showed that the presence of Dps does not cause any changes in transcription behavior and RNAP is capable to transcribe DNA without substantial perturbation through the compacted Dps-DNA complex.

To conclude, single-molecule approach made it possible to test wide range of different conditions by varying few parameters and explore the process of Dps compacting DNA. A new model proposed for cooperative binding revealed the intrinsic features of Dps-Dps and Dps-DNA neighboring interactions in response to the environmental changes. These experiments gave a detailed biophysical and kinetical view of Dps binding to DNA providing us with better insight into the process of genome packaging and cell functioning. Further characterization and modeling of the processes of DNA compaction by Dps can provide substantial information to the whole picture of genome organization together with other proteins and result in important medical impact for treatment of the bacterial diseases.

Samenvatting

Samenvatting

Ieder door de natuur gecreëerd afgesloten cellulair volume dat een DNA molecule bevat valt in de categorie “levend organisme”. Alle informatie over dit organisme is gecodeerd in DNA molecule in genen, met als enige uitzondering het lot. Samen met het DNA molecuul dat de genetische drager representeert, kan zowel het organisme als het genoom niet functioneren zonder eiwitten. Eiwitten vormen de bouwstenen waaruit cellen zijn opgebouwd. Daarnaast zijn eiwitten in staat om bepaalde genen te activeren of buiten werking te stellen, zodoende spelen ze een cruciale rol in DNA replicatie, alsmede de bescherming en reparatie van DNA. Om de functie van elk individueel eiwit en zijn rol in het gehele cellulaire metabolisme te begrijpen, zijn we genoodzaakt om het via verscheidene invalshoeken te karakteriseren. Zonder deze vergaarde kennis zal het onmogelijk zijn om een compleet beeld te vormen van de vitale cellulaire processen en blijven er onherroepelijk zeer belovende trajecten voor de behandeling van velerlei ziekten onontdekt.

In dit proefschrift richten we ons op het karakteriseren van DNA-bindend eiwit Dps (*DNA-binding protein from starved cells*). Dps is een bacterieel eiwit dat aan het bacteriële genoom bindt onder de specifieke omstandigheden van cellulaire stresssituaties zoals uithongering. Dps zorgt er in deze situaties voor dat het bacteriële genoom een zeer compacte vorm aanneemt, waardoor de in het DNA gecodeerde erfelijke informatie beschermd blijft. De bestaande kennis van Dps-gemedieerde DNA verdichting schiet echter tekort in het licht van het volledig beschrijven van de kinetische aspecten en biofysische parameters van Dps-DNA complexvorming. Zodoende wordt in dit proefschrift *in vitro* onderzocht hoe Dps DNA verdicht. Op deze manier onthullen we in real time de dynamische aspecten en biofysische eigenschappen van respectievelijk Dps-DNA-complexvorming en -interactie.

We hebben twee enkel-molecuulonderzoeken ontwikkeld om de Dps-gemedieerde DNA verdichting te kunnen meten: de een maakt gebruik van fluorescentiemicroscopie, de ander van de magnetische pincettechniek. In **Hoofdstuk 2** beschrijven we deze in ons onderzoek gebruikte experimentele technieken en methoden in detail. De chemische modificatieprotocollen voor de DNA en Dps moleculen zijn specifiek voor deze enkel-molecuulmetingen

ontwikkeld. Verder hebben we de nodige controle-experimenten uitgevoerd om de natuurlijke activiteit van onze gemodificeerde Dps-eiwitten te controleren.

Hoofdstuk 3 is gewijd aan de beschrijving van de aard van de interacties tussen Dps en DNA dat we hebben onderzocht door middel van de bovengenoemde fluorescentiemicroscopie- en magnetische pincettechnieken. Door de bindingsactiviteit van Dps aan DNA te onderzoeken hebben we ontdekt dat Dps-binding een zeer coöperatief proces is. Dit leiden we af uit onze observatie dat DNA in uitgestrekte vorm abrupt ineenstort tot de compacte vorm in aanwezigheid van Dps, zelfs als er een substantiële kracht aanwezig is die de ineenstorting tegenwerkt. Bovendien vonden we verrassend genoeg een reproduceerbare hysteresis in het compactie- en decompactieproces van het Dps-DNA complex. In dit hoofdstuk verschaffen we een gedetailleerd zicht op deze Dps-bindingstransities en hebben laten zien dat de geobserveerde hysteresis extreem stabiel is over tijdschalen in een bereik van seconden tot uren. Daarnaast laten we ook zien dat de standaard gebruikte coöperatieve modellen het Dps-DNA coöperatieve proces niet adequaat kunnen omschrijven. Geïnspireerd door het Ising model met betrekking tot ferromagnetisme, beschrijven we onze observatie aangaande coöperatieve Dps-binding met hysteresis daarom gebruikmakend van een gemodificeerd Ising model. We ontdekten hierbij dat de door ons geobserveerde langdurige hysteresis natuurlijk voortvloeit uit de sterke mate van coöperatie die het Dps eiwit bezit in de limiet van grote complexen.

Uit de verkregen Dps-bindings- en dissociatiedata hebben we de kinetische kenmerken van Dps-DNA complexvorming kunnen destilleren. In **Hoofdstuk 4** hebben we de hierboven beschreven processen vanuit een kinetisch perspectief bekeken door DNA-verdichtingsdynamiek te volgen en verschillende factoren die Dps activiteit beïnvloeden te variëren. Door gebruik te maken van fluorescentiemicroscopie-onderzoek hebben we vergeleken hoe verschillende hoeveelheden van monovalent zout de affiniteit van Dps voor DNA veranderen. We ontdekten hierbij dat verhoogde ionenconcentraties het moment waarop Dps aan het DNA binden zeer vertragen.

Gebruikmakend van de magnetische pincettechniek hebben we de mechanische krachten gemeten die kenmerkend zijn voor de interacties tussen Dps en DNA. Door een breed scala aan op het DNA molecuul aangebrachte trekkrachten te testen hebben we de bindings- en dissociatiesnelheden van Dps kunnen extraheren. Gebaseerd op deze data hebben we de snelheid en gemiddelde stapgrootte van DNA wikkeling en afwikkeling in de aanwezigheid van Dps geschat.

Om het fenomeen van hysteresis in het proces van Dps-gemedieerde DNA-verdichting vanuit een kinetisch perspectief te begrijpen, hebben we het globale vrije energiediagram van ons gemodificeerde Ising model en andere coöperatieve modellen geplot. We concluderen hieruit dat coöperatie kan leiden tot hysteresis voor een scala aan mechanistische aannames. We concluderen echter ook dat ons gemodificeerde Ising model bij uitstek geschikt is voor het modelleren van Dps-DNA complexformaties.

In **Hoofdstuk 5** zijn, gebruikmakend van het magnetisch pincet, verschillende buffervariaties gebruikt die de veranderingen in de cellulaire omgeving bij stress nabootsen, om zo de elektrostatistische interacties tussen Dps en DNA te onderzoeken. We ontdekten dat de affiniteit van Dps voor DNA sterk wordt beïnvloed door het zoutgehalte, het magnesiumgehalte, de concentratie van andere grote moleculen en de pH van de oplossing. Met ons gemodificeerd Ising model voor Dps-DNA complexvorming hebben we de mate van hysteresis gekoppeld aan elk van de geteste omstandigheden. Door experimentele data met ons model te fitten hebben we gedemonstreerd dat deze intracellulaire omstandigheden de kracht van de aangrenzende interacties (de mate van coöperatie dus) tussen gebonden Dps en DNA beïnvloeden. Als direct gevolg hiervan verandert de hoeveelheid hysteresis. De mate van hysteresis is dus een mate voor de coöperativiteit van Dps. We hebben daarom een Dps-coöperativiteitsparameter en dissociatieconstante gedefinieerd en deze voor elk van de geteste omstandigheden bepaald.

In de vorige hoofdstukken, hebben we gedemonstreerd dat niet-getordeerd DNA door Dps verdicht wordt middels een coöperatief Ising mechanisme. Aan torsiekrachten onderworpen DNA is echter onlosmakelijk verbonden met

verscheidene cellulaire en chromosomale processen en daardoor van vitaal belang voor de cel. In **Hoofdstuk 6** hebben we ons daarom gericht op de affiniteit van Dps voor andere DNA conformaties, waarbij we in het bijzonder aandacht hebben besteed aan plectonemisch DNA als een van de toestanden van (super)getordeerd DNA. Gebruikmakend van fluorescentiemicroscopie hebben we de voorkeur van Dps voor het binden aan verschillende DNA vormen getest. Hierbij ontdekten we dat Dps geen affiniteit heeft voor gestrekt DNA, maar de nabijheid van twee DNA strengen vereist om een (bindings)kern te vormen op het DNA. Eerst vormt Dps een kern op DNA plectonemen, dan op gebogen DNA en pas als laatste op lineair DNA, echter pas nadat de spanning erop is weggehaald. Nucleatie van Dps leidt daardoor tot Dps-DNA complexformatie. Dps-DNA complexen kunnen daarnaast ook nog een overschot aan vrije DNA-plasmide accommoderen.

Gebruik makend van het magnetisch pincet hebben we bekeken hoe de aanwezigheid van Dps invloed heeft op het door torsie aangebrachte oprollen van DNA onder een constante trekkracht. We laten zien dat de aanwezigheid van Dps de DNA rotatie-extensie verhouding beïnvloedt door plectonemevorming te bevorderen en deze te stabiliseren op het DNA. Dps-DNA complexen hebben ook hysteresis laten zien tussen toenemende en afnemende aangelegde torsie voor zowel positieve als negatieve (super)getordeerde DNA toestanden. Hiernaast hebben we onze kracht versus extensie metingen op niet-getordeerd DNA (beschreven in hoofdstuk 2) uitgebreid met eenzelfde meetserie aan supergetordeerd DNA. Verrassend genoeg zorgt de aanwezigheid van voorgevormde plectonemes op DNA voor een geleidelijke afname in DNA uitstrekking, in plaats van de abrupte ineenstorting zoals eerder bij niet-getordeerd DNA door ons geobserveerd was. Ook nemen we een verkleining van de hysteresis in vergelijking met Dps-DNA complexen bij nul draaiing waar. In de aanwezigheid van supergetordeerd DNA gedraagt Dps zich minder coöperatief dan het geval is bij niet-getordeerd DNA. De bereikte resultaten laten duidelijk zien hoe supergetordeerde DNA toestanden de Dps-binding en Dps-affiniteit beïnvloeden.

Doordat de door Dps verdichte bacteriële chromosomen zeer strak onder spanning staan, moet de RNA polymerase (RNAP) hyper-gecondenseerde genomen transscriberen. Hoe de RNAPs dit voor elkaar krijgen en zich een weg door een Dps-DNA complex weten te banen is tot nu toe een onopgehelderd vraagstuk. Het kennen van biofysische parameters alsmede de kinetika van de Dps-DNA complexvorming heeft het mogelijk gemaakt om experimenten te ontwerpen die het proces van RNAP transcriptie door Dps-DNA complexen registreert. In **Hoofdstuk 7** beschrijven we de metingen aan individuele *Escherichia coli* RNAPs op het moment dat ze het door Dps verdichte DNA transscriberen. Verrassend laten deze *in vitro* experimentele resultaten zien dat de aanwezigheid van Dps geen veranderingen in het RNAP transcriptiegedrag veroorzaken en RNAP in staat is om door Dps verdicht DNA te transscriberen zonder substantiële verstoring of vertraging.

In conclusie maakte een enkel-molecuulbenadering het mogelijk om een breed scala aan toestanden te onderzoeken waarop Dps DNA verdicht, door een paar parameters te variëren. Een door ons voorgesteld nieuw model voor coöperatieve binding heeft de intrinsieke kenmerken van Dps-Dps en Dps-DNA aangrenzende interacties onthuld, alsmede de respons van het systeem in veranderende omstandigheden. Deze experimenten geven ons een gedetailleerde biofysische en kinetische kijk op Dps binding aan DNA en verschaft ons zo een beter inzicht in het proces van genoomverpakking en cellulaire werking. Verdere karakterisering en modellering van de processen die gepaard gaan met door Dps gemedieerde DNA verdichting kan aanzienlijke informatie opleveren voor het totaalplaatje van hoe genoomorganisatie afhangt van andere eiwitten. Dit kan op zijn beurt weer een aanzienlijke invloed hebben op hoe we bacteriële ziekten voorkomen, bestrijden, en behandelen.

Acknowledgements

First and foremost, I would like to thank my family for their unconditional love and support throughout my life. My parents, Mr. and Mrs. [Name], have always been my pillars of strength and encouragement. I am also grateful to my siblings, [Name] and [Name], for their constant companionship and understanding.

I would like to express my deep appreciation to my teachers and mentors who have guided me through my academic journey. In particular, I thank [Name] for their inspiring leadership and [Name] for their unwavering support during my most challenging times.

My friends, [Name] and [Name], have been a source of joy and laughter throughout my life. Their friendship has made every moment more meaningful and memorable. I am grateful for their presence and the love they have shown me.

I also want to thank my community and the many people who have supported me in various ways. From the staff at [Name] to the volunteers at [Name], everyone has played a role in shaping my life and helping me achieve my dreams.

Finally, I would like to thank myself for never giving up and for always striving for excellence. I am proud of the person I have become and the journey I have taken. I look forward to the future with hope and optimism.

With love and gratitude,
[Name]

I am grateful to all who have read this book and to those who will read it in the future. May it inspire and uplift everyone who encounters its pages.

Thank you for being a part of my life and for sharing in my journey. I am truly grateful for every moment we have spent together.

With love and appreciation,
[Name]

A.I Story of my PhD adventure

Most of the PhD students experience periodical declines and climbs on their research path. My climbs usually occurred due to help of my colleagues without whom this project would not have reached its success. If you are on this page of my thesis you must be the one who played an essential role in my PhD research. Here I would like to acknowledge my colleagues who guided, supported, and inspired me through my PhD path.

First person I met on my PhD horizon 4,5 years ago was my supervisor Elio Abbondanzieri. I am endlessly grateful to him for giving me - physicist without any experience in the biolab, an opportunity of doing a PhD project in the discipline I knew less than I was passionate about. Thus, I realized my passion in hardcore experimental biology in one of the most successful universities and departments. Thank you for guiding me through this project and being always available for advice, discussions, patient explanations and new ideas. Thank you for keeping your faith in me when I was lost. Additional gratitude I express for the contribution into my personal development by sending me to the Cold Spring Harbor Advanced Bacterial Genetic Course at the sunrise of my PhD and allowing me to do an internship at Philips at the sunset of my project.

The second person I met was Anne Meyer. Anne, you were the one who revealed to me all known fascinating insights of Dps protein and provided me with necessary resources for launching my project. Thanks to your whole group with whom we had very intertwined projects and, therefore, valuable knowledge exchange: Michel, Ilja, Vlad and Mathia.

Another ice breaking meeting occurred with Chirlmin Joo who shed a light on the basics of the single-molecule fluorescence assay. Also, thanks to the whole group of Chirlmin: Anna, Stanley, Jetty, Malwina and Mohamed. You were always kind to Abbobandzieri lab - sharing knowledge, protocols and chemicals.

Next shot of inspiration I received from Bertus Beaumont. You made my first day at work when I attended the course of yours. You are the best presenter I ever seen! Your charge of inspiration and curiosity is still in me.

Jetty, thank you for providing me a right angle on the view of Dutch culture and the weather during my intake interview. You told me only the truth! Anna and Michela, thank you for a great dinner on the evening after the interview, that was necessary social activity for me that day. You fulfilled me with the right energy for this decision to become a PhD.

Vlad Karas, thank you for explaining me a great part of my project at the beginning in pure Russian. I was so lucky to have you around at that time when I needed it so much!

Anna Haagsma, you become a necessary trainer for me. Under your supervision I have learnt the most basic and not so basic techniques I needed in order to start my project. Under your control I performed my first pipetting move, my first buffer preparation, my first agarose gel, my first autoclave, and at the end my first protein purification. You assisted me with all my first steps. Thank you for your time and patience!

Then was an era of a clean room. Thank you Xander for introducing me to our clean room. Thank you Felix for agreeing to be my mentor, when all refused. Thank you Yaron for a lively lesson with the nitric spill. I learnt to be extremely careful and finally started to enjoy working there. Thank you Magnus for educational EBEAM sessions.

Mahipal Ganji – my one and only one labmate. It was a pleasure to work with you shoulder to shoulder. You always provided me with numerous of great suggestions when I was encountered to the problems. I am glad that at least at the end of our PhDs we could perform a little bit of a common research.

Special gratitude to Margreet Docter who came up with an amazing and complex script for my fluorescence data analysis. This script allowed me to understand how Dps works at the very first step of my research as well as it fulfilled the missing puzzles at the very end.

David Dulin – thank you for revealing me the power of magnetic tweezers! This technique in one day changed the direction of my study and brought me the most fruitful results. Now three quarters of my thesis consists of the results obtained with the setup you developed. These conclusions I could never draw without your professional look. From the very beginning of my project I was supported by you in my growth as a scientist.

Particularly grateful to people who were involved in the magnetic tweezers and provided me trainings, support, assistance and feedback: Mariana, Richard, Orkide and Bojk. Special thank you to Richard Janissen for dragging me into Dps-RNAP project. It was a very pleasant collaboration, always neatly organized, planned and analyzed.

Yera – thank you for such a wonderful graphical support to my thesis. So many pictures and figures were made by you or with your help. Not only that, but also for critically judging my work and correcting my first manuscript.

The experimental work would not have been possible without technical support of the following people: Serge, Susana, Erwin, Anna, Ilja, Jaco, Theo, Inge, Margreet and Daniel. At different stages of the research you were always there to help and solve the problem very fast and efficiently. I thank Jelle for his golden arms and professionalism in making extremely customized devices.

Among others, I have benefited greatly from the discussions with people from Bionanoscience department: Maarten, Fabai, Pauline, Zohreh, Sriram, Andrew, Charl, Regis, Simon, Kuba, Adithya, Felix, Jelmer, Allard, Zhongbo, Gautam, Eugene and Greg Bokinsky. I have seen so much openness and wiliness to help from you that I never was left alone and always felt a ground under my feet.

I am proud to have excellent scientists as members of my committee: Nynke Dekker, Andreas Engel, Tom Shimizu, Gijs Wuite, John van Noort, David Grainger, and Marileen Dogterom. Thank you for your time that you spent on reviewing my thesis and critically assessing it.

Additional gratitude I express to my promotor Nynke Dekker - you were always supportive, kind and fair to me. You allowed me to integrate in your

group and I felt as a member. Thank you for caring about my project and my well-being through these years.

Dijana Boric, Jolijn Leeuwenburgh, Angela de Ceuninck van Capelle and Esther Reinders provided me a great support in all organizing issues.

I acknowledge TU Delft, Casimir Research School, NanoFront, Bionanoscience Department and Kavli Institute of Nanoscience for the financial support of my project and investments into my personal development.

Overall, I am incredibly glad that I had a chance to work with all of these people so interesting and so smart what always intellectually stimulated me; so kind and patient to help me through all frustrating moments I had; so diverse and multicultural that made the atmosphere happy and friendly.

A.II Story of my live during PhD adventure

I was also lucky to meet many interesting people outside of my department. If you are on this page of my thesis you must be the one who played a great role in my personal life during these years of my PhD. Here, I would like to acknowledge people who contributed to my spirit and encouraged me morally in making it through my PhD.

Some of them I met during the PhD Start Up course: Olga, Nikolas, Dena and Aldo. All of you became my friends from the very beginning and remained them through the all years. Thank you for all fun and gatherings we had together! Ольга, спасибо за поддержку и мудрые советы, спасибо за твою бесконечную заботу!

Sacha Khaiboulov, your endless enthusiasm and optimism always amazed me! You are a great listener. Thank you for always being in a good mood and supporting me in all my initiatives! Your help and assistance in everything that I asked made my life much easier.

Eugen and Roy – thank you for the fun we had during our business trips! Robert and Rashiq thank you for dragging me into Thai Boxing! Joris – so much fun we had in our tandem meetings, I am grateful to you for my Dutch

knowledge and that you are always ready to help me with translation, including the samenvatting of this thesis. Jinhee, thank you for the wonderful cover design you made! Thank you to all who supported my stretching classes: Joris, Rossiza, Eline, Caroline, Misha and others. Serge, thank you for your open-mindedness and great time we spent at the performances of NDT.

So many housemates I changed through these years in Delft and so much of your culture precipitated in me because of you girls: Basia, Mariana and Helena. Thank you for sharing yourself and the houses with me.

Отдельную благодарность выражаю всем моим русскоговорящим друзьям, кто всегда помогал полезными советами, поддерживал, делился опытом и посещал мои мероприятия: Глеб, Никита, Лена, Коля, Таня и Олег, Леша, Маша Р., Катя М., Маша З., Надя, Катя У., Иван, Аня, Женья, Сергей и Инна.

Дорогие мои друзья, живущие на родине: Ряба, Аля, Эрик, Павлуша, Гром и Митяй. Спасибо тем, кто меня навестил и спасибо тем, кто всегда ждет моего прибытия в Москву!

Ира, ты дала мне уверенность в моем выборе аспирантуры и поддержала меня с самого начала до самого конца. Ты была и есть рядом всегда, особенно когда мне это необходимо. Не только ты, но и твоя семья оказала мне огромную поддержку, что сильно облегчило мне мой переезд. Спасибо!

Миша, твоя рассудительность, взвешенность, благоразумие и профессионализм позволяют мне принимать правильные решения и достигать многого. Твоя любовь и забота стоят за моими свершениями. Ты готов выслушать, помочь и поддержать все мои начинания, за что я тебе бесконечно благодарна!

Спасибо моей семье: папе, маме и сестре. Благодаря вам моя научная деятельность стала возможной и приобрела для меня большое значение.

Delft,
July 2016

Curriculum Vitae

Natalia Vtyurina

25-02-1988

Born in Moscow, Russia

2001-2005

High School

Lyceum № 1580 at Bauman Moscow State
Technical University
Moscow, Russia

2005-2011

B.Sc. Physics

Lomonosov Moscow State University
Department of Photonics and Microwave Structures
Thesis: "The influence of electromagnetic radiation on
biological systems within urban environment"
Moscow, Russia

2008-2011

M.Sc. Biophysics

Engelhardt Institute of Molecular Biology, Russian
Academy of Sciences
Thesis: "The cleavage of DNA molecule induced by laser
excitation at 193 nm"
Moscow, Russia

2012-2016

Ph.D. Bionanoscience

Delft University of Technology
Thesis: "What makes long DNA short? Modulation of
DNA structure by Dps protein: cooperating & reorganizing"
Delft, the Netherlands

List of Publications

1. Vtyurina NN, Dulin D, Docter MW, Meyer AS, Dekker NH, & Abbondanzieri EA (2016) Hysteresis in DNA compaction by Dps described by an Ising model. *Proc Natl Acad Sci USA*, 113, 4982-4987.
2. Vtyurina NN, Docter MW, Meyer AS, Dekker NH, & Abbondanzieri EA (2016) The kinetics of the cooperative condensation of DNA by Dps. *In preparation*.
3. Vtyurina NN, Ganji M, Meyer AS, Dekker NH, & Abbondanzieri EA (2016) DNA topology modulates Dps binding. *In preparation*.
4. Vtyurina NN, Meyer AS, Dekker NH, & Abbondanzieri EA (2016) Effect of DNA supercoils on Dps induced collapse of DNA. *In preparation*.
5. Vtyurina NN, Janissen R, Artsimovitch I, Dekker NH, & Abbondanzieri EA (2016) RNAP transcribes through Dps-DNA complexes. *In preparation*.

Propositions

accompanying the dissertation

What makes long DNA short? Modulation of DNA structure by Dps protein: cooperating & reorganizing

by

N. Vtyurina

1. Cooperativity engenders efficiency and singularity.
2. Fate is not stored in your DNA: evolution is not gifted with precognition and does not plan the future.
3. Scientific results are always interpreted through a researcher's perspectives.
4. The amount of memory needed to encode all cellular processes exceeds the amount of information that a human brain can process.
5. Biology is a programming language designed by Nature.
6. The laws of physics apply on both sides of the cell boundary regardless of whether the researcher is a physicist or a biologist.
7. Only fundamental science can give rise to genuine innovation.
8. Understanding the technique chosen for tackling a scientific problem provides insight into researcher's conclusions.
9. There is a direct link between the discovery of the simplest organism in Delft by Antonie van Leeuwenhoek and the success of the Bionanosience department.
10. Keeping yourself busy is the cheapest and most effective medicine.

These propositions are regarded as opposable and defensible, and have been approved as such by the promotor Prof.dr.ir. N.H. Dekker and the copromotor Dr. E.A. Abbondanzieri.

Утверждения

к диссертации

Что делает длинную ДНК короткой? Модуляция структуры ДНК протеином Dps: кооперативность & реорганизация

Н. Втюрина

1. Кооперативность порождает эффективность и сингулярность.
2. Судьба не хранится в ДНК: эволюция лишена дара предвидения и не строит планов.
3. Научные результаты всегда интерпретируются через призму сознания исследователя.
4. Количество памяти необходимое для кодировки всех клеточных процессов превышает количество информации, которое может обработать человеческий мозг.
5. Биология – это язык программирования, придуманный Природой.
6. Законы физики работают одинаково и внутри и за пределами клетки, независимо от того, является ли исследователь физиком или биологом.
7. Только фундаментальная наука может дать толчок к настоящим инновациям.
8. Понимание техники, выбранной для решения научной проблемы, позволяет понять выводы исследователя.
9. Существует прямая связь между открытием простейшего организма Антони Левенгуком в Делфте и успехом бионанонаучной кафедры.
10. Быть все время занятым является наиболее эффективной и дешевой медициной.

Эти утверждения одобрены проф., д.ф.-м.н. Н.Х. Деккер и д.ф.-м.н. Э. А. Аббонданзиери, могут быть оспорены и представлены к защите.




The protein Dps protects the bacterial chromosome from hostile environments. In one way this protection is achieved through cooperative Dps binding to chromosomal DNA that rapidly alters its shape and forms a protective shell around the genome.

This thesis examines how binding of Dps modulates the DNA structure *in vitro*. It gives a detailed biophysical view of the Dps-DNA interaction and provides new insights into bacterial survival strategies.

Elucidation of Dps properties has important medical impact on the treatment of bacterial diseases.





Casimir PhD series 2016-10
ISBN: 978.90.8593.262.8